Fall 2024 InSAR Survey of Ground Displacement and Subsidence Monitoring Report

Sulphur Mines Salt Dome

ANNUAL SURVEY

Prepared for:

Westlake US 2, LLC

Prepared by:

Lonquist & Co., LLC
12912 Hill Country Blvd. / Suite F-200
Austin, TX 78738

Louisiana Firm License Number EF-5937

September 2025

Fall 2024 InSAR Survey of Ground Displacement and Subsidence Monitoring Report

Sulphur Mines Salt Dome

ANNUAL SURVEY

CERTIFIED BY:
Lonquist & Co., LLC
Louisiana Registration No. EF5937

Teresa H. Rougon, P.G.
Date Signed: September 19, 2025
Baton Rouge, LA

Teresa H. Rougon, P.G.
Principal Geologist
Louisiana License No. 330

Nathaniel L. Byars
Date Signed: September 19, 2025
Austin, TX

Nathaniel L. Byars, P.E.
Principal Engineer
Louisiana License No. 40697

Executive Summary

Lonquist and Co., LLC ("Lonquist") was contracted by the three (3) operators at the Sulphur Mines Salt Dome to prepare a subsidence monitoring plan that utilizes InSAR (Interferometric Synthetic Aperture Radar) data to detect ground displacement. TRE Altamira ("TREA") was contracted by Lonquist to collect, process, and analyze the data across the dome and surrounding area. Upon completion of the InSAR subsidence analysis by TREA, Lonquist is providing the Louisiana Department of Energy and Natural Resources ("LA DENR"), Injection Mining Division ("IMD"), with a detailed review of the reported data and a supplementary evaluation of the subsidence trends that have been observed over the dome.

Statewide Order 29-M-3 and Statewide Order 29-M (Rev. 3), require that both brine mining operators and hydrocarbon storage operators conduct subsidence monitoring surveys on an annual basis during the same period. Monitoring at Sulphur Mines is carried out in the fall of each year. The analysis performed by TREA serves as the Fall 2024 subsidence survey for the dome.

The evaluation discussed herein details ground displacement measurements as captured from two satellite orbits observing from the east and west of the monitoring area. True vertical displacement and east-west displacement were identified via triangulation of the two satellite datasets during the February 2023 - December 2024 timeframe when data was collected from both satellite orbits.

The utilized method of subsidence evaluation follows guidance provided by the IMD in 2019 for estimation of subsidence rate trends and apparent rate changes for survey monuments over the dome. The charts provided within this report illustrate the historical ground displacement and subsidence trends within areas of interest (AOIs) in lieu of survey monument locations. The contour maps generated from this data depict the spatial distribution and present condition of vertical and east-west ground displacement across the dome.

No anomalous subsidence trends or regions have been identified in the Fall 2024 survey. This indicates that rates of cavern closure and other factors of influence are continuing to act in a consistent manner at this time.

As the third annual survey performed with InSAR data, this report is also intended to provide evaluation and clarification of the following: 1) Discussion of InSAR technology and modifications to the subsidence evaluation methodology over the dome, 2) Comparison of current and prior annual subsidence rates indicated by InSAR, 3) Review of the 8-year 1-D SNT dataset to confirm historical rate consistency, and 4) Review of preliminary data trends from InSAR corner reflectors installed in 2024.

Table of Contents

APPENDICES

Acronyms and Abbreviations

1-D	1-Dimensional – Line of Site Displacement
2-D	2-Dimensional – Vertical and East-West Displacement
AOI	Area of Interest
CR	Corner Reflector
GNSS	Global Navigation Satellite System
IMD	Injection and Mining Division
InSAR	Interferometric Synthetic Aperture Radar
LA DENR	Louisiana Department of Energy and Natural Resources
LOS	Line of Sight
SNT	Sentinel 1 Satellite
SPR	Strategic Petroleum Reserve
TREA	TRE-Altamira
TSX	TerraSAR-X Satellite
TSX-A	TerraSAR-X Satellite – Ascending Dataset
TSX/PAZ	TerraSAR-X and PAZ Satellite Constellation – Descending Dataset

1.0 Background

Salt caverns are created through a process called solution mining. This is achieved by drilling into a salt formation and circulating water into the drilled hole to dissolve the salt. This process forms a brine-filled cavern within the salt body. Salt caverns can then be used to store various fluids such as natural gas and refined hydrocarbon products. Salt domes have been known to experience deformation due to gradual closure of the mined spaces within the salt formation or other geological processes related to the salt and overlying caprock. The gradual closure of cavern space is formally known as salt creep and stops only when the cavern has reached a geostatic equilibrium with the surrounding rock. Factors such as cavern depth, ground temperature, salt properties, regional stresses, overburden density, operating pressures, and the geometry of and proximity to neighboring caverns affect the magnitude of salt creep.

Due to salt creep, the overburden rock layers begin to move downward towards the caverns. This can be seen on the surface as subsidence (or ground displacement) vertically and to a lesser extent horizontally toward the center of the subsidence basin. Consequently, it is anticipated that surface subsidence will transpire over all solution-mined caverns in domal and bedded salt to varying extents. The vertical displacement rate over a solution-mined cavern generally ranges from less than ¼ inch annually to several inches per year. Pursuant to the provisions of Statewide Order 29-M (LAC 43: XVII. Subpart 3) and Statewide Order 29-M-3 (LAC 43: XVII. Subpart 5), subsidence must be measured annually over all solution-mining and storage caverns.

1.1 Monitoring History

Subsidence monitoring over salt caverns allows operators and regulators to prepare for and respond to potential stability issues in a proactive manner. Monitoring of surface elevations has been undertaken for a number of years by individual companies operating on the Sulphur Mines Salt Dome. The data provided to Lonquist & Co., LLC (“Lonquist”) indicates level surveying for subsidence monitoring was initiated in 1993 by Westlake US 2, LLC (“Westlake”) (formerly Eagle US 2, LLC and PPG Ind., Inc. – Ind. Chem. Div.) and was generally conducted on a two-year basis. These elevation surveys were conducted internally by a PPG staff surveyor. In addition to the surveys being performed by Westlake, surveys were also conducted by American Surveyors, LLC, on behalf of Liberty Gas Storage, LLC (“Liberty”) and Boardwalk Louisiana Midstream, LLC (“Boardwalk”).

In 2015, an agreement was reached between all three (3) operators to conduct a coordinated precision level survey across the Sulphur Mines Salt Dome utilizing a common set of benchmarks and monuments. Hydro Consultants, Inc. (“Hydro Consultants”), a

professional land surveying company, was subcontracted by Lonquist to conduct the survey. A survey plan was created, and a set of benchmarks and monitoring stations were selected to be surveyed. Level surveys were performed in accordance with this plan through the Fall 2021 survey. Following that survey, the decision was made to transition to InSAR subsidence monitoring for the next annual survey in Fall 2022 and subsequent surveys going forward.

Since the coordinated monitoring effort began in 2015, continual and relatively consistent ground displacement has been observed. The greatest subsidence rates have been identified over the central portion of the dome with a gradual tapering toward the dome flank.

1.2 Sulfur Extraction

Although the current monitoring program is affiliated with cavern operations on the dome, the primary source of subsidence has been attributed to past sulfur extraction from the overlying caprock. Between 1902 and 1924, the caprock was heavily drilled and molten sulfur was mined through wellbores resulting in a total production of 10.5 million US tons of sulfur. This tonnage equates to 28 million barrels or 3,600 acre-feet of extracted volume. Over the approximately 75 acres of caprock extent, an average 48-foot thickness of sulfur is estimated to have been removed. By the time mining was completed in the late 1920's, the collapse of voids left by the sulfur extraction had resulted in surface subsidence in excess of 20 feet. This led to the creation of a lake extending across the mined area, surrounding the present-day salt cavern locations.

Subsidence continued at lesser rates over the following century and large sections of the lake were backfilled to support infrastructure and well pads. Dredging of the surrounding area to provide fill material is what led to the creation of the large lakes that surround the site. A study performed in 1965 comparing data from wells drilled before and after the sulfur mining operations, resulted in the development of a caprock collapse map identifying changes in caprock thickness below ground. Large collapses up to 163 feet were identified in some places, but most values ranged between 25 and 50 feet across the mined area.

In a 1980 study commissioned by the Strategic Petroleum Reserve ("SPR"), subsidence was estimated from level survey data to be occurring at an average rate of about 1.2 inches/year above the existing SPR cavern locations (PPG Nos. 2, 4, 5, 6, and 7). The study noted that this rate of subsidence had been occurring for some time and was likely to continue into the foreseeable future. These subsidence rates agree with current survey data, indicating that the trend has remained consistent to present day. The study concluded that subsidence over the dome was the result of the following factors: 1)

Continual closure of caprock voids from the past sulfur mining, 2) Consolidation of soils used to fill subsided regions, and 3) Natural dissolution of evaporite layers and collapse of preexisting voids from groundwater flow within the caprock.[1] Although not acknowledged as a factor in the report, creep closure in the Sulphur Mines salt caverns may have been contributing in some degree to the rates of observed subsidence.

1.3 Westlake US 2, LLC

Westlake US 2, LLC operates only Class III Solution-Mining caverns which are regulated by SWO 29-M-3. The statutory compliance requirements found therein mandate that Westlake perform an annual survey as part of the ongoing monitoring program established at the dome. The InSAR survey and this supplementary evaluation report are being submitted to fulfill the annual monitoring effort for the Fall of 2024.

2.0 Fall 2024 InSAR Survey

Beginning with the Fall 2022 subsidence evaluation, the decision was made to employ an alternative survey method known as Interferometric Synthetic Aperture Radar, or "InSAR". This method of data collection relies on satellite-based ground displacement readings calculated from radar imagery. Compared to traditional level surveys, data resolution is improved both spatially and temporally, allowing for the analysis of thousands of ground locations on regular, multi-day intervals. InSAR is a high-accuracy, remote sensing technology that effectively provides an updated level survey of a target area with each successive pass of an orbiting satellite. Spatial density of the measurement points varies, but in areas of non-vegetated ground cover, a substantial number of ground targets can be surveyed on a regular basis. The Fall 2024 survey is the third annual survey to employ InSAR data for subsidence monitoring.

TRE-Altamira ("TREA"), a global leader in InSAR ground displacement monitoring, was contracted by Lonquist to collect, process, and analyze ground displacement data over the Sulphur Mines site. TREA utilizes an advanced, proprietary form of InSAR data processing that tracks ground movement by analyzing a stack of radar images collected over time. This technology, termed "SqueeSAR®", provides a collection of spatially distributed measurement points that each contain a time series of ground deformation measurements reported to a 0.1 mm (0.004 inch) scale. Measurement accuracy is on par with traditional rod and level surveys in terms of error range with vertical displacement rate precision being estimated at ±0.02 in/yr. The analysis report prepared by TREA has

[1] **Whiting, G H. 1980.** "Strategic Petroleum Reserve (SPR) geological site characterization report, Sulphur Mines Salt Dome: Section I, Section II, and Section III". United States.

been provided for reference as Appendix F. The report contains a general description of subsidence related observations over the analysis area as well as a detailed description of the InSAR monitoring system and data processing method.

2.1 Data Properties

Imagery collected via satellites over successive orbital passes is used to identify and define measurement points on the ground. Objects or ground features providing a stable reflection of radar energy such as buildings, roads, and infrastructure produce the highest quality of measurement points. Measurement points can be generated in some areas with vegetation, but data quality is affected by changing ground characteristics over time, leading to data gaps in areas with dense vegetation, farming or wetlands. In the absence of stable reflectors, additional datapoints can sometimes be generated in areas with lower but homogenous signal return by averaging groups of readings into a single measurement point.

InSAR uses phase and amplitude in the radar signal images to measure the distance between the satellite sensor and the measurement points on the ground. The data generated from the InSAR technique results in a time series of displacement values at each measurement point. These displacement values are reported in relation to the original distance measured for each point in the dataset.

When a measurement point on the ground moves, whether that be vertically or laterally, the phase value detected by the sensor on the satellite is impacted due to a change in the distance between the sensor and ground target. Displacement values generated in this way are referred to as 1-D Line-of-sight (“LOS”) measurements, referring to the line-of-sight of the satellite to the ground target. Data collected in this manner is understood to convey a movement distance that is not purely vertical. This distinction only affects the assignment of a precise direction to the movement identified. As the primary component of the observed displacement is often vertical, InSAR analyses based on 1-D data are regularly used to identify and monitor the consistency of deformation trends related to ground subsidence.

If precise delineation of vertical deformation is required, datasets from a pair of satellite orbits can be utilized to calculate the vertical component of ground displacement via triangulation. Data generated from a pair of 1-D LOS datasets processed in this manner are referred to as 2-D measurements. These datasets identify vertical and horizontal ground displacement. Due to the orbital direction of the satellites, radar images are always captured from an eastern or western direction relative to the target area. Therefore, horizontal ground deformation identified via InSAR is defined as east-west

displacement. The north-south component of ground deformation is unknown in 2-D datasets, and cannot be identified via InSAR due to the viewing direction of the satellites. Analysis of an InSAR dataset allows for the identification of displacement velocity in inches/year and acceleration in inches/year^2. Measurement precision is affected by the satellite sensor resolution and the timeframe of the dataset. Average accuracy ranges for individual measurements can vary between ±0.20 inches for a low-resolution satellite and ±0.03 inches for a high-resolution satellite. With time, velocity trends can be measured with high accuracy yielding standard deviations in the range of ±0.01 inches/year.

2.2 Reference Point

The InSAR survey method relies on the selection of a local reference point from among the measured ground targets. The reference point is represented as static in order to produce calculations of relative movement at all other measurement points. In this way the reference point is similar to the off-dome, deep-rod benchmark monuments used in past level surveys at the site. However, unlike benchmark monuments, the reference point is chosen more for its motion behavior and radar properties than its location and construction. The reference point used for the evaluation of each dataset must exhibit high-quality signal return and not be affected by fluctuating surface movement within the time period evaluated.

Movement, if present at the reference point, is confirmed to be linear and assumed to be representative of broad regional deformation trends that extend beyond the analysis area. Once this movement is zeroed out at the reference point, regional movement is assumed to be excluded from the displacement rates calculated at other measurement points. This is similar to historical ground surveys that relied on relative measurements from benchmark monuments. Ideally, the reference point will not change between surveys, but subsequent non-linear movement or increased signal noise may require selection of a new location.

As discussed in the following sections, multiple InSAR datasets were evaluated as part of the Fall 2024 survey efforts. The reference points for each of these datasets are located near to each other, 1.68 miles to the southeast of the approximate dome center. The off-dome benchmark used in past surveys was located at a similar distance from the site at 1.79 miles to the south-southwest of the dome center.

2.3 Satellite Data Sources

Two satellite datasets were used in the InSAR analysis which were acquired from satellites on both ascending and descending orbits. An ascending orbit denotes the satellite's

longitudinal course from south to north as it passes over the site and radar images from ascending orbits are captured in an eastward direction. In descending orbits, the satellite moves from north to south and images are captured with a westward viewing direction.

In prior InSAR surveys, the 1-D LOS ascending dataset came from a Sentinel 1 ("SNT") low-resolution satellite. The dataset timeframe covered an 8-year period from October 4, 2016 to December 21, 2024 with a 12-day image capture frequency. Data from this satellite was originally processed and evaluated in May 2022. Given the availability of a multi-year data span from the SNT satellite, the objective at that time was to compare subsidence trends identified via InSAR to the historical level surveys, and to establish historical baseline trends for future InSAR surveys. That evaluation led to the following conclusions: 1) Trends were identified as matching historical level surveys in the degree of consistency of linear ground movement observed, 2) Horizontal ground displacement was evident necessitating the use of a second satellite in future surveys to triangulate the vertical and lateral components, and 3) Due to data gaps in vegetated and marshy areas, the second dataset would need to come from a high-resolution satellite to maximize the spatial density of data point capture.

For the Fall 2022 survey, the second 1-D LOS dataset was gathered via the TerraSAR-X ("TSX") high-resolution satellite from a descending orbit track with an 11-day revisit frequency. The high-resolution designation refers to the 3 x 3-foot pixel size of the TSX imagery as compared to the 65 x 16-foot pixel size in the SNT imagery. The dataset timeframe covered a 6-month period from June 16, 2022 to December 20, 2022. High-resolution commercial satellites must be tasked for data capture so historical data preceding the selection of the satellite for monitoring was not available.

In January 2023, the decision was made to transition to a new source for high-resolution descending satellite data to better serve a continuous InSAR monitoring effort that is currently active over the dome. This dataset is gathered from a pair of satellites, the TerraSAR-X satellite and the PAZ satellite, which share the same descending orbit and capture with a westward viewing direction. Both satellites orbit with an 11-day revisit frequency but their imaging periods are offset which provides the benefit of more frequent data collection. This data source is referred to as the TSX/PAZ Constellation ("TSX/PAZ"). The PAZ satellite passes over the site 4 days after the TSX satellite which results in a combined image frequency that transitions between 4- and 7-day intervals. This dataset provides the second 1-D LOS dataset for use in this evaluation and covers a 23-month period from January 24, 2023 to December 28, 2024.

In February of 2023, the TerraSAR-X satellite was additionally tasked to capture imagery from an ascending orbit track. This dataset was planned to eventually replace the SNT ascending data as the imagery source from the west of the dome. An improvement in

measurement accuracy and ground target density was anticipated but the decision was made to delay use of the ascending TSX-A data beyond the Fall 2023 report to allow development of a longer data history. The relative duration of the SNT data history was seen as the primary justification for its continued use.

The transition to the ascending TSX data ("TSX-A") was re-evaluated for the Fall 2024 report and ultimately deemed appropriate. To date, there has been no deviation from the linear deformation trends in the SNT data across any areas of the dome. Similar behavior observed in the two-year span of TSX-A data provides mutual support and substantial overlap between the datasets. As anticipated, measurement precision and spatial ground target density was improved with the incorporation of the TSX-A data, and increased co-location of measurement points between the two LOS datasets has led to a higher grid density and measurement point count in the resulting 2-D dataset.

Table 1 below provides information on the satellite image parameters for the two high-resolution datasets currently utilized in this evaluation. Figure 1 provides a diagram of the satellite orbital paths in relation to the Sulphur Mines site and Figure 2 depicts the data capture timeline. The 8-year SNT dataset was also evaluated as part of this review, and a short discussion on the continuity of the displacement trends is provided in Section 6.1.

Table 1 – Satellite Data Parameters

Analysis Characteristics	LOS Ascending (TSX-A)	LOS Descending (TSX/PAZ)
Satellite Properties		
Band (Wavelength)	X-band (1.22 in)	X-band (1.22 in)
Track	T52	T67 & T120
Pixel resolution	3 x 3 ft	3 x 3 ft
Revisit frequency	11 days	4 & 7 days
Orbit (LOS Angle, θ)	Ascending (44.00°)	Descending (37.05°)
Data Properties		
Period covered	02/04/2023 - 12/28/2024	01/24/2023 - 12/28/2024
No. of images processed	56	123
Reference Point location - *NAD 83*	Lat: 30.236147 Long: -93.392421	Lat: 30.236132 Long: -93.392306
No. of measurement points	106,384	129,421
Average point density	7,769 pts/mi^2	9,451 pts/mi^2
Average displacement rate standard deviation	< ± 0.04 in/yr	< ± 0.04 in/yr
Average displacement measurement error bar	± 0.06 in	± 0.07 in

Figure 1 – Satellite Orbit Visualization

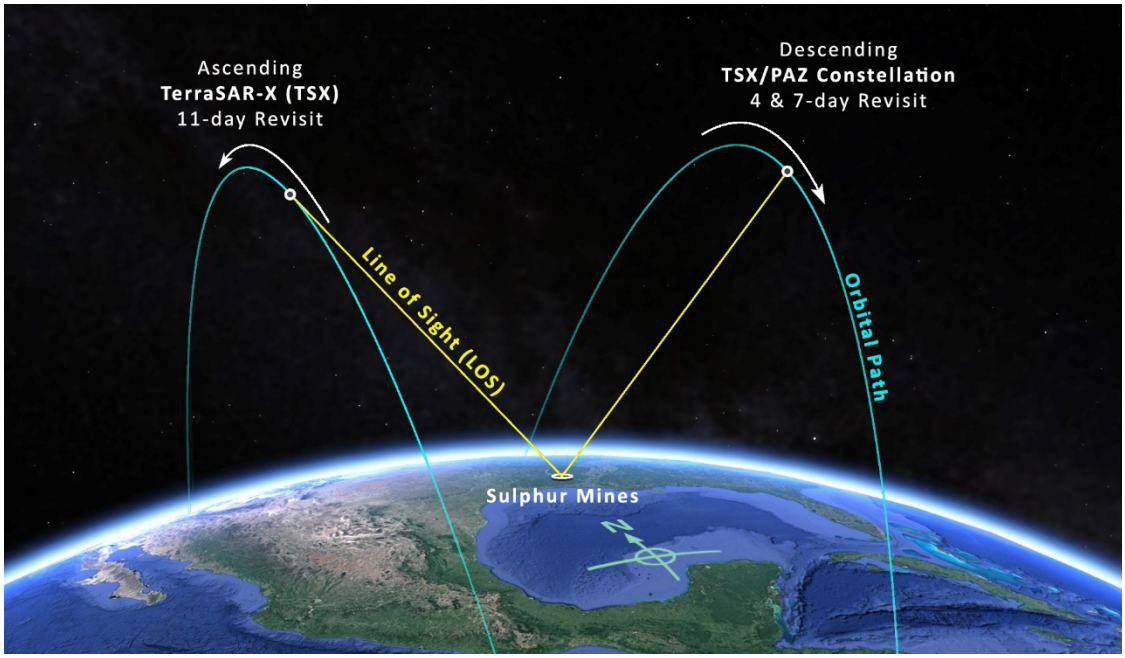

Figure 2 – Satellite Data Timeline

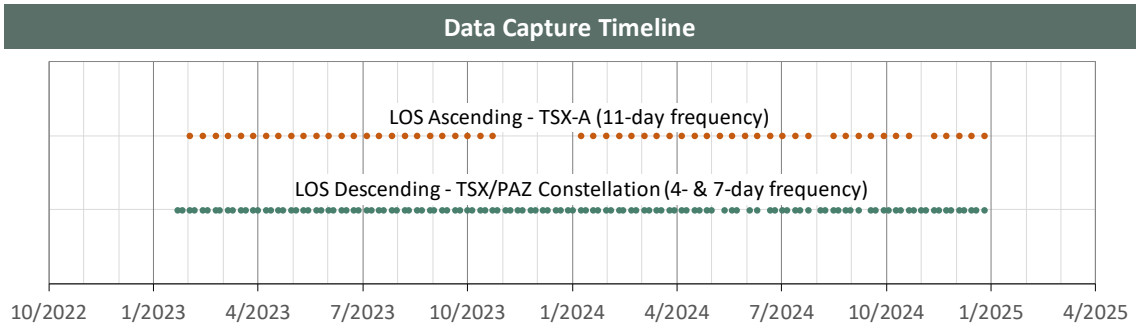

The 1-D LOS InSAR datasets generated from the two satellite orbits each cover a 13.7-square mile area that extends roughly 1.85 miles out from the center of the Sulphur Mines Salt Dome. Figure 3 below depicts the measurement point locations, reference points, and data extent for the TSX-A and TSX/PAZ datasets in relation to the dome structure contours. Areas of dense data capture are situated over roadways and infrastructure associated with dome operations and the city of Sulphur, Louisiana to the southeast. Areas showing farmland, forests, and water bodies can be seen to lack measurement data.

Figure 3 – TSX-A and TSX/PAZ 1-D LOS Measurement Points

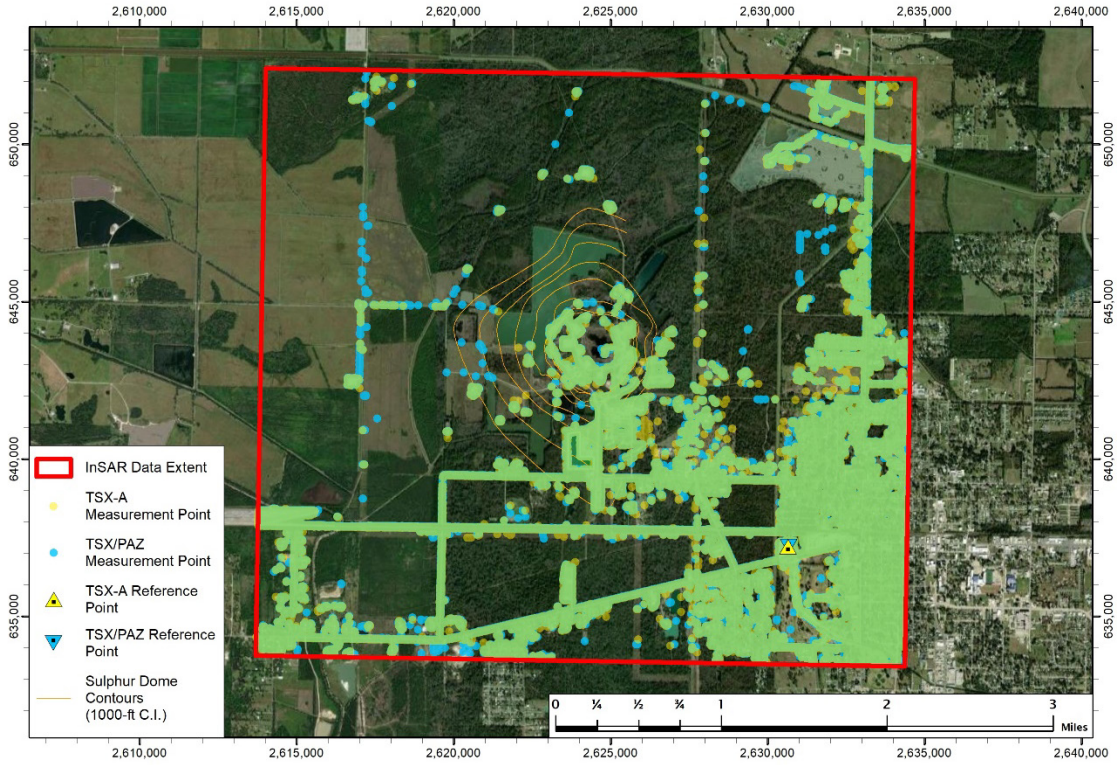

2.4 Vertical and East-West Data

In order to generate the 2-D dataset from the 1-D LOS data, a grid of cells measuring 33 x 33 feet was created across the 13.7-square mile data extent. For cells that contained at least one measurement point from each of the ascending and descending 1-D datasets, a vertical and east-west displacement value was calculated by triangulation of the 1-D displacement values. If multiple 1-D measurement points from the same dataset were present within a particular cell, those values were averaged to produce a single 1-D time series of displacement values prior to the calculation. The 2-D measurement points are located within the center of each cell for which the calculation was performed.

Two datasets were generated from this process, a vertical displacement and an east-west displacement dataset, with a time series of displacement values for each calculated measurement point. The time series for these two datasets span the 23-month overlap of the data, February 4, 2023 to December 28, 2024. Interpolation of the data in time allows for a displacement value to be calculated for each date of data capture from either

satellite orbit. As a result, the 2-D measurement schedule mirrors the more frequent TSX/PAZ 4- and 7-day acquisition intervals. Table 2 below provides additional information on the 2-D parameters. Figure 4 shows a diagram of the calculated displacement components in relation to the Sulphur Mines site and Figure 5 displays the calculated data timeline.

Table 2 – 2-D Data Parameters

Analysis Characteristics	Vertical	East-West
Period covered	02/04/2023 - 12/28/2024	
No. of images processed	117	
Reference Point location - *NAD 83*	Lat: 30.236113 Long: -93.392315	
No. of measurement cells	17,187	
Cell size	33 x 33 ft	
Average displacement rate standard deviation	± 0.02 in/yr	± 0.02 in/yr

Figure 4 – 2-D Displacement Visualization

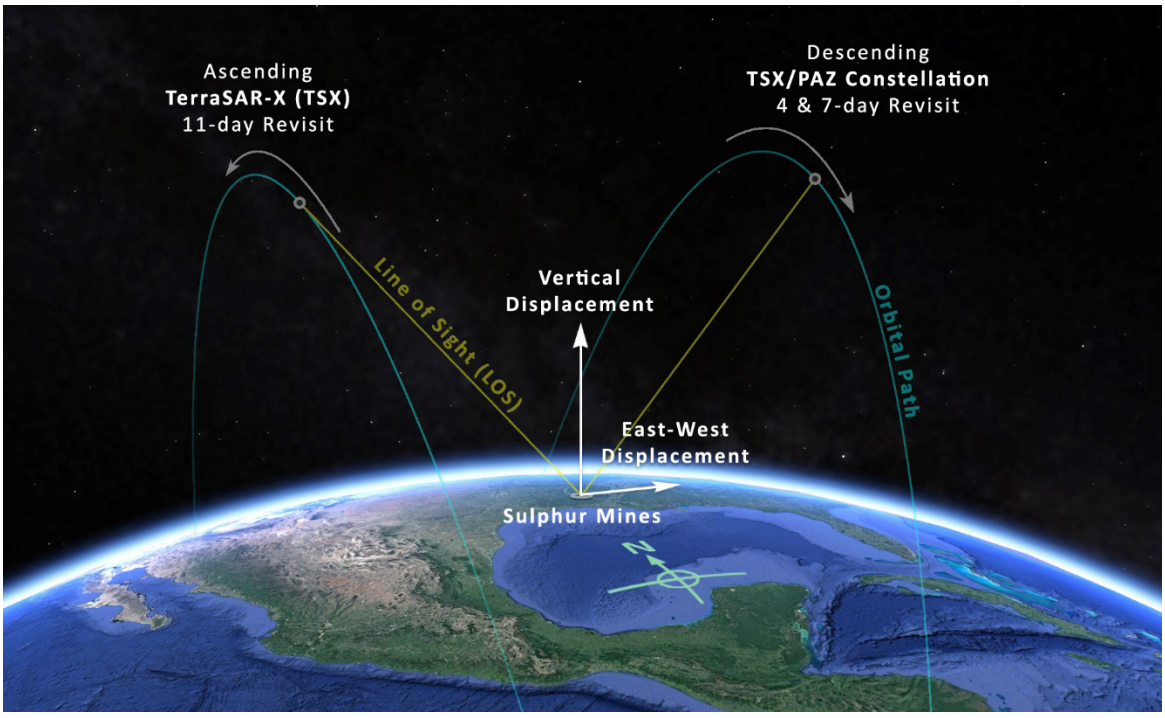

Figure 5 – 2-D Data Timeline

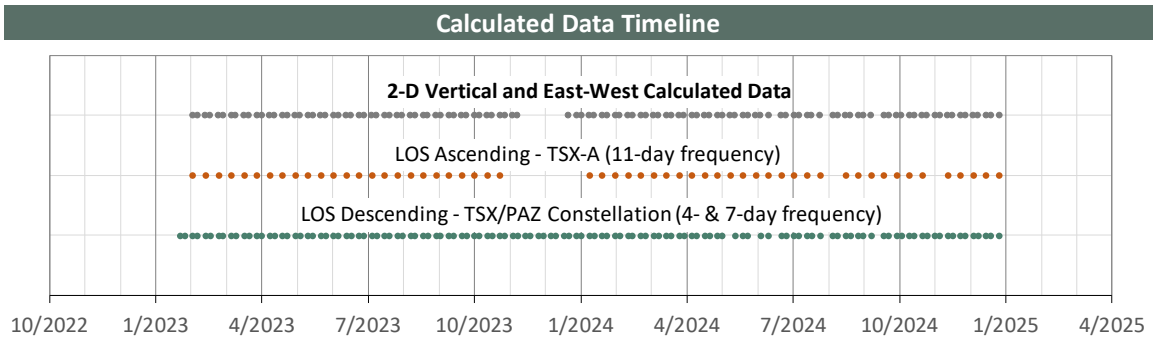

The vertical and east-west 2-D datasets generated from the 1-D LOS data cover the same 13.7-square mile area. Figure 6 below depicts the grid cell positions with calculated measurement points in relation to the dome structure contours. Data coverage indicates areas where both TSX-A and TSX/PAZ data were present within the data extent.

Figure 6 – 2-D Vertical and East-West Measurement Points

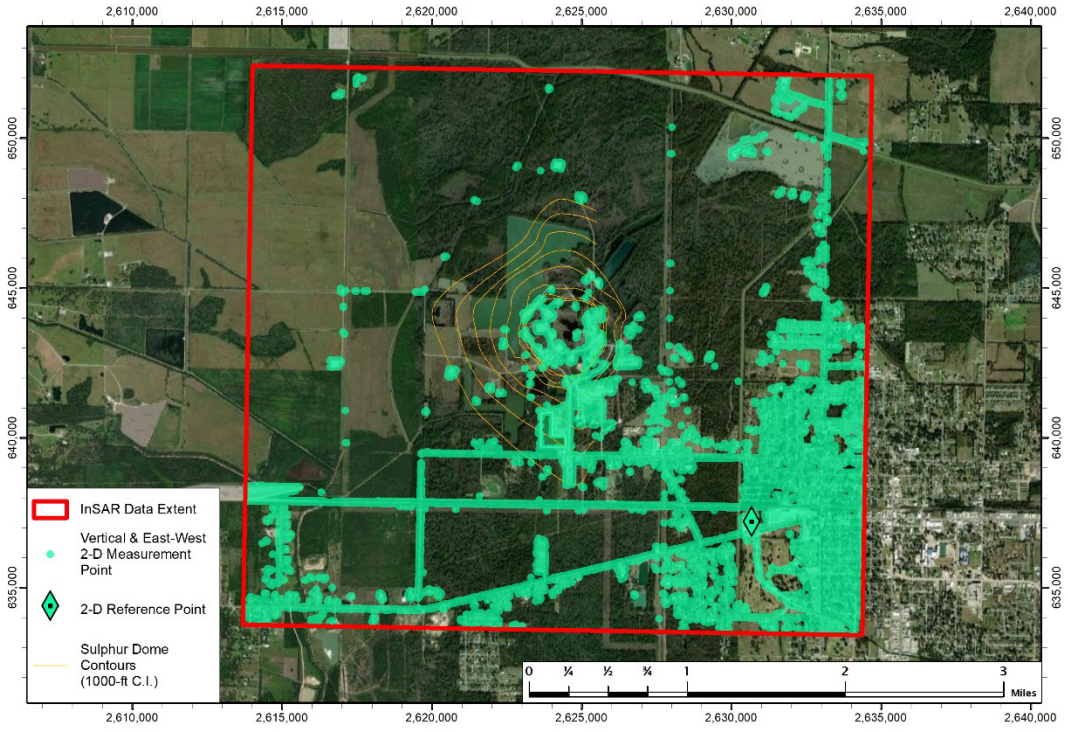

2.5 Corner Reflectors and GNSS Monitoring Stations

Conditions on the western side of the dome related to Caverns PPG 6 and PPG 7 have prompted the implementation of additional systems to detect or provide early indicators of potential surface deformation. These include microseismic sensor arrays, a network of precision tiltmeters, six (6) GNSS stations, and fifteen (15) artificial reflectors to supplement InSAR data collection.

The artificial reflectors used at the site are referred to as corner reflectors due to the orthogonal orientation of the metallic surfaces that comprise their structure. The corner reflectors are installed atop a 4-inch diameter steel pipe that has been cemented into the ground to a depth of 30 feet. InSAR measurement points are typically derived from the radar signals returned by natural reflectors, but data density and quality are strongly influenced by ground conditions. The corner reflectors were positioned to improve data availability in areas with less coverage and to maximize reliability in areas of particular interest. InSAR measurements from corner reflectors offer higher precision than those from natural reflectors, due to the stronger and more coherent returned radar signal. The deep anchoring of the corner reflectors also reduces the influence of near-surface seasonal deformation on the captured readings.

Installation of the corner reflectors was completed in July 2024. Their displacement is monitored by the same pair of TSX orbital tracks that generate the natural reflector datasets. The displacement measurements from the corner reflectors are contained within separate datasets than the natural reflectors with a shorter time span that begins after installation on July 27, 2024. As with the natural reflectors, separate datasets are maintained for the corner reflector readings, including LOS measurements from the ascending and descending satellite tracks and calculated vertical and east-west 2D displacement.

Concurrent with the corner reflector installation, an array of GNSS (Global Navigation Satellite System) stations was installed across a similar footprint on the western side of the dome. The GNSS antennas are mounted on cemented vertical steel pipes, following the same installation approach as the corner reflectors. Five of the stations are described as receiver stations and they record ground displacement at approximately 30-second intervals. A sixth station, located about one mile west-northwest of the dome center, serves as the off-dome reference station. This station provides a fixed baseline for calculating relative displacement at the receiver stations and is used to correct for common GNSS errors such as atmospheric delays and satellite clock drift. This differential positioning technique is commonly referred to as Differential GPS (DGPS).

Displacement data from the five GNSS receiver stations are reported in a global reference frame, representing their absolute positions on the Earth's surface. To evaluate local ground movement, these data can be converted to a local reference frame by removing the displacement component associated with regional tectonic plate motion near the dome.

The corner reflector InSAR datasets lack an off-dome reference point as utilized in the natural reflector datasets. For this reason, three of the GNSS stations were co-located with corner reflectors to enable integration of InSAR and GNSS data. This can enable transformation of the broader corner reflector displacement data based on measured displacement rates at the GNSS stations. To enable the calculation of InSAR displacement values, corner reflector 10 (CR10), which is co-located with the most stable DGPS trend at GNSS station REMSW, is used as the reference point for the corner reflector InSAR datasets. Displacement at all other corner reflectors is calculated in relation to CR10.

The corner reflector and GNSS data can provide valuable context and validation for the long-standing primary InSAR datasets. However, because these data span only a short period, their trends cannot yet be assessed with confidence. As such, this report focuses on preliminary observations, which are discussed in Section 6.2. Figure 7 below shows the timespan and image count used in the corner reflector InSAR datasets. Figure 8 depicts the corner reflector and GNSS station locations in relation to the dome structure contours and historical maximum cavern extents. The corner reflector and GNSS station positions are additionally included on the map in Appendix A for reference. Table 3 specifies the coordinate positions of the corner reflector and GNSS stations.

Figure 7 – Corner Reflector Data Timeline

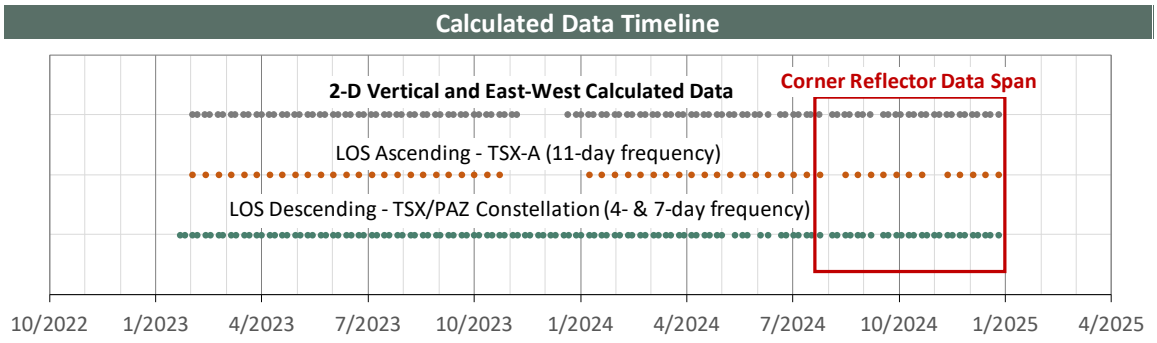

Figure 8 – InSAR Corner Reflector and Differential GNSS Station Locations

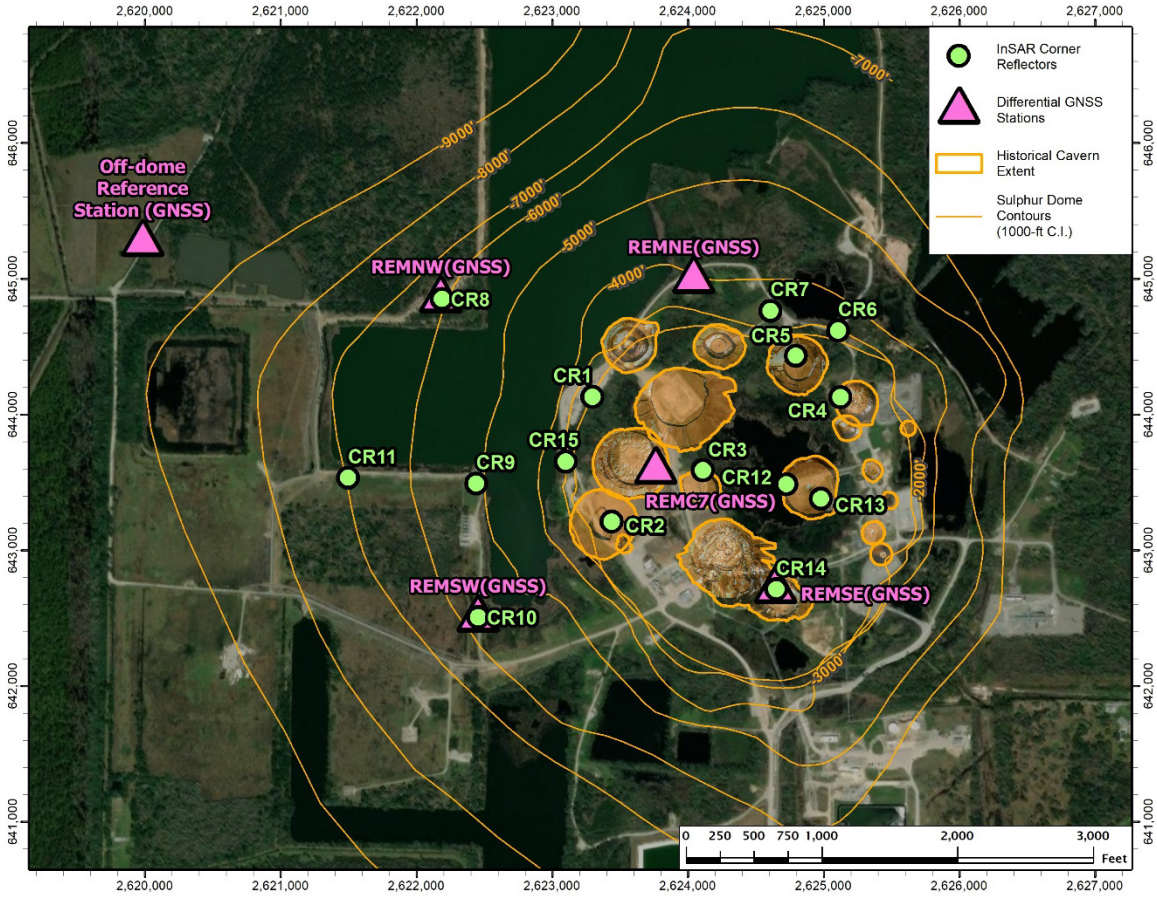

Table 3 – InSAR Corner Reflector and Differential GNSS Station Coordinates

InSAR Corner Reflectors	Latitude *(WGS 84)*	Longitude *(WGS 84)*
CR1	30.254790	-93.416096
CR2	30.252269	-93.415597
CR3	30.253343	-93.413486
CR4	30.254871	-93.410311
CR5	30.255690	-93.411364
CR6	30.256220	-93.410390
CR7	30.256594	-93.411973
CR8	30.256711	-93.419652
CR9	30.252985	-93.418770
CR10	30.250285	-93.418668
CR11	30.253054	-93.421764
CR12	30.253085	-93.411533
CR13	30.252805	-93.410720
CR14	30.250956	-93.411722
CR15	30.253470	-93.416690

Differential GNSS Stations	Latitude *(WGS 84)*	Longitude *(WGS 84)*
GPS NE	30.257206	-93.413782
GPS NW	30.256713	-93.419670
GPS Cavern 7 Pad	30.253327	-93.414588
GPS SE	30.250953	-93.411739
GPS SW	30.250263	-93.418668
GPS Off-dome Reference Station	30.257750	-93.426649

3.0 Areas of Interest

Past level surveys were performed on a set of thirty-six (36) physical monuments located on cavern wellheads, abandoned cavern well caps, and additional monuments positioned over and around the dome. Of this total, there were two (2) off-dome benchmark deep-rod monuments, twelve (12) additional rod monuments, and twenty-two (22) wells. Fifteen (15) of the wells are owned by Westlake, five (5) wells by Boardwalk, and two (2) by Liberty.

This system was designed to provide comprehensive monitoring for any areas that may be subject to subsidence as a result of current or past cavern operations. Survey measurements of these monument elevations were used to develop time series charts of the elevation changes and movement trends as well as contour maps of the interpolated subsidence velocity and acceleration across the dome.

With InSAR data, the displacement values for each measurement point can similarly be used to generate contour maps of displacement velocity and acceleration, indicating the spatial distribution of subsidence magnitudes. Velocity and acceleration rates are determined via trend analysis of the displacement time series for each individual measurement point. In total, 17,187 calculated measurement points are available in the 2-D dataset for generation of contour maps. Roughly 900 of the points are located in close proximity to the dome top and cavern locations.

Given this number of measurement locations, a data reduction method must be considered to visually convey and evaluate trend consistency in displacement time series charts. This can be achieved by the grouping of measurement points to generate time series of the averaged displacement values for each group. Averaging of the displacement data within point groups also allows for the reduction of scatter (noise) in the plotted displacement values associated with individual measurement accuracy.

3.1 AOI Boundary Definition

Past level surveys measured elevations at cavern wellheads and at supplemental monuments over the dome. In an effort to maintain a similar mode of reporting and analysis, Areas of Interest (AOIs) were drawn to group measurement points over individual cavern extents and to encompass the dome-wide coverage achieved in prior monitoring.

In total, twenty-one (21) AOIs were created to evaluate displacement trend consistency across the dome. The AOIs were numbered and eighteen (18) of the twenty-one (21) AOIs encompass cavern extents and were additionally labeled with acronyms denoting the associated cavern. Table 4 below provides a list of the AOIs and 2-D measurement point counts within each AOI. Figure 9 depicts the AOI boundaries in relation to the historical maximum cavern extents and past level survey monuments.

Table 4 – InSAR Point Group Parameters

AOI Name	Area (Acres)	2-D Point Count
AOI 1 (LGS 1)	3.75	10
AOI 2	2.71	9
AOI 3	3.01	6
AOI 4	4.71	32
AOI 5 (PPG 21)	5.92	19
AOI 6 (PPG 6)	9.49	66
AOI 7 (PPG 7)	6.35	61
AOI 8 (PPG 22)	5.46	25
AOI 9 (SMS A1)	5.92	15
AOI 10 (PPG 2)	8.18	129
AOI 11 (PPG 5)	4.43	23
AOI 12 (PPG 4)	9.74	60
AOI 13 (PPG 18)	8.24	15
AOI 14 (PPG 16)	8.83	4
AOI 15 (PPG 20)	7.51	59
AOI 16 (LGS 2)	8.71	6
AOI 17 (SS 4)	5.40	75
AOI 18 (SS 2)	3.23	56
AOI 19 (SS 5)	2.86	61
AOI 20 (SS 1)	4.20	37
AOI 21 (SS 3)	3.10	56

Figure 9 – InSAR Point Group AOI Boundaries

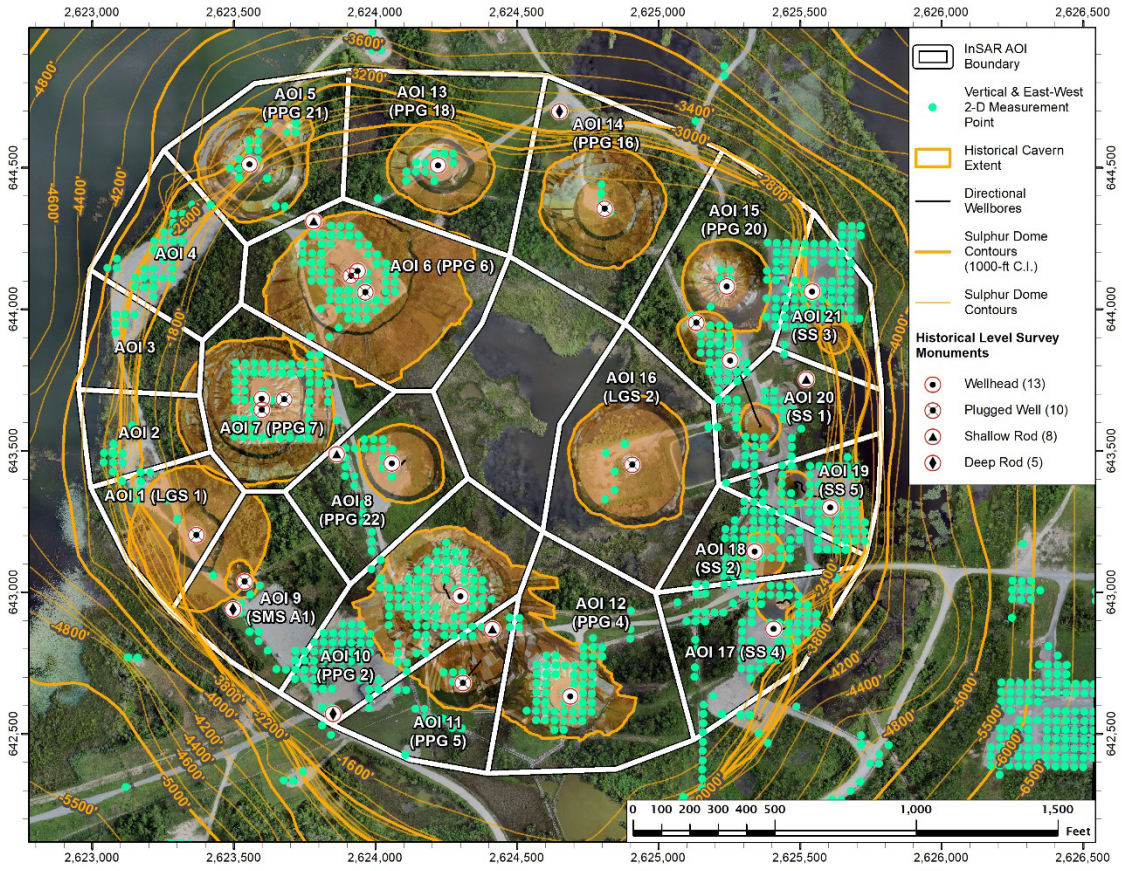

A larger format map has been included as Appendix A that depicts the AOI regions in relation to the 2-D measurement point locations. The map also depicts the surface locations of cavern wells along with well names, serial numbers, and statuses.

4.0 Subsidence Rate Determination

Per guidance issued by the Injection and Mining Division of the LA DNR in 2019, a determination of the current rate of subsidence over each survey point is to be evaluated. This is considered the "velocity" of ground displacement at each monument. Additionally, the guidance requests that the rate at which this "velocity" is changing be determined if non-linear movement trends are identified. This rate of change is considered the "acceleration" of ground displacement at each monument. In place of monument elevations, the displacement values associated with each measurement point in the InSAR

survey are used. The historical displacement data provides the basis for determining these ground movement rates through analysis of the long-term trends.

4.1 Selection of Trend Equation

Trend analysis data was generated by plotting average displacement values over time for the measurement point groups within the AOI regions. The use of non-linear trend equations was evaluated which could yield acceleration estimates in addition to velocity. This was avoided in the 2023 evaluation due to the relatively short 11-month timeframe of the data in combination with the accuracy range of the measurements. Calculated accelerations varied dramatically at the time and were found to lack statistical significance.

A review of the 2024 dataset of 2-D data showed the emergence of predominantly linear trends, which are characteristic of the site's historical subsidence behavior. With the longer 23-month dataset, the reliability of a non-linear trend analysis has increased and was considered appropriate for this review. This change will allow for assessment of any observed accelerations in ground displacement going forward.

4.2 Quadratic Regression Analysis

To evaluate subsidence trends in the 2-D displacement data, a quadratic least squares regression model was computed to define a time-dependent representation for each AOI dataset. In least squares regression analysis, the sum of the squared difference between model-predicted and actual data is minimized by a computationally derived set of model variables. The model formula is shown below in Equation 1.

$$D(t) = \beta_0 + \beta_1 t + \beta_2 t^2 \qquad \text{Equation 1}$$

where $D(t)$ is the predicted displacement at time (t), and β_0, β_1, and β_2 are fit parameters determined by the regression model computed on the historical dataset for each AOI.

Once this model has been defined, the predicted rate of displacement can be calculated by taking the derivative of the model equation with respect to time. The formula used to approximate the instantaneous rate of displacement at a particular moment in time is provided below in Equation 2.

$$d/dt\,[D(t)] = \beta_1 + 2\beta_2 t \qquad \text{Equation 2}$$

where $d/dt\ [D(t)]$ is the predicted rate of displacement at time (t). This value represents the velocity of ground displacement estimated by the model for each AOI. In the vertical data, negative velocity values represent downward rates of ground displacement and positive values represent upward displacement. In the east-west data, negative values are associated with westward displacement rates, and positive values are eastward.

The time-dependent component of the velocity equation represents the modeled acceleration of ground displacement with time. This can be calculated by taking the second derivative of the model equation with respect to time as shown in Equation 3.

$$d^2/dt\ [D(t)] = 2\beta_2 \qquad \text{Equation 3}$$

where $d^2/dt\ [D(t)]$ is the estimated acceleration in ground displacement observed throughout the historical dataset for each AOI. A positive vertical acceleration value derived from this equation represents a slowing in the rate of subsidence with time, whereas a negative value represents and increasing rate of subsidence. A positive east-west acceleration represents a slowing westward displacement or increasing eastward displacement, and a negative acceleration represents a slowing eastward displacement or an increasing westward displacement.

5.0 Data Analysis

5.1 Time Series Plots

Averaged displacement values for vertical and east-west movement were plotted for each AOI with respect to time. The resulting time series charts provide a visual depiction of the calculated trends and associated data. These plots are shown for reference in Appendix B. The modeled trends for each AOI are shown by the dashed lines that overlay the displacement measurements on each plot. No divergence was seen between the data and the quadratic trend lines that would imply more complex or higher-order trends in ground displacement. Overall, the data exhibited relatively low scatter and consistent near-linear trends in all AOIs evaluated.

AOIs with higher point counts were generally found to exhibit less fluctuation and scatter in the plotted data, indicating that the accuracy limitations in individual measurement point values were mitigated through data averaging. The properties of the 1-D TSX/PAZ and TSX-A source data likely also play a role in the relative measurement precision depicted in the charts. The specific number and distribution of the 1-D measurement

points and the quality of the radar targets within each AOI region will lead to variation in measurement quality for the averaged 2-D displacement data.

The trend models generated for each AOI were used to identify the vertical and east-west displacement velocity in units of inches/year. In non-linear trends, velocity is time dependent, and is calculated for a specific date. In past years, when precision level surveys were performed in the fall, quadratic trend fits were used to estimate monument velocities on November 1st of that year. For consistency all velocities noted in this report are calculated for the date of November 1, 2024.

The trend models for each AOI were additionally used to identify vertical and east-west acceleration in units of inches/year^2. The acceleration component in a quadratic trend is irrespective of time and represents the average rate of change in velocity over the full dataset history. The calculated values of vertical velocity and acceleration are provided in Table 5 below for each AOI. Velocity and acceleration values in the east-west direction are provided in Table 6.

5.2 Displacement Velocity and Acceleration Maps

The same process that was followed to generate trend equations for the AOI point groups was also performed on each individual measurement point in the 2-D dataset. The velocity values calculated for each point were used to generate contours to illustrate the spatial distribution of displacement velocities across the surveyed region. Contouring was additionally performed on the displacement acceleration values for each measurement point. Vertical velocity and acceleration contours are provided on a pair of maps in Appendix C for reference. East-west velocity and acceleration contours are similarly provided on a pair of maps in Appendix D.

Table 5 – InSAR Point Group Vertical Displacement Velocity and Acceleration Values

AOI Name	Vertical Displacement			
	Velocity *(Inches/Year)*	Velocity Direction	Acceleration *(Inches/Year^2)*	Acceleration Direction
AOI 1 (LGS 1)	-0.51	Downward	+0.10	Upward
AOI 2	-0.55	Downward	+0.06	Upward
AOI 3	-0.58	Downward	-0.05	Downward
AOI 4	-0.53	Downward	-0.01	Downward
AOI 5 (PPG 21)	-0.51	Downward	+0.06	Upward
AOI 6 (PPG 6)	-0.96	Downward	-0.11	Downward
AOI 7 (PPG 7)	-0.90	Downward	-0.05	Downward
AOI 8 (PPG 22)	-1.15	Downward	+0.03	Upward
AOI 9 (SMS A1)	-0.62	Downward	+0.15	Upward
AOI 10 (PPG 2)	-1.06	Downward	-0.08	Downward
AOI 11 (PPG 5)	-0.93	Downward	-0.04	Downward
AOI 12 (PPG 4)	-1.07	Downward	-0.06	Downward
AOI 13 (PPG 18)	-0.69	Downward	+0.03	Upward
AOI 14 (PPG 16)	-0.68	Downward	+0.18	Upward
AOI 15 (PPG 20)	-0.91	Downward	-0.09	Downward
AOI 16 (LGS 2)	-1.61	Downward	-0.11	Downward
AOI 17 (SS 4)	-0.80	Downward	+0.08	Upward
AOI 18 (SS 2)	-1.07	Downward	-0.07	Downward
AOI 19 (SS 5)	-0.90	Downward	-0.06	Downward
AOI 20 (SS 1)	-1.02	Downward	-0.10	Downward
AOI 21 (SS 3)	-0.64	Downward	-0.07	Downward

Table 6 – InSAR Point Group East-West Displacement Velocity and Acceleration Values

AOI Name	East-West Displacement			
	Velocity *(Inches/Year)*	Velocity Direction	Acceleration *(Inches/Year^2)*	Acceleration Direction
AOI 1 (LGS 1)	+0.39	Eastward	+0.02	Eastward
AOI 2	+0.40	Eastward	+0.02	Eastward
AOI 3	+0.30	Eastward	-0.04	Westward
AOI 4	+0.32	Eastward	-0.01	Westward
AOI 5 (PPG 21)	+0.24	Eastward	+0.02	Eastward
AOI 6 (PPG 6)	+0.32	Eastward	+0.06	Eastward
AOI 7 (PPG 7)	+0.48	Eastward	+0.04	Eastward
AOI 8 (PPG 22)	+0.45	Eastward	+0.09	Eastward
AOI 9 (SMS A1)	+0.44	Eastward	+0.14	Eastward
AOI 10 (PPG 2)	+0.28	Eastward	+0.05	Eastward
AOI 11 (PPG 5)	+0.15	Eastward	+0.03	Eastward
AOI 12 (PPG 4)	-0.20	Westward	-0.04	Westward
AOI 13 (PPG 18)	+0.10	Eastward	+0.03	Eastward
AOI 14 (PPG 16)	-0.44	Westward	-0.06	Westward
AOI 15 (PPG 20)	-0.60	Westward	-0.01	Westward
AOI 16 (LGS 2)	-0.53	Westward	-0.07	Westward
AOI 17 (SS 4)	-0.53	Westward	-0.05	Westward
AOI 18 (SS 2)	-0.69	Westward	-0.08	Westward
AOI 19 (SS 5)	-0.67	Westward	-0.05	Westward
AOI 20 (SS 1)	-0.72	Westward	-0.04	Westward
AOI 21 (SS 3)	-0.48	Westward	+0.02	Eastward

5.3 Comparison to Fall 2023 Survey

This review will summarize a few notable observations in relation to the prior Fall 2023 InSAR survey. For the sake of clarification and to qualify these comparisons a few variables are noted below that differ between the current and prior 2023 analysis:

1) The transition from the lower-resolution SNT dataset to higher-resolution TSX-A data has improved the quality and coverage of the 2-D dataset. Increased data density and accuracy, along with changes in the overlap of LOS measurements, are expected to influence displacement trends by shifting the locations and types of ground features being sampled.

2) The Fall 2023 survey relied on an 11-month 2D InSAR dataset, constrained by limited overlap in the available 1-D LOS inputs. This shorter record increased the potential for seasonal ground movement to bias velocity trends, whereas the current 23-month dataset may influence trend behavior with an anticipated improvement in long-term accuracy.

3) The higher spatial density of 2-D data in the current dataset has led to higher point counts in the AOIs by a factor of about 3.5x. This should improve reliability in the AOI trend variables compared to prior analyses. Most notably, AOI 14 (PPG 16) previously contained no 2-D measurement points, and its analysis relied on evaluation of 1-D LOS data. The current dataset provides four 2-D measurement points in that AOI allowing for vertical and east-west trend calculation over that area of the dome.

4) The transition from linear to non-linear trend computation is expected to influence the calculated velocity values. While historical observations indicate predominantly linear ground displacement over the dome, limitations in measurement accuracy may introduce artificial curvature in the trends, affecting velocity estimates. These effects are considered secondary, however, to the improved ability of non-linear analysis to reveal genuine deviations from linear behavior.

5.4 Observations

In general, the subsidence rate is greatest over the eastern-central portion of the dome with a gradual tapering toward the dome edges. Subsidence rates continue to slow at further distances from the dome, but the slowing trend is less uniform as evidenced to the southeast of the dome where data coverage is more densely present. Regions of near-zero subsidence were noted near the perimeter of the data extent at distances of roughly 1.5 to 2 miles from the dome center.

The AOI point groups with the highest rates of calculated subsidence were AOI 8 (PPG 22), AOI 10 (PPG 2), AOI 12 (PPG 4), AOI 16 (LGS 2), AOI 18 (SS 2), and AOI 20 (SS 1). The maximum rate of subsidence was -1.61 inches/year at AOI 16 which overlies the plugged and abandoned Liberty Gas Storage No. 002 cavern. The other point groups listed above surround AOI 16 in the south-central portion of the dome with similar subsidence values

averaging around -1.07 inches/year. The position of maximum subsidence in AOI 16 is consistent with past reviews, with an indicated subsidence rate of -1.90 and -1.91 inches/year in the prior 2023 and 2022 reports, respectively. The reduced subsidence rate in the current review may be attributable to the factors outlined in Section 5.3 relating to changes in data properties and calculation methods.

The mapped geometry of the vertical velocity contours shows general agreement with prior annual monitoring maps generated from analysis of ground survey data. Additionally, the mapped geometry of the subsidence velocity contours and the calculated velocities of the AOI point groups in the present evaluation were found to agree broadly with the results of the Fall 2023 InSAR analysis.

AOI subsidence velocities were compared between the present and prior survey. On average subsidence rates were seen to have decreased roughly 26% compared to the 2023 review. Two of the most substantial decreases were observed at AOI 9 (SMS A1) and AOI 17 (SS 4) with decreases of 54% and 44%, respectively. Notably these were the two areas where a marked increase in subsidence rate was reported in the 2023 review in comparison to the 2022 data. No AOI was shown to have an increased subsidence rate relative to the 2023 review. The consistent linear nature of the AOI trends in the time series plots suggests that these subsidence rate revisions are likely due to the factors covered in Section 5.3 and not related to actual changes in ground displacement trends.

East-west displacement velocities in the present analysis generally indicate inward lateral movement toward the center of the dome. Such lateral displacement is commonly associated with vertical subsidence, as compaction or volume loss at depth induces both downward settlement and horizontal convergence toward the subsidence basin center. Although the current dataset is limited to east-west motion, it is reasonable to expect similar north-south displacement is occurring radially inward toward the center of an approximately symmetric subsidence basin.

The region of zero horizontal movement in the east-west velocity contours divides the dome from north to south and passes about 500 feet to the west of the area of greatest vertical subsidence. It is possible that the greatest subsidence rates are coincident with this contour; however, no measurement points exist in this region over the center of the dome where a small lake is present. On the eastern side of the dome, horizontal east-west velocities are seen to be generally greater than velocities on the western side of the dome.

Additionally, it appears that horizontal displacement exhibits more spatial irregularity than vertical displacement across the AOI regions. Similar magnitudes of east-west

displacement observed within the dome footprint are also observed sporadically across the full analysis area.

The AOI point groups with the highest rates of westward movement were AOI 18 (SS 2), AOI 19 (SS 5), and AOI 20 (SS 1). The highest east-west displacement rate was calculated as -0.724 inches/year at AOI 20 which overlies the active Sulphur Storage No. 001 cavern. All three of these AOIs are centrally located on the eastern edge of the dome and encompass the region with the greatest calculated rates of westward displacement over the dome. The AOI point groups with the highest rates of eastward movement were AOI 7 (PPG 7), AOI 8 (PPG 22), and AOI 9 (SMS A1). The highest eastward displacement rate was calculated as +0.479 inches/year at AOI 7 which overlies the active PPG No. 007 cavern. These three AOIs are centrally located near the western side of the dome and contain the area with the greatest rates of calculated eastward displacement over the dome.

The general division of eastward and westward movement remained consistent over the dome relative to the Fall 2023 analysis. However, a general westward shift was broadly noted among the AOI velocities. On average, east-west velocities moved about -0.23 inches/year in the west direction which contributed to about 50% higher rates of east-west displacement on the eastern side of the dome relative to the west. This is the opposite of a change that was noted in the 2023 InSAR review in comparison to the prior 2022 data. This supports an observed tendency for the east-west InSAR data to fluctuate from year to year, and generally exhibit less uniformity and linearity than the vertical data in the time series plots. It is assumed that future surveys will exhibit less change in the east-west interpretation once a longer-term dataset is compiled.

After reviewing the vertical and east-west velocity trends against the 2023 results, and considering the potential influences discussed in Section 5.3, the observed differences in the calculated annual rates are not interpreted as evidence of changing ground displacement. For the current reporting period, conditions across the dome are assumed to remain consistent with prior behavior.

The acceleration components of the vertical and east-west AOI trends were reviewed and found to generally support the linearity of the datasets. Vertical acceleration values averaged -0.01 inches/year^2 among the AOIs. The greatest negative or downward acceleration was calculated as -0.11 inches/year^2 at AOI 6 which overlies the active PPG No. 006 cavern, and the greatest positive or upward acceleration was +0.18 inches/year^2 at AOI 14 which overlies the plugged and abandoned PPG No. 016 cavern. The greatest eastward acceleration was observed as +0.14 inches/year^2 in AOI 9 which overlies the plugged and abandoned Sulphur Mines Storage A-1 cavern and the greatest westward

acceleration was calculated as -0.08 inches/year^2 at AOI 18 which overlies the active Sulphur Storage No. 002 cavern.

These acceleration values are relatively minor and may reflect the limited duration of the dataset. If linear behavior persists, acceleration values should decline as additional data are incorporated in future analyses. Review of the vertical and east-west acceleration contour maps likewise revealed minor values, with evenly distributed fluctuations that are more likely indicative of limitations in data accuracy than actual changes in displacement trends. Direct comparison with the prior 2023 survey is not possible regarding displacement acceleration due to the use of linear trends in the prior review.

6.0 Supplementary Discussion

A few additional reviews were performed using the 1-D SNT LOS data and InSAR corner reflector data to supplement the observations made in the 2-D data evaluation. The results of these reviews are described in this section.

6.1 Sentinel 1 (SNT) 8-Year InSAR Dataset

A 5.5-year dataset from the Sentinel 1 (SNT) low-resolution satellite was originally processed and evaluated in May 2022. A supplementary evaluation of the updated 6-year dataset was then presented in the Fall 2022 annual report. Both reviews revealed consistent near-linear subsidence in all areas of the dome and provided a link to past level survey monitoring results.

The updated 8-year SNT dataset was evaluated for a final time as part of this review. The primary objective was to confirm general continuation of ground displacement trends from 2016 to present. Time series charts were generated for each of the current AOI regions and reviewed for recent trend consistency. This was done to confirm that the subsidence trends identified using the 23-month 2-D data could be considered continuations of the historical trends within each AOI. Figure 10 below provides two examples of the AOI time series that were reviewed as part of the historical evaluation of the SNT 1-D LOS data.

No acute deviations from the historical trends were observed during the 2024 timeframe that warranted further investigation. Overall, the subsidence rates identified through quadratic regression of the 23-month 2-D dataset are believed to generally agree with historical trends and to provide a reliable representation of ground displacement rates within the AOI regions.

Figure 10 – Sample SNT 1-D Displacement Time Series of AOI Regions

SNT 1-D LOS Point Group – AOI 6 (PPG 6) – Point Count: 134

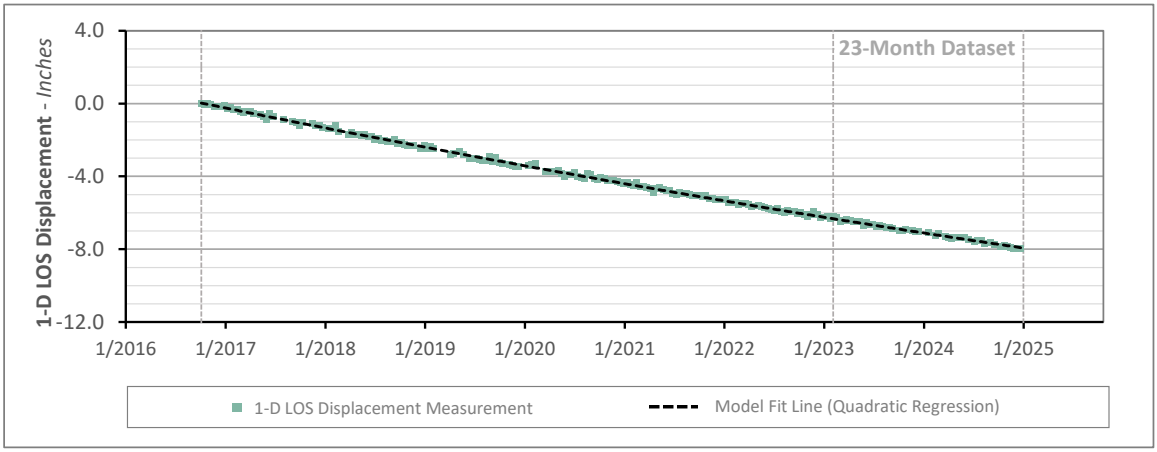

SNT 1-D LOS Point Group – AOI 9 (SMS A1) – Point Count: 58

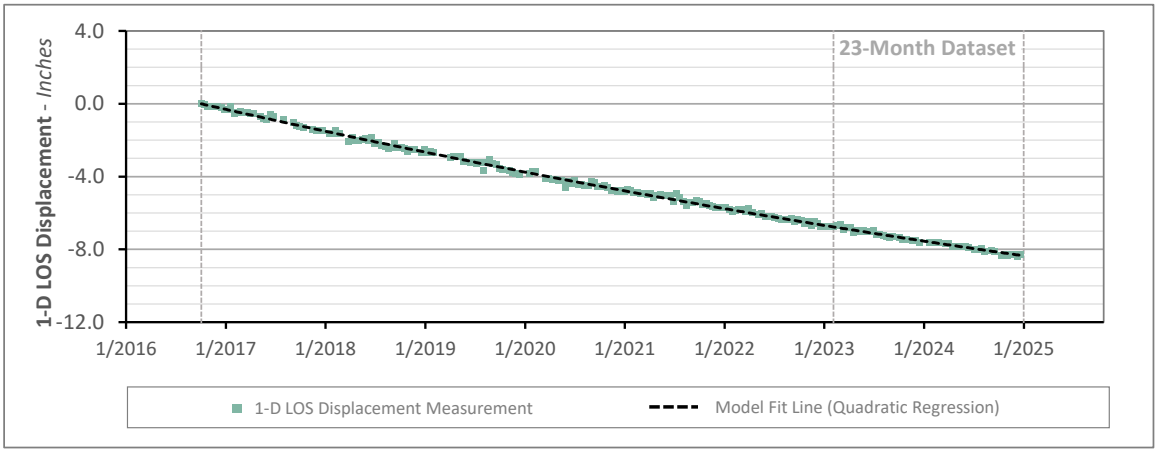

6.2 InSAR Corner Reflectors and Differential GNSS Stations

As discussed in Section 2.5, a 5-month dataset of InSAR measurements was available for review for the recently installed network of fifteen (15) corner reflectors from July 27, 2024 to December 28, 2024. The vertical and east-west data was modeled and linear trends were applied to generate velocity estimates. Time series plots of these datasets, with equivalent scaling to the AOI time series for comparison, are available for reference in Appendix E.

The displacement trends were observed to exhibit higher degrees of scatter in comparison to the AOI trends. This is due to the input data coming from a single point for each rather than the data averaging that is utilized in the AOI point groups. However, on

an individual point basis the corner reflector measurements provide a higher degree of accuracy than an individual natural reflector due to their highly reflective surface and physical stability.

The scatter in the radar data and the short time frame lessen the utility of the corner reflectors for trend analysis in the current review. It is anticipated that future analyses will incorporate local displacement rates identified at the reference point (CR 10) from the co-located GNSS station REMSW to transform the dataset values.

In the current review, the velocities estimated from the linear trends were seen to roughly approximate the values observed in the AOI trends. Vertical velocities ranged from +0.06 to -1.43 inches/year with the lowest value being observed at CR12. This reflector is located in AOI 16 on the Liberty Gas Storage No. 002 well pad where the greatest rate of subsidence was identified in the vertical dataset of natural reflectors. An overlay of the two datasets is provided for reference in Figure 11 below. The east-west velocity trends ranged from -0.45 to +0.33 inches/year with lateral velocities generally indicating inward movement toward the dome center.

Figure 11 – Sample Corner Reflector Dataset vs. AOI Point Group

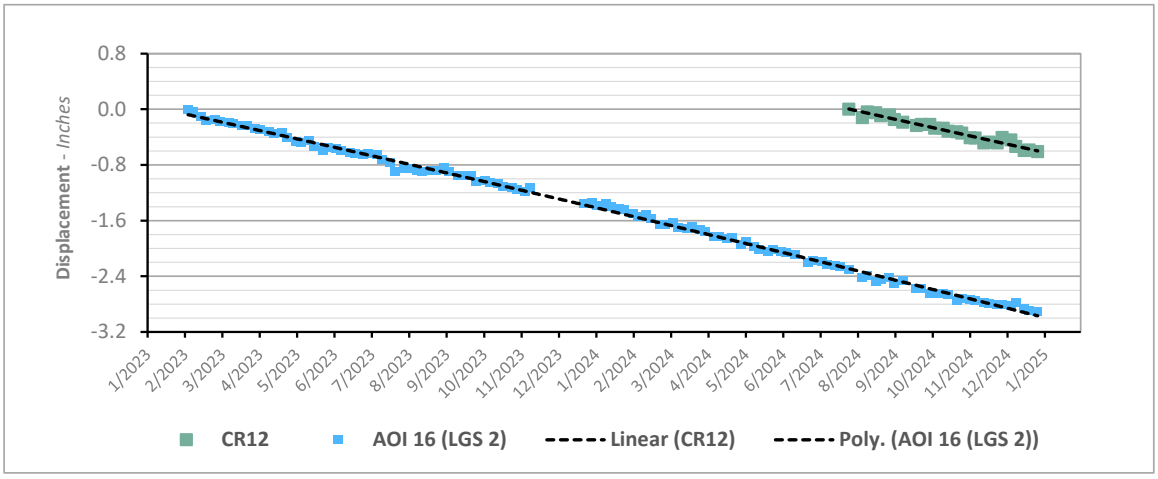

6.3 Fall 2024 Trend Consistency

Based on the evaluation of the calculated 2-D data and supplementary review of the SNT and corner reflector datasets, subsidence trends appear to be continuing as historically defined in past InSAR and precision level surveys. This indicates that rates of cavern closure and other local factors of influence are continuing to act in a consistent manner at this time.

7.0 Conclusions

1. The third annual InSAR survey of the Sulphur Mines Salt Dome showed sustained trend continuity and geometry of the subsidence basin, in terms of both vertical and lateral displacement.

2. In general, the subsidence rate is greatest over the eastern-central portion of the dome with a gradual tapering toward the dome edges. At further distances from the dome, subsidence rates continue to slow but exhibit more variability in the mapped contours. The greatest subsidence rates were identified at AOI 8 (PPG 22), AOI 10 (PPG 2), AOI 12 (PPG 4), AOI 16 (LGS 2), AOI 18 (SS 2), and AOI 20 (SS 1), with the maximum rate being -1.61 inches/year at AOI 16 which overlies the plugged and abandoned Liberty Gas Storage No. 002 cavern.

3. East-west displacement velocities were seen to generally indicate that lateral ground displacement is occurring toward the center of the dome. The highest westward displacement rate was calculated as -0.724 inches/year at AOI 20 (SS1) and the highest eastward displacement rate was calculated as +0.479 inches/year at AOI 7 (PPG 7). Both AOIs were located respectively near the western and eastern sides of the dome where the highest rates of lateral displacement were observed.

4. Subsidence rates identified in the InSAR analysis agree well with the trends established through past monitoring surveys of the site. Based on the evaluation of the calculated 2-D data and the supplementary review of the 8-year SNT dataset and corner reflector data, subsidence trends appear to be progressing as historically defined. This indicates that rates of cavern closure and other local factors of influence are continuing to act in a consistent manner at this time.

Appendix A – Map of 2-D InSAR Measurement Points and AOI Boundaries

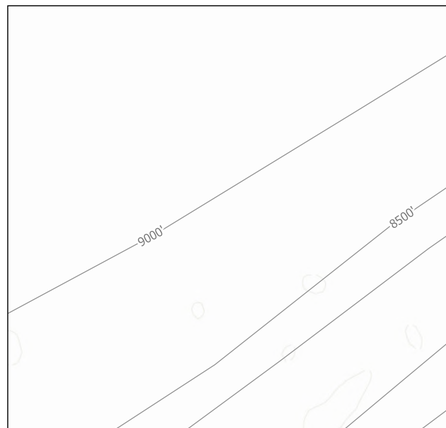

Fall 2024 Subsidence Monitoring InSAR Survey

2-D InSAR Measurement Points and AOI Boundaries

with Historical Cavern Extents and Top of Salt Contours

Sulphur Mines Salt Dome

Calcasieu Parish, LA

Appendix A

Drawn by: Steven Larcom	Date: 9/19/2025	Approved by: Nathaniel Byars

PCS: NAD 1983 State Plane LA-S FIPS 1702 (US Ft.)

LONQUIST

Louisiana Registration No. EF5937

Sulphur Cavern Well Surface Hole Locations

- 09 - ACTIVE INJECTION (14)
- 29 - DRY AND PLUGGED (10)
- 30 - PLUGGED AND ABANDONED (1)
- Directional Wellbores
- InSAR Point Group AOI Boundaries
- Historical Cavern Extent
- InSAR Data Extent
- Vertical & East-West 2D Measurement Point
- 2D InSAR Reference Points
- InSAR Corner Reflectors
- Differential GNSS Stations
- 2,000' Salt Contour (subsea depth)
- Top of Salt Contours (CI = 500', subsea depth)

1:1,900

0 500 1,000 2,000 Feet

Appendix B – Vertical & East-West Displacement Time Series – AOI Point Groups

Averaged Vertical Displacement Time Series - AOI Point Groups

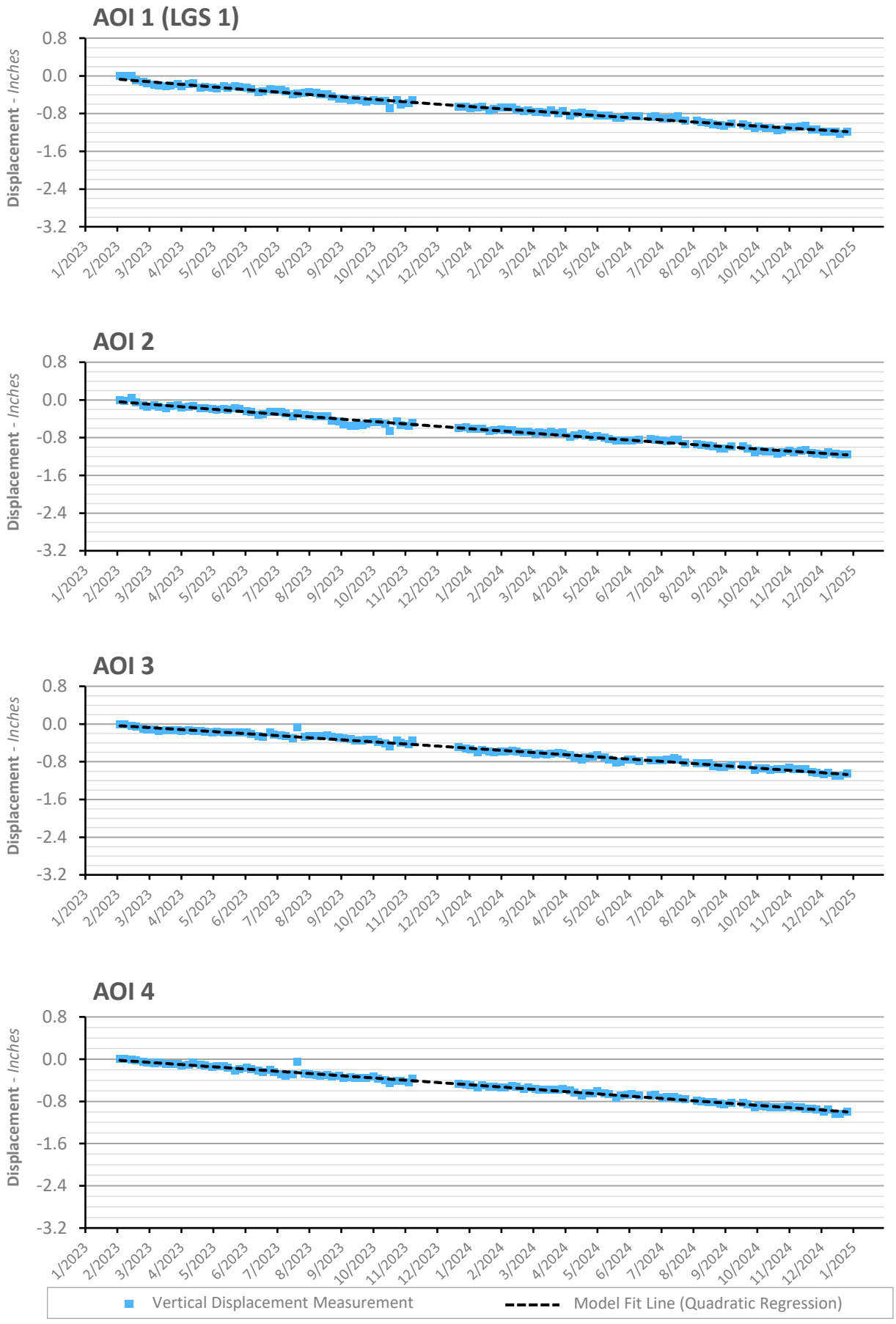

Averaged Vertical Displacement Time Series - AOI Point Groups

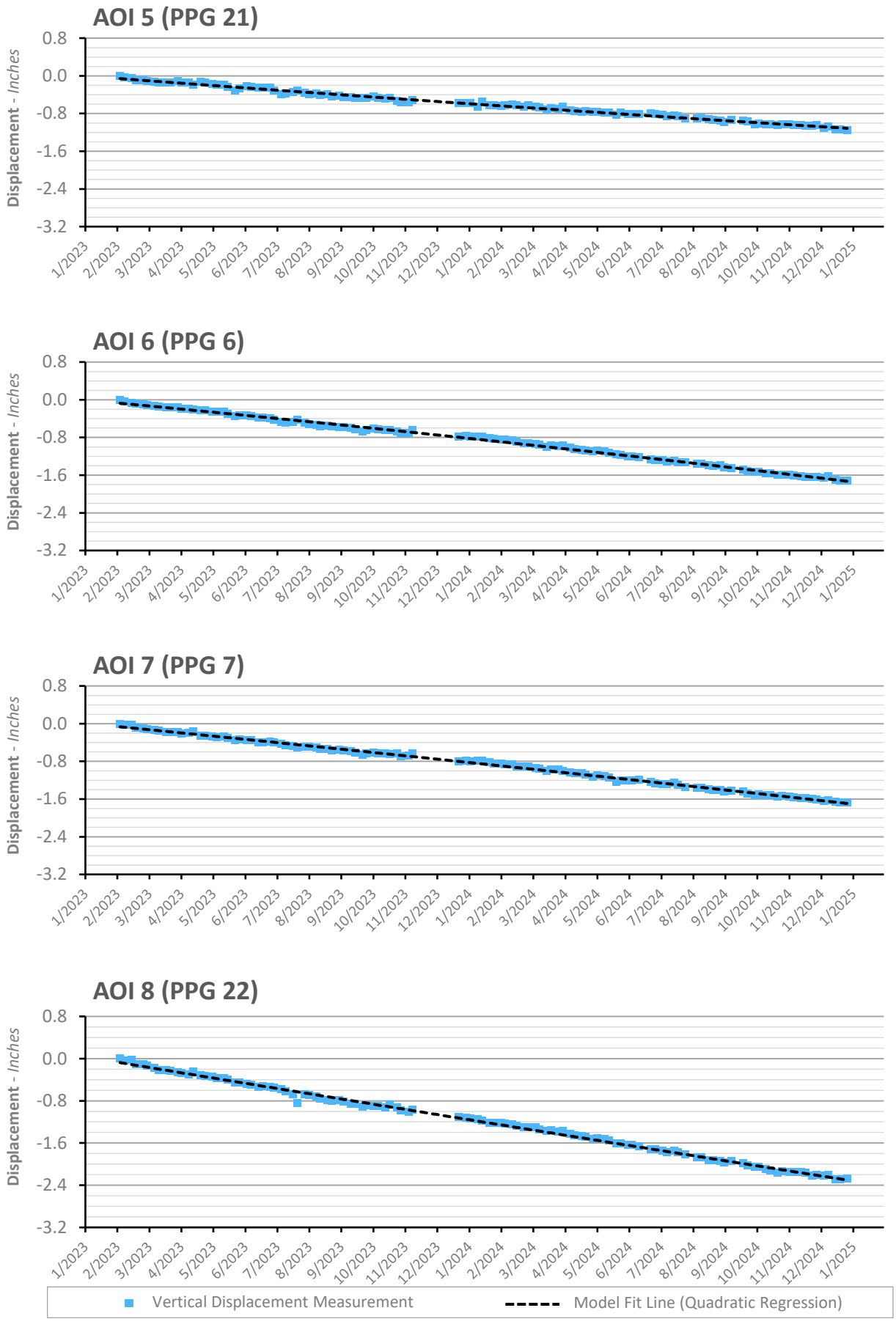

Averaged Vertical Displacement Time Series - AOI Point Groups

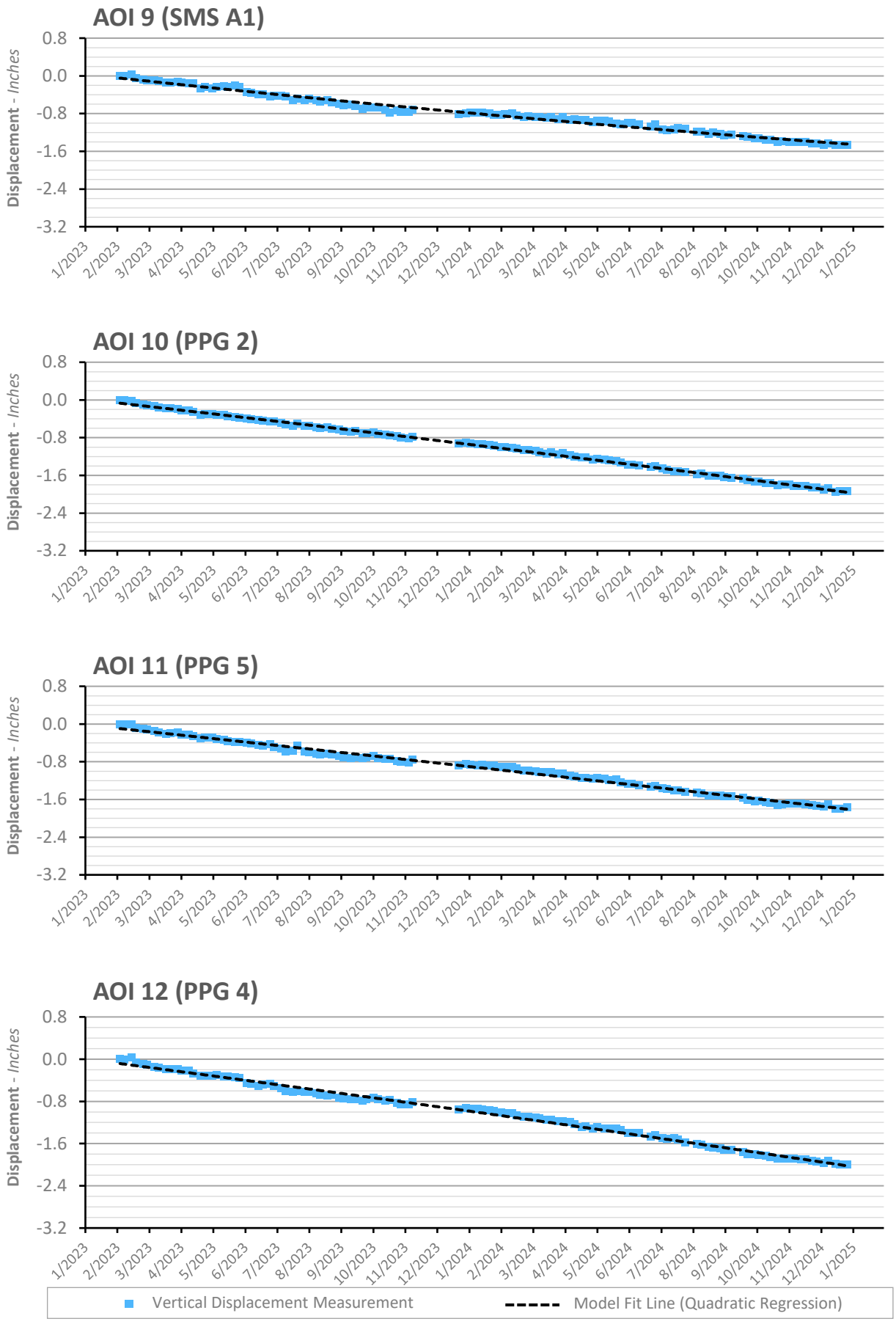

Averaged Vertical Displacement Time Series - AOI Point Groups

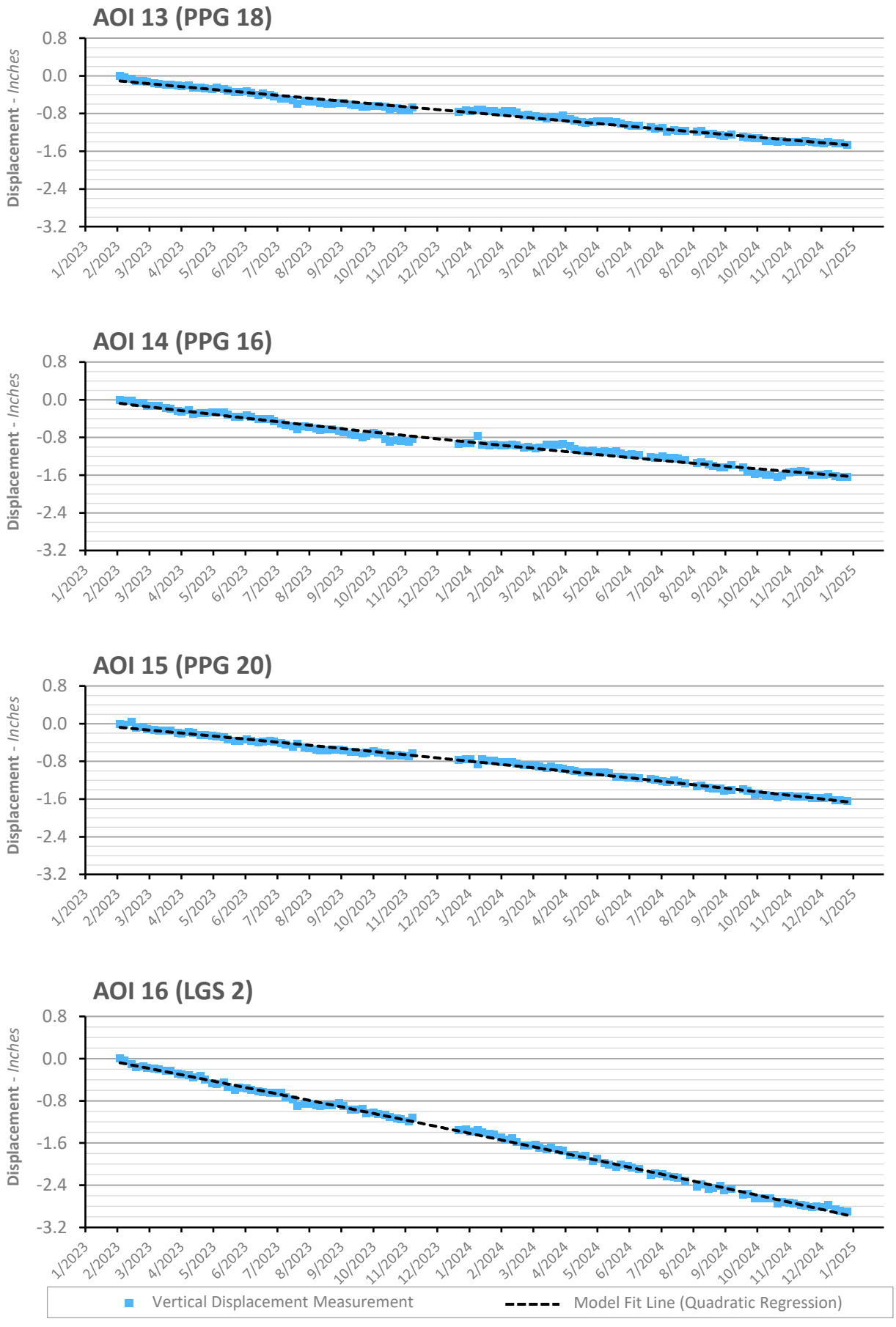

Averaged Vertical Displacement Time Series - AOI Point Groups

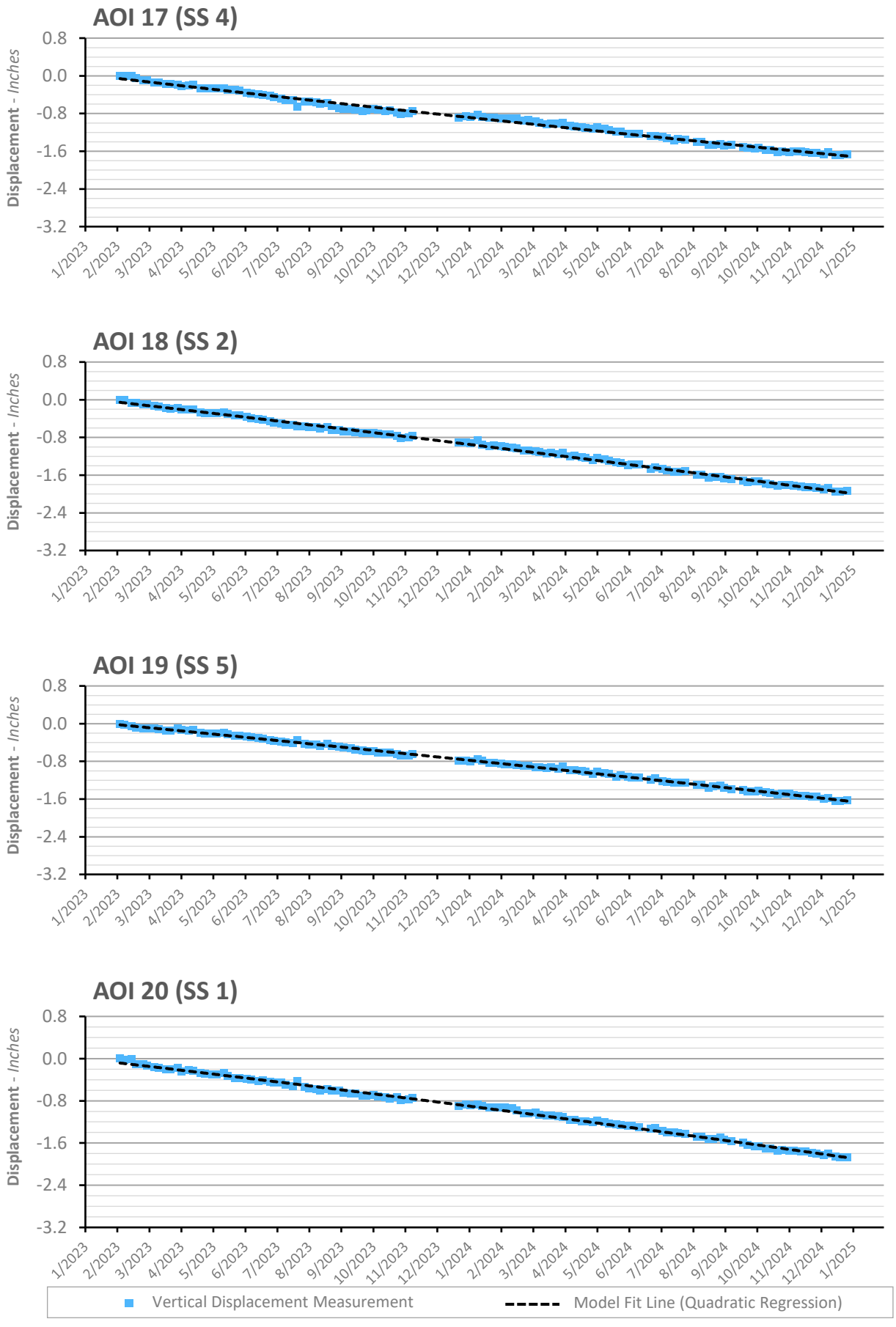

Averaged Vertical Displacement Time Series - AOI Point Groups

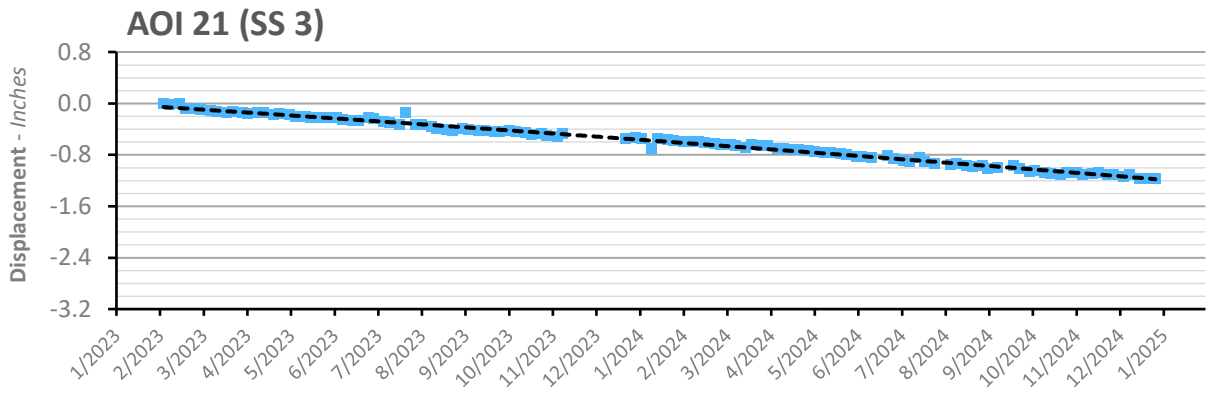

Vertical Displacement Measurement — Model Fit Line (Quadratic Regression)

Averaged East-West Displacement Time Series - AOI Point Groups

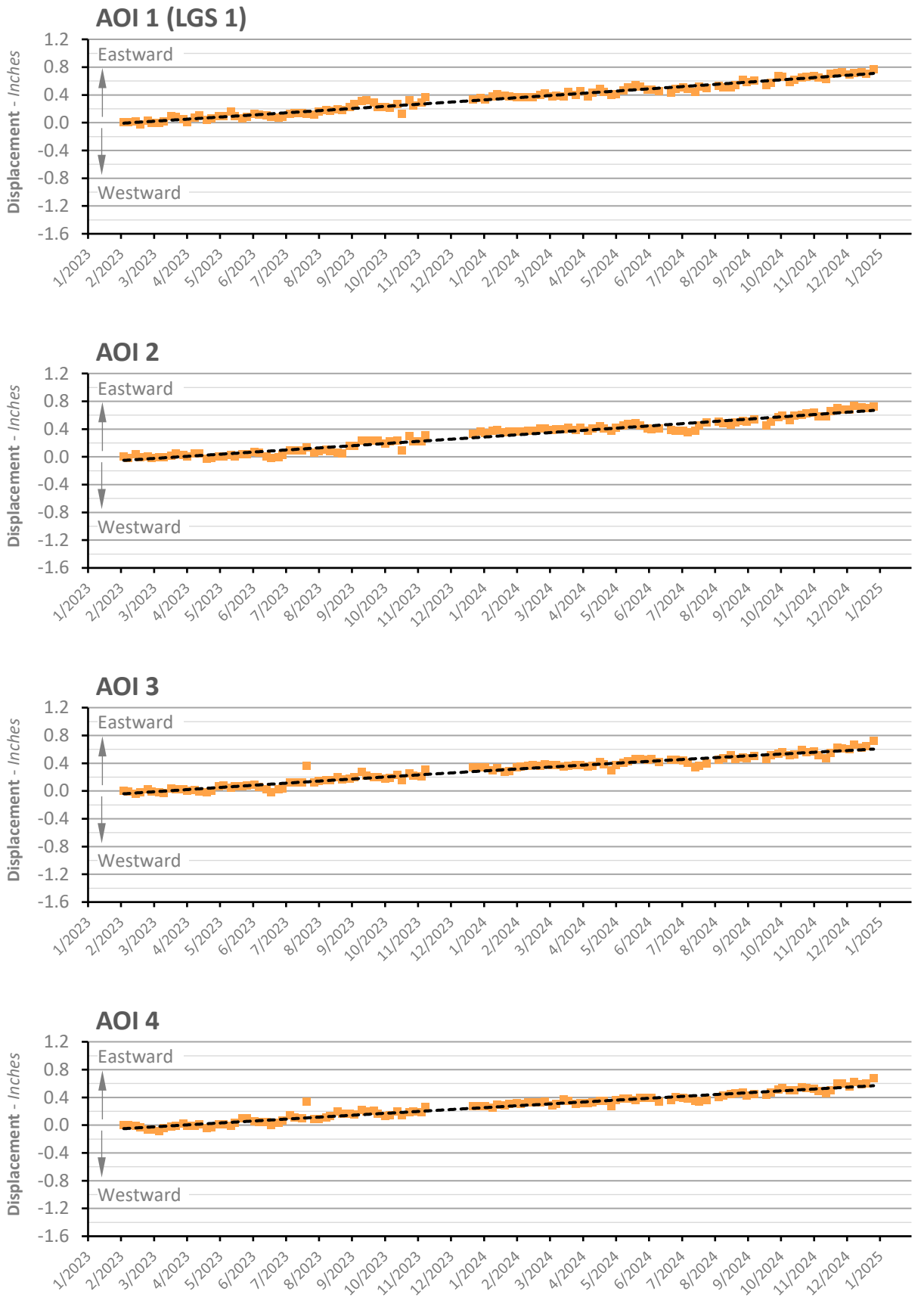

Averaged East-West Displacement Time Series - AOI Point Groups

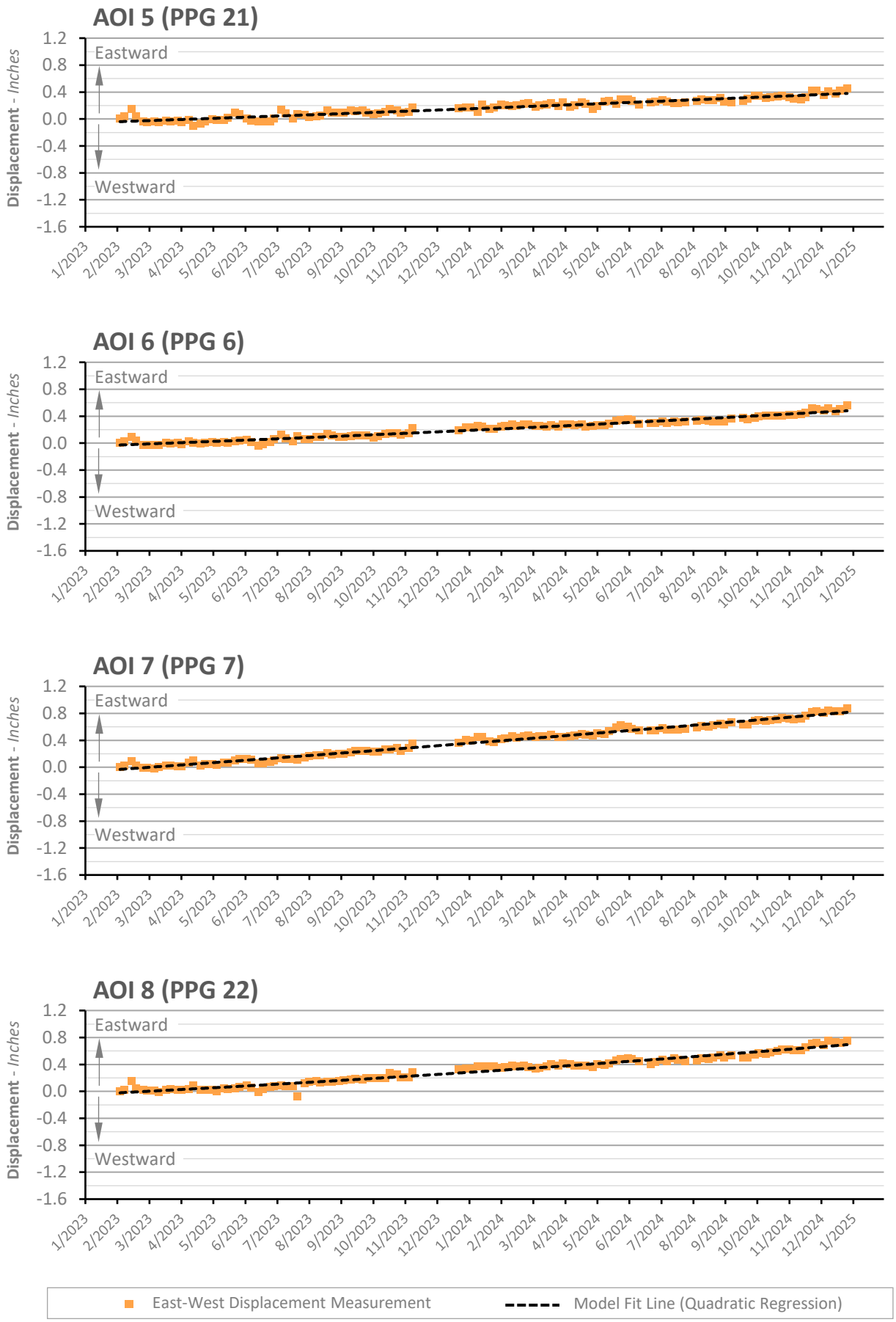

Averaged East-West Displacement Time Series - AOI Point Groups

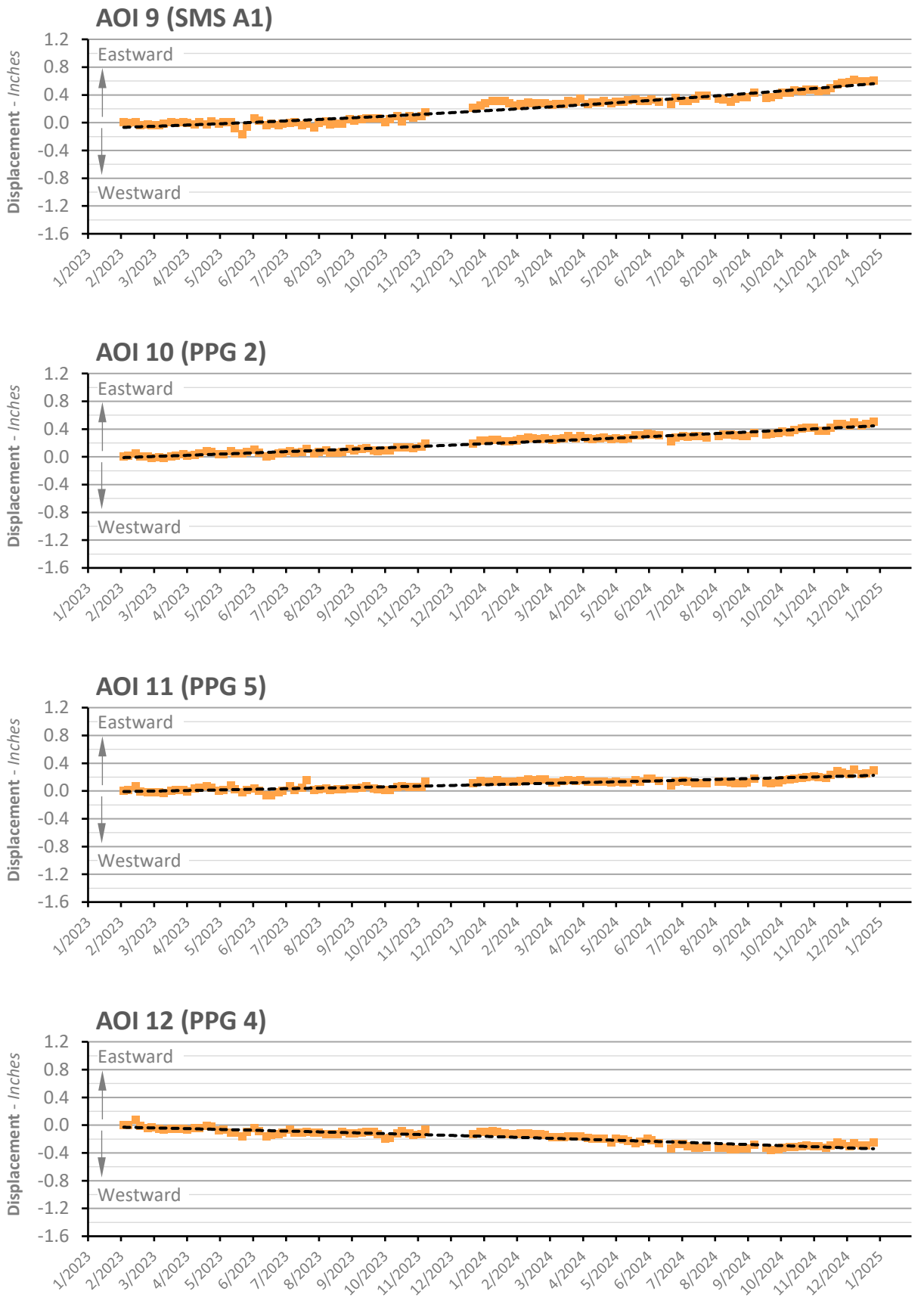

Averaged East-West Displacement Time Series - AOI Point Groups

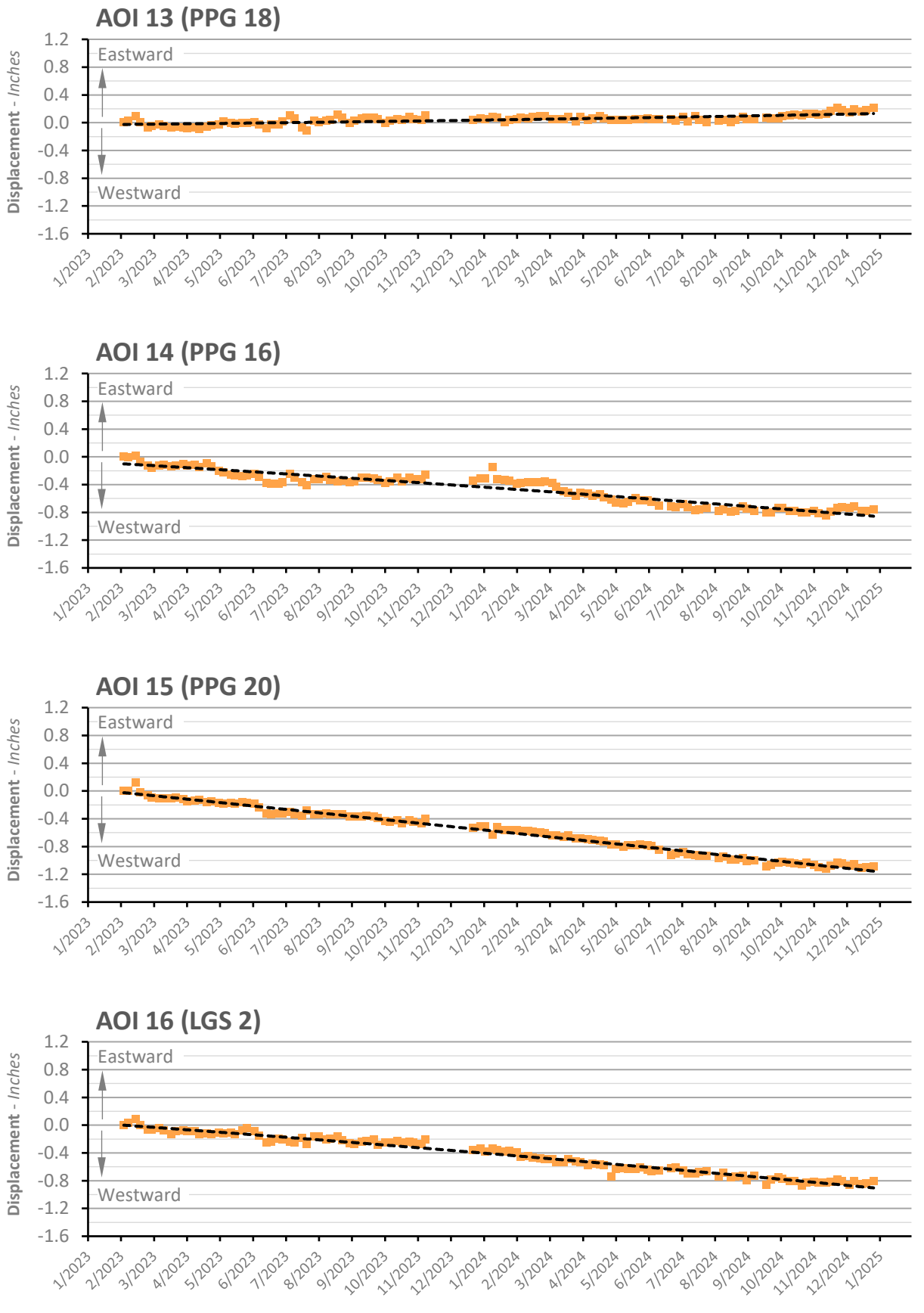

Averaged East-West Displacement Time Series - AOI Point Groups

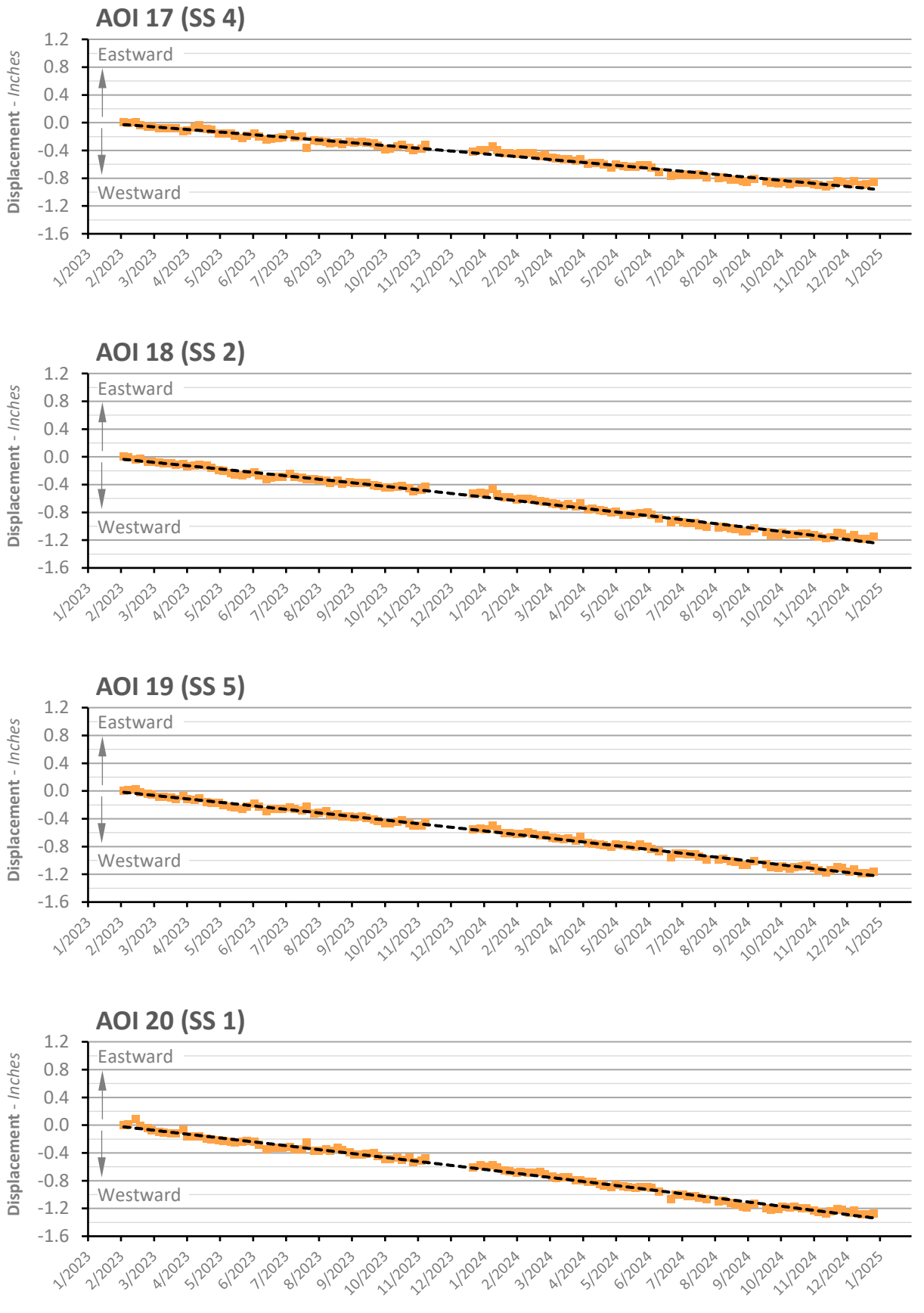

Averaged East-West Displacement Time Series - AOI Point Groups

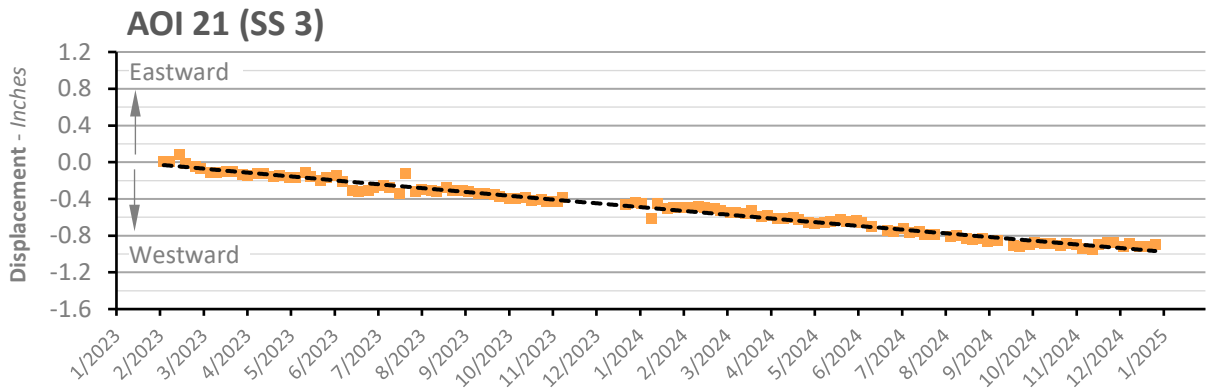

East-West Displacement Measurement Model Fit Line (Quadratic Regression)

Appendix C – Velocity and Acceleration Contour Maps – Vertical Displacement

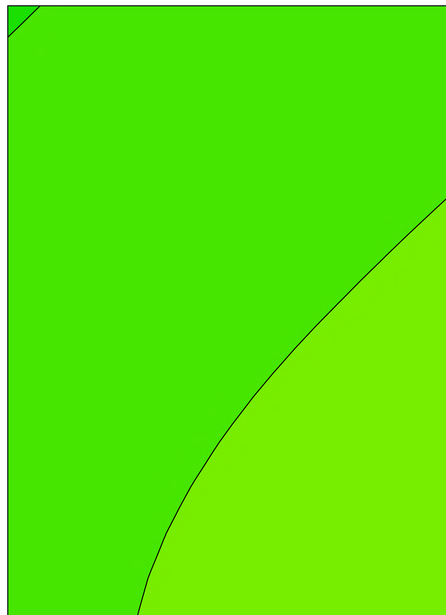

Fall 2024 Subsidence Monitoring InSAR Survey
Vertical Displacement Velocity Contours (in/yr)
with 2-D InSAR Measurement Points and AOI Boundaries
Sulphur Mines Salt Dome
Calcasieu Parish, LA

Appendix C-1

Drawn by:	Date:	Approved by:
Steven Larcom	9/19/2025	Nathaniel Byars

PCS: NAD 1983 State Plane LA-S FIPS 1702 (US Ft.)

LONQUIST

Louisiana Registration No. EF5937

Sulphur Cavern Well Surface Hole Locations

- 09 - ACTIVE INJECTION (14)
- 29 - DRY AND PLUGGED (10)
- 30 - PLUGGED AND ABANDONED (1)
- Directional Wellbores
- InSAR Point Group AOI Boundaries
- Historical Cavern Extent
- InSAR Data Extent
- 2,000' Salt Contour (subsea depth)
- 2D InSAR Reference Points
- Vertical 2-D Measurement Point
- Vertical Velocity Contours (CI = 0.1 in/yr)

-1.7 | 0 | 1.0 in/yr

1:1,400

0 | 500 | 1,000 | 2,000 Feet

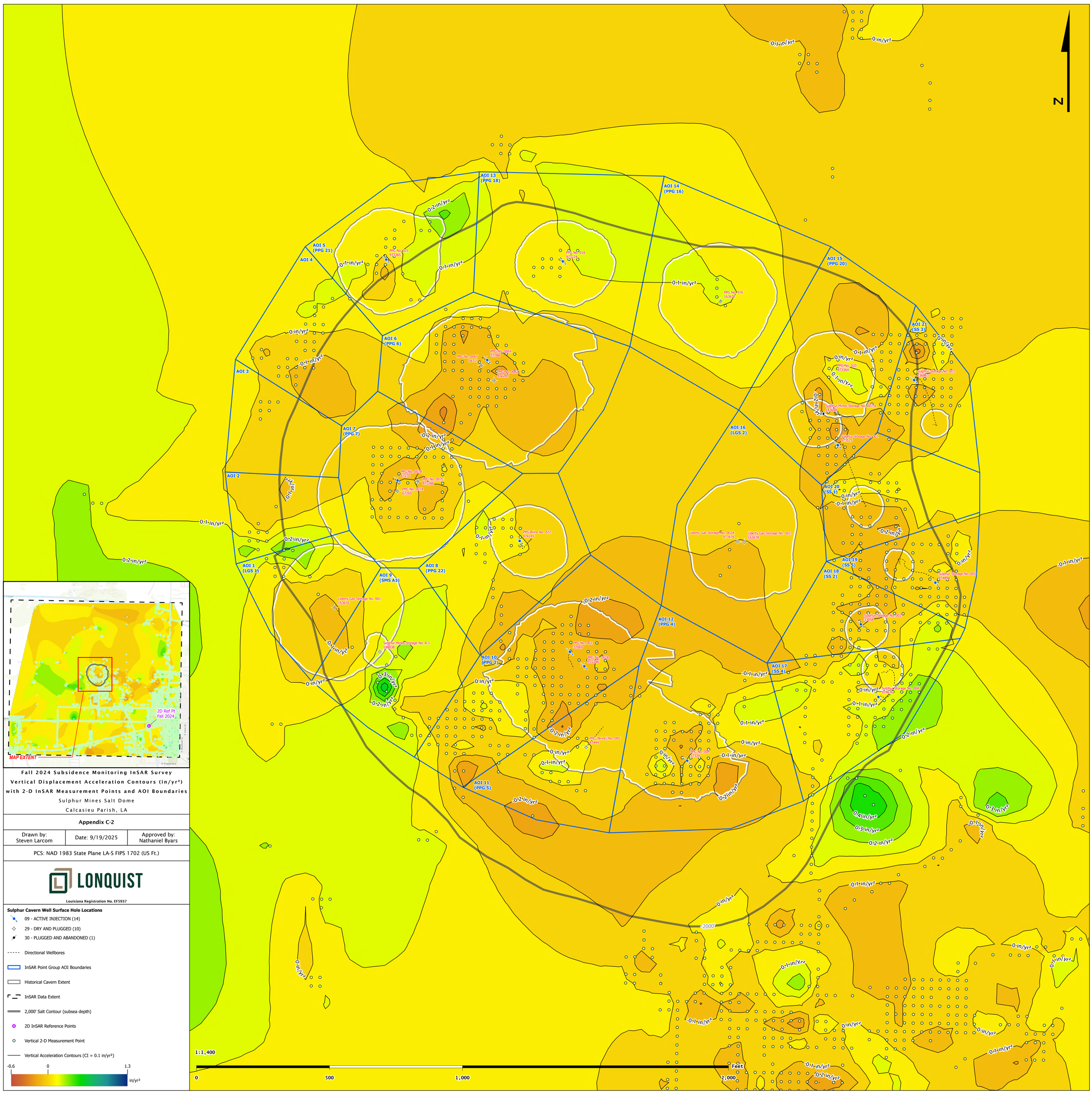

Fall 2024 Subsidence Monitoring InSAR Survey

Vertical Displacement Acceleration Contours (in/yr²) with 2-D InSAR Measurement Points and AOI Boundaries

Sulphur Mines Salt Dome

Calcasieu Parish, LA

Appendix C-2

Drawn by: Steven Larcom	Date: 9/19/2025	Approved by: Nathaniel Byars

PCS: NAD 1983 State Plane LA-S FIPS 1702 (US Ft.)

LONQUIST

Louisiana Registration No. EF5937

Sulphur Cavern Well Surface Hole Locations

- 09 - ACTIVE INJECTION (14)
- 29 - DRY AND PLUGGED (10)
- 30 - PLUGGED AND ABANDONED (1)
- Directional Wellbores
- InSAR Point Group AOI Boundaries
- Historical Cavern Extent
- InSAR Data Extent
- 2,000' Salt Contour (subsea depth)
- 2D InSAR Reference Points
- Vertical 2-D Measurement Point
- Vertical Acceleration Contours (CI = 0.1 in/yr²)

-0.6 0 1.3 in/yr²

1:1,400

0 500 1,000 Feet 2,000

Appendix D – Velocity and Acceleration Contour Maps – East-West Displacement

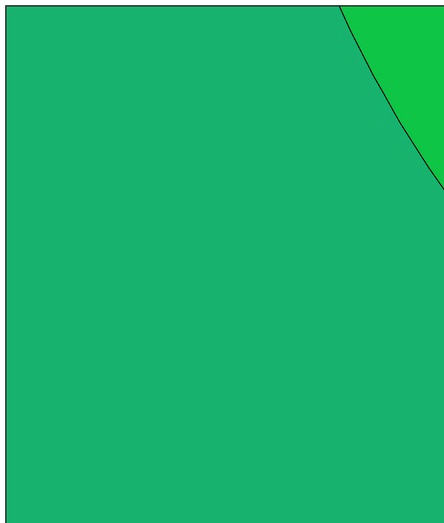

Fall 2024 Subsidence Monitoring InSAR Survey

East-West Displacement Velocity Contours (in/yr)

with 2-D InSAR Measurement Points and AOI Boundaries

Sulphur Mines Salt Dome

Calcasieu Parish, LA

Appendix D-1

Drawn by:	Date:	Approved by:
Steven Larcom	9/19/2025	Nathaniel Byars

PCS: NAD 1983 State Plane LA-S FIPS 1702 (US Ft.)

LONQUIST

Louisiana Registration No. EF5937

Sulphur Cavern Well Surface Hole Locations

- 09 - ACTIVE INJECTION (14)
- 29 - DRY AND PLUGGED (10)
- 30 - PLUGGED AND ABANDONED (1)
- Directional Wellbores
- InSAR Point Group AOI Boundaries
- Historical Cavern Extent
- InSAR Data Extent
- 2,000' Salt Contour (subsea depth)
- 2D InSAR Reference Points
- East-West 2D Measurement Point
- East-West Velocity Contours (CI = 0.1 in/yr)

-1.1 0 0.8 in/yr

1:1,400

0 500 1,000 Feet 2,000

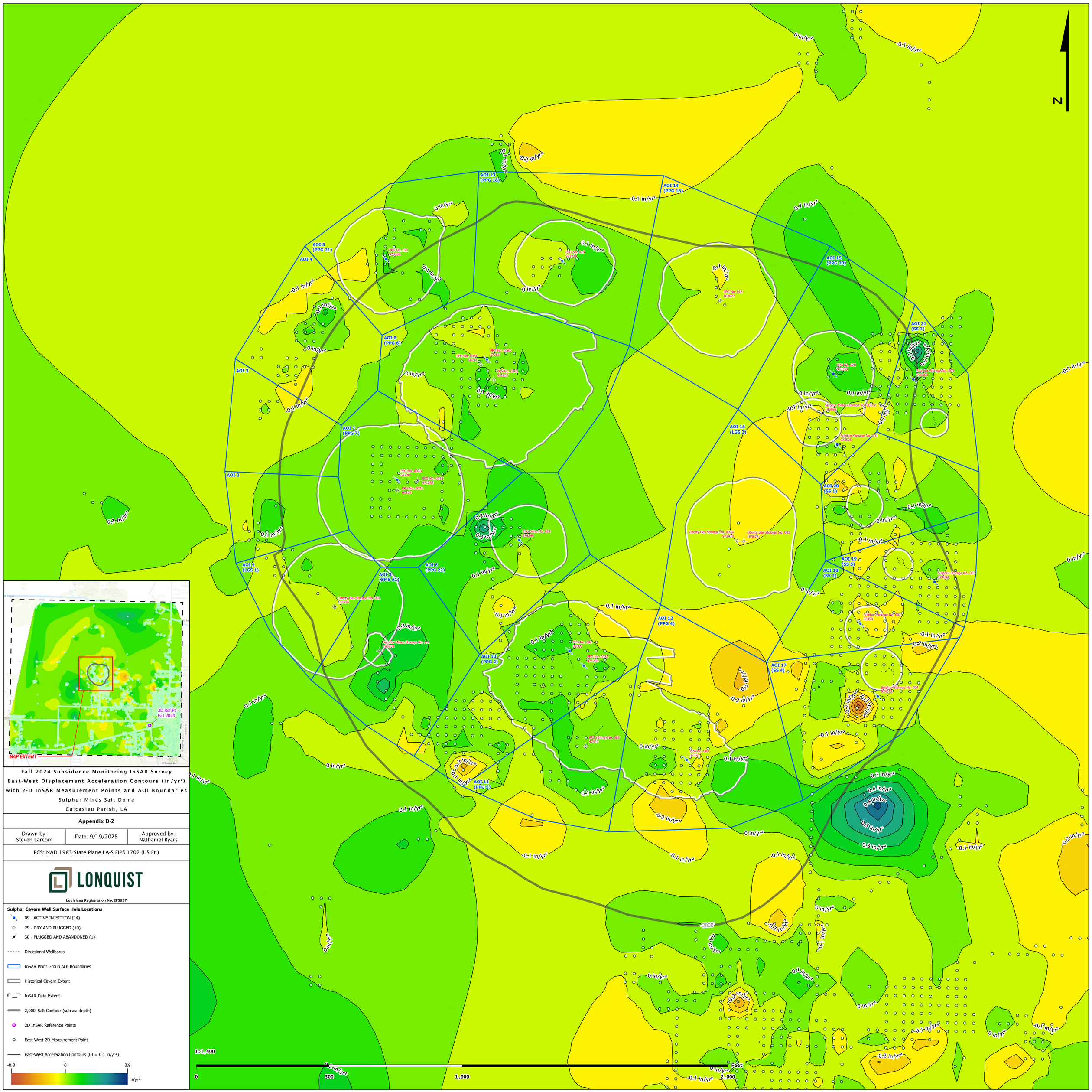

Fall 2024 Subsidence Monitoring InSAR Survey

East-West Displacement Acceleration Contours (in/yr²)

with 2-D InSAR Measurement Points and AOI Boundaries

Sulphur Mines Salt Dome

Calcasieu Parish, LA

Appendix D-2

Drawn by:	Date:	Approved by:
Steven Larcom	9/19/2025	Nathaniel Byars

PCS: NAD 1983 State Plane LA-S FIPS 1702 (US Ft.)

LONQUIST

Louisiana Registration No. EF5937

Sulphur Cavern Well Surface Hole Locations

- 09 - ACTIVE INJECTION (14)
- 29 - DRY AND PLUGGED (10)
- 30 - PLUGGED AND ABANDONED (1)
- Directional Wellbores
- InSAR Point Group AOI Boundaries
- Historical Cavern Extent
- InSAR Data Extent
- 2,000' Salt Contour (subsea depth)
- 2D InSAR Reference Points
- East-West 2D Measurement Point
- East-West Acceleration Contours (CI = 0.1 in/yr²)

-0.8 | 0 | 0.9 in/yr²

Appendix E – Vertical & East-West Displacement Time Series – Corner Reflectors

Vertical Displacement Time Series - Corner Reflectors

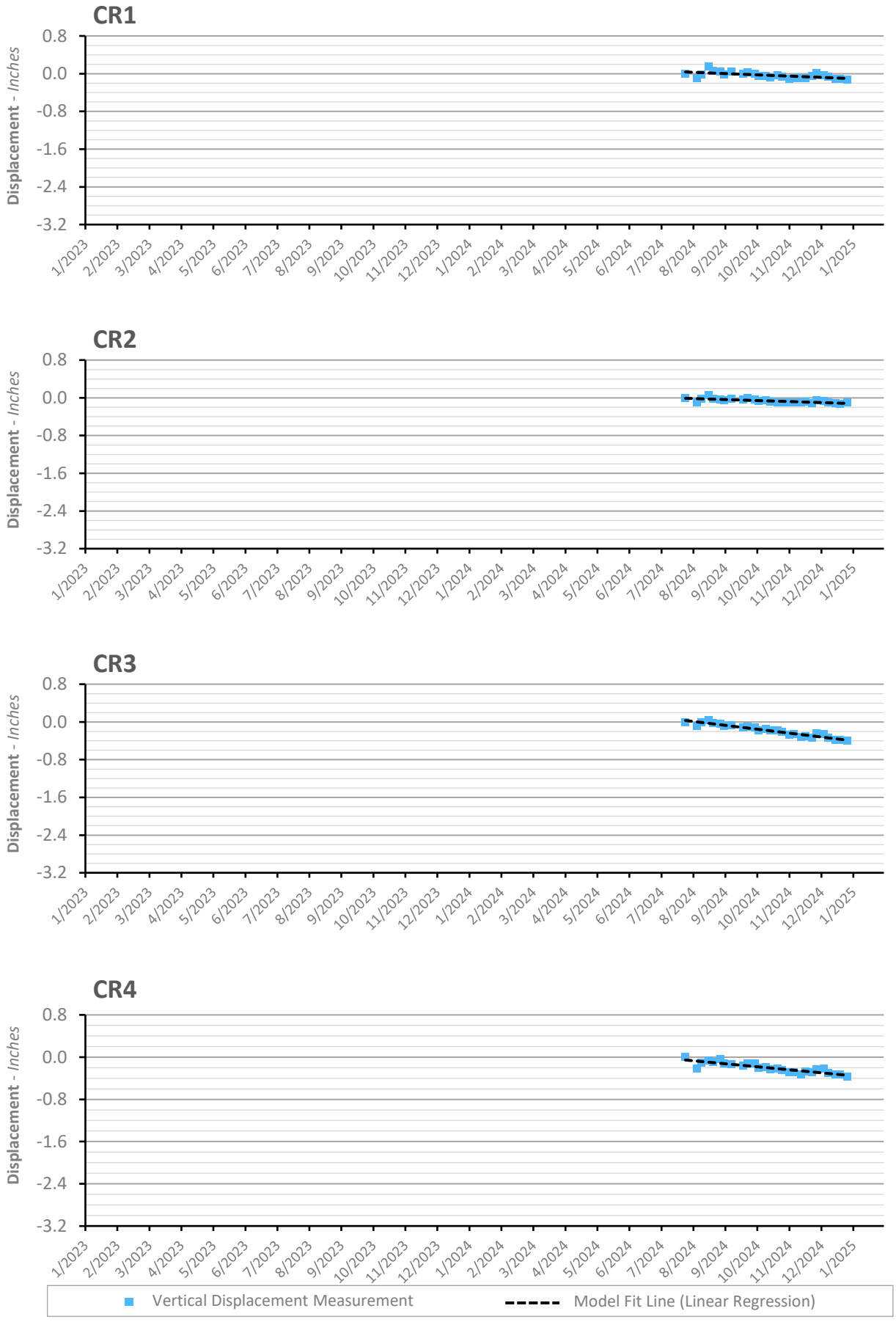

Vertical Displacement Time Series - Corner Reflectors

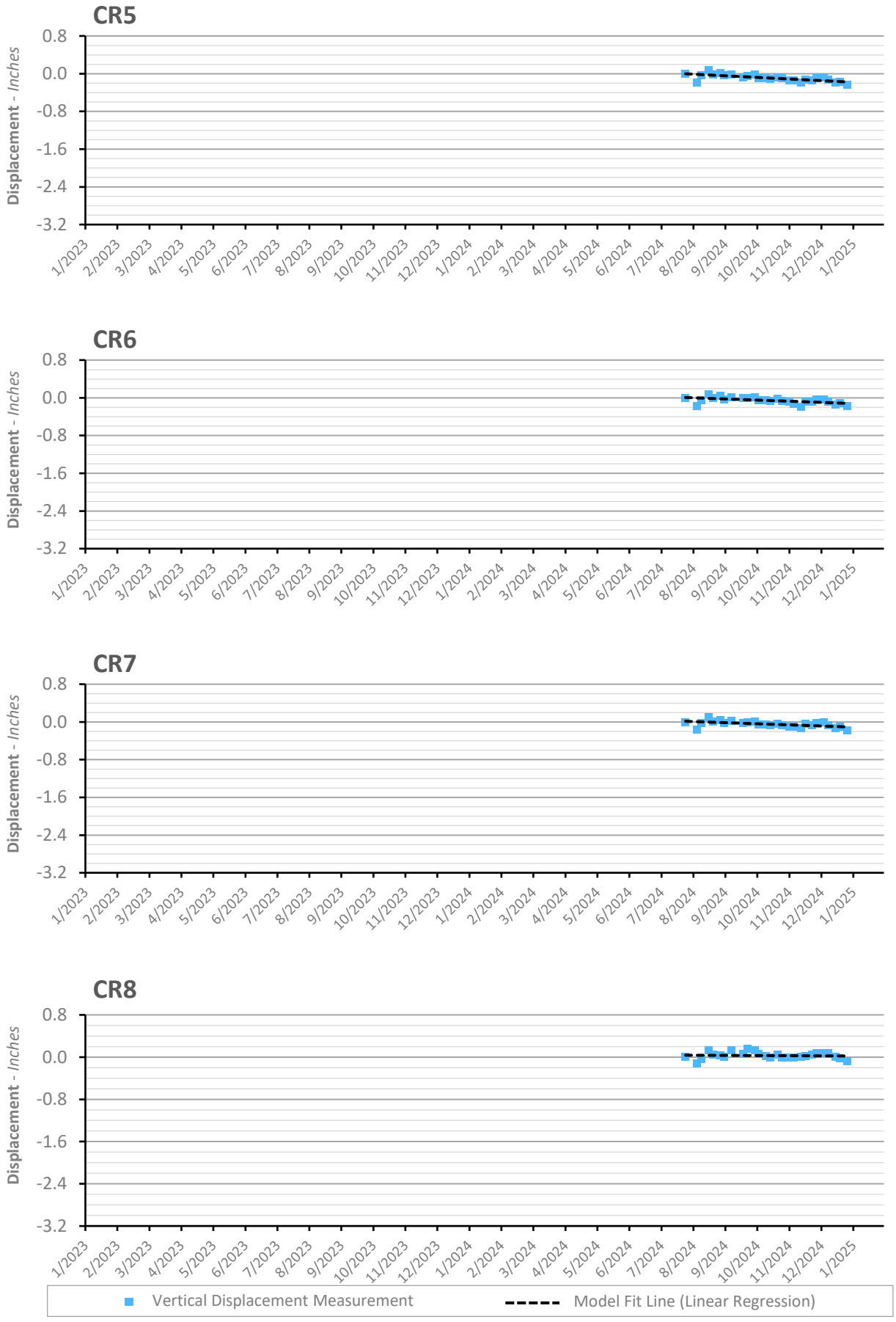

Vertical Displacement Time Series - Corner Reflectors

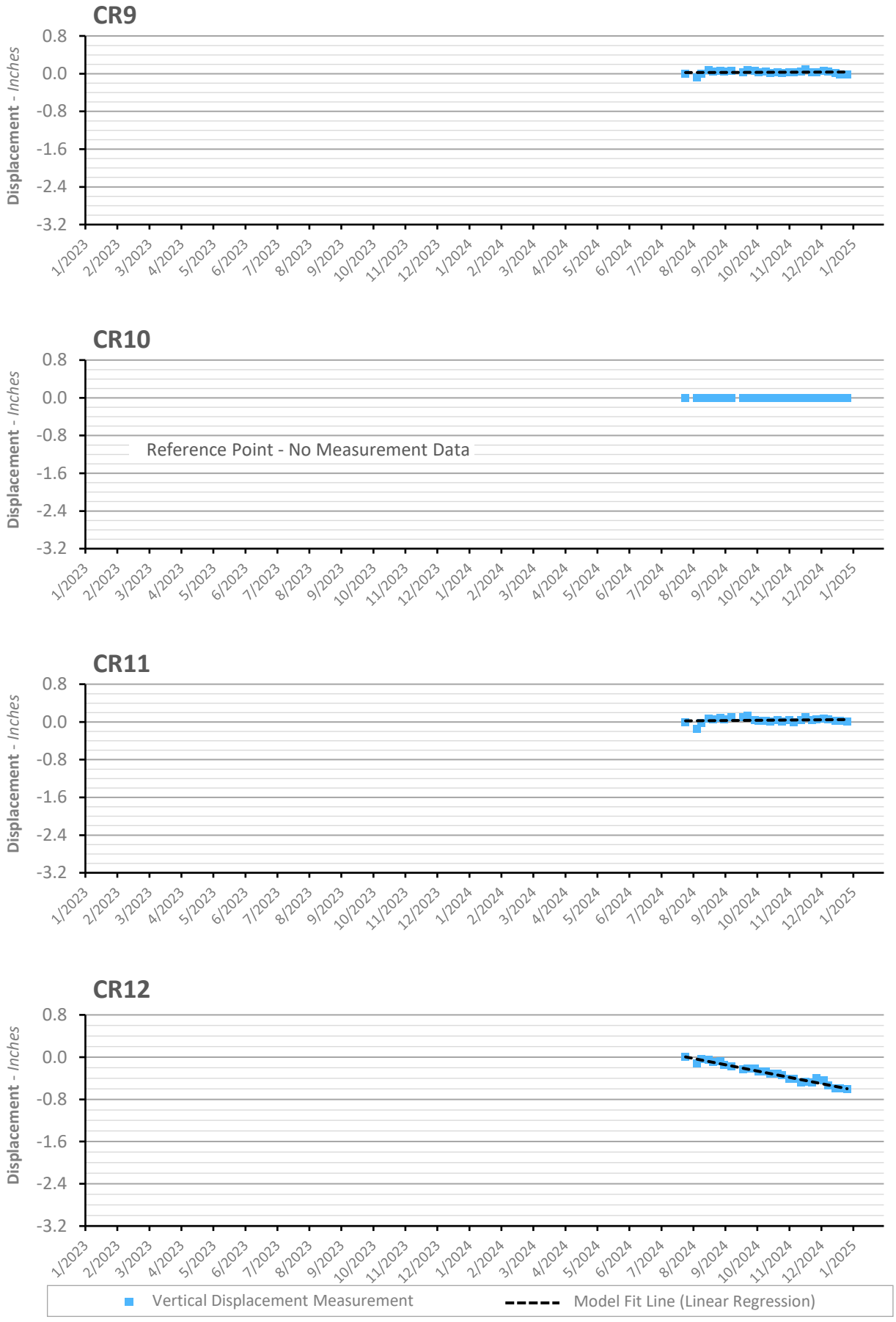

Vertical Displacement Time Series - Corner Reflectors

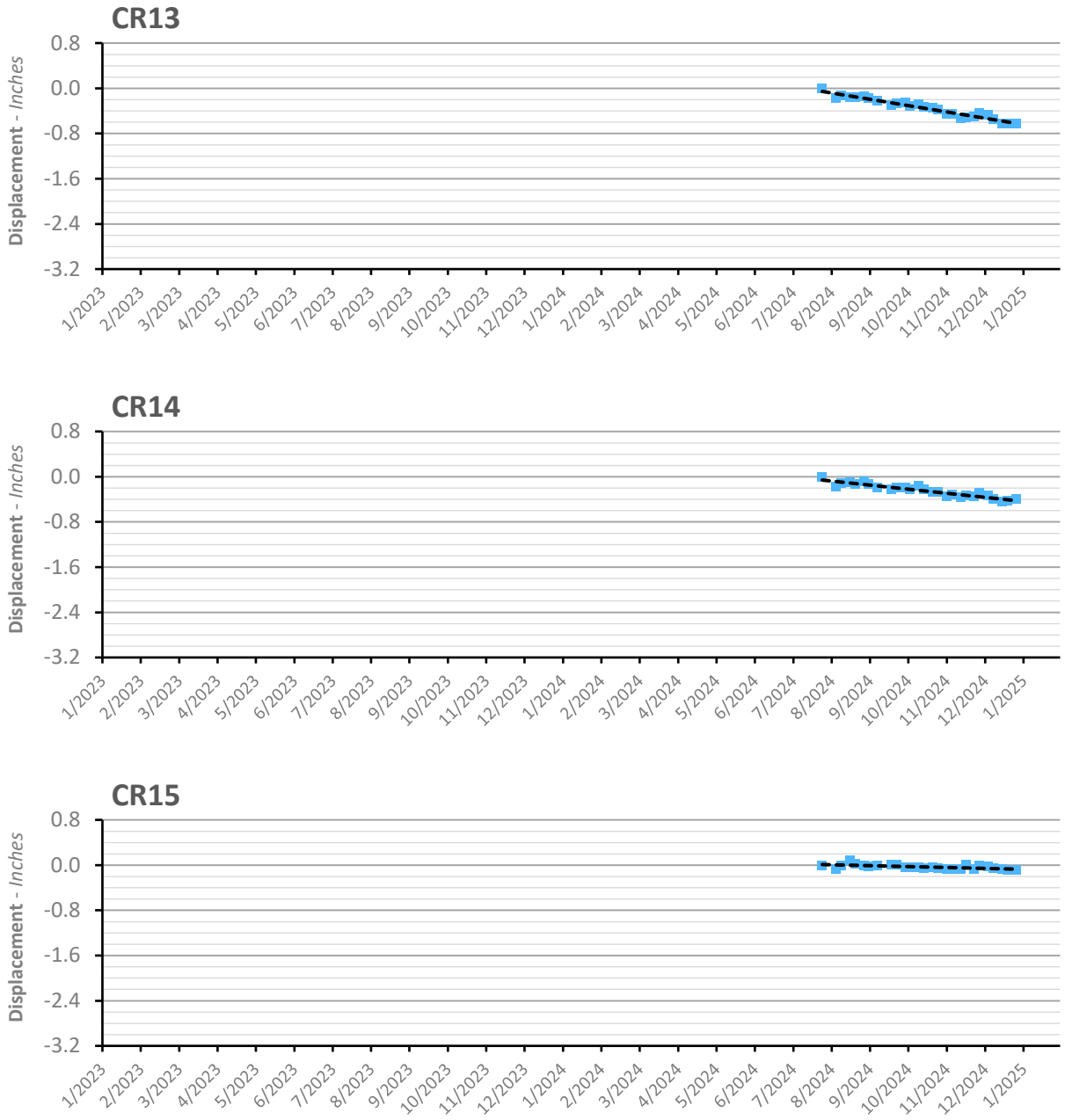

East-West Displacement Time Series - Corner Reflectors

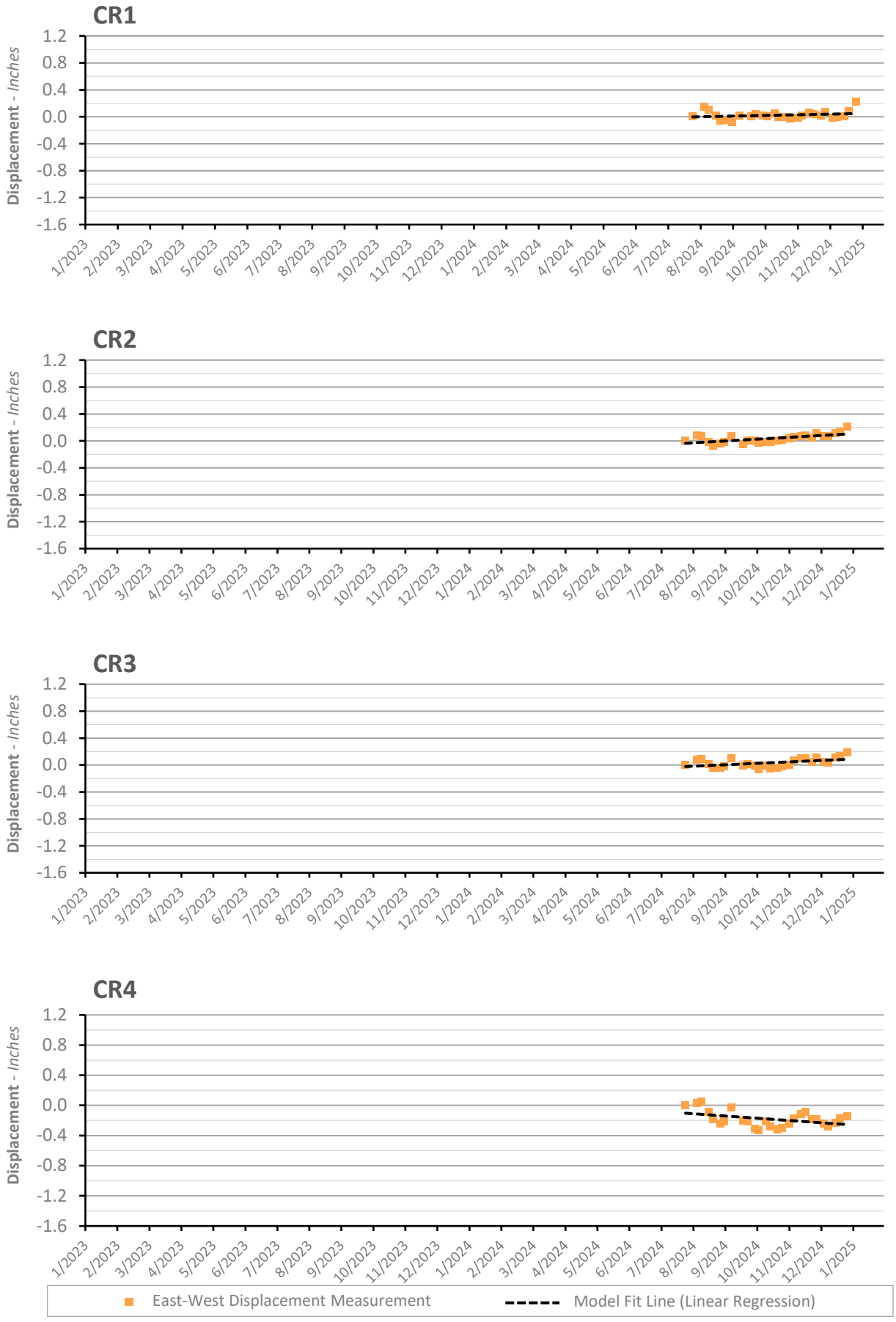

East-West Displacement Time Series - Corner Reflectors

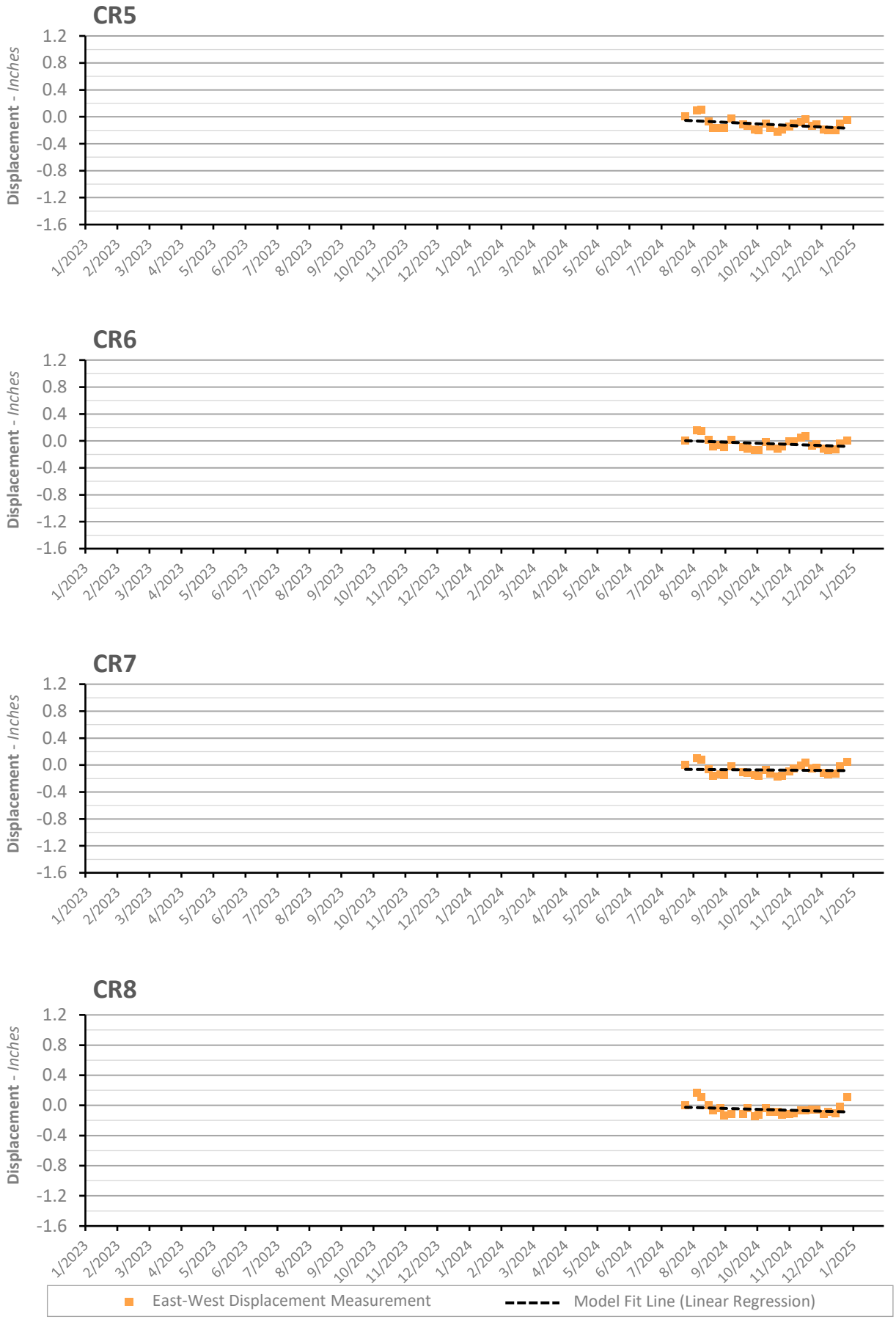

East-West Displacement Time Series - Corner Reflectors

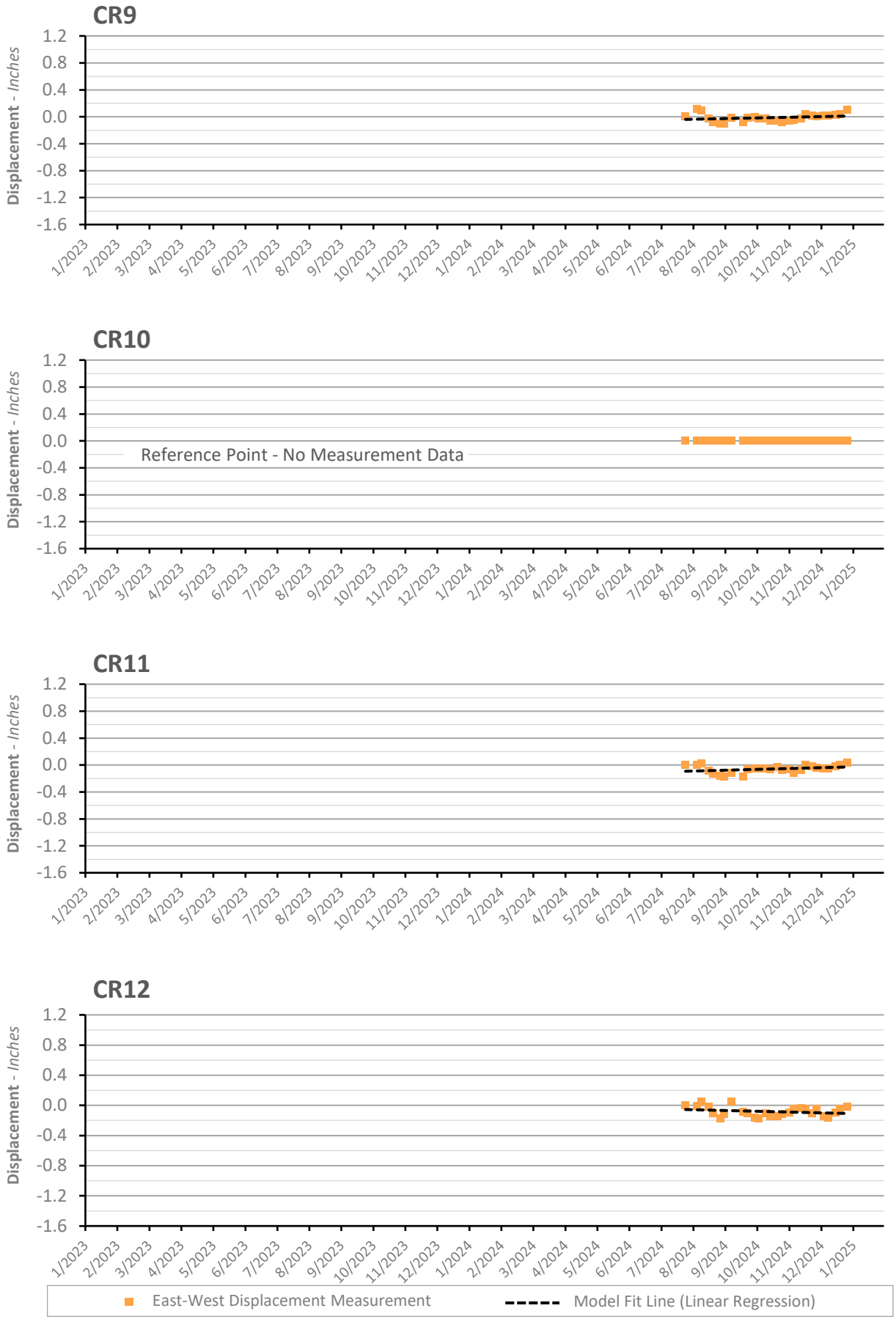

East-West Displacement Time Series - Corner Reflectors

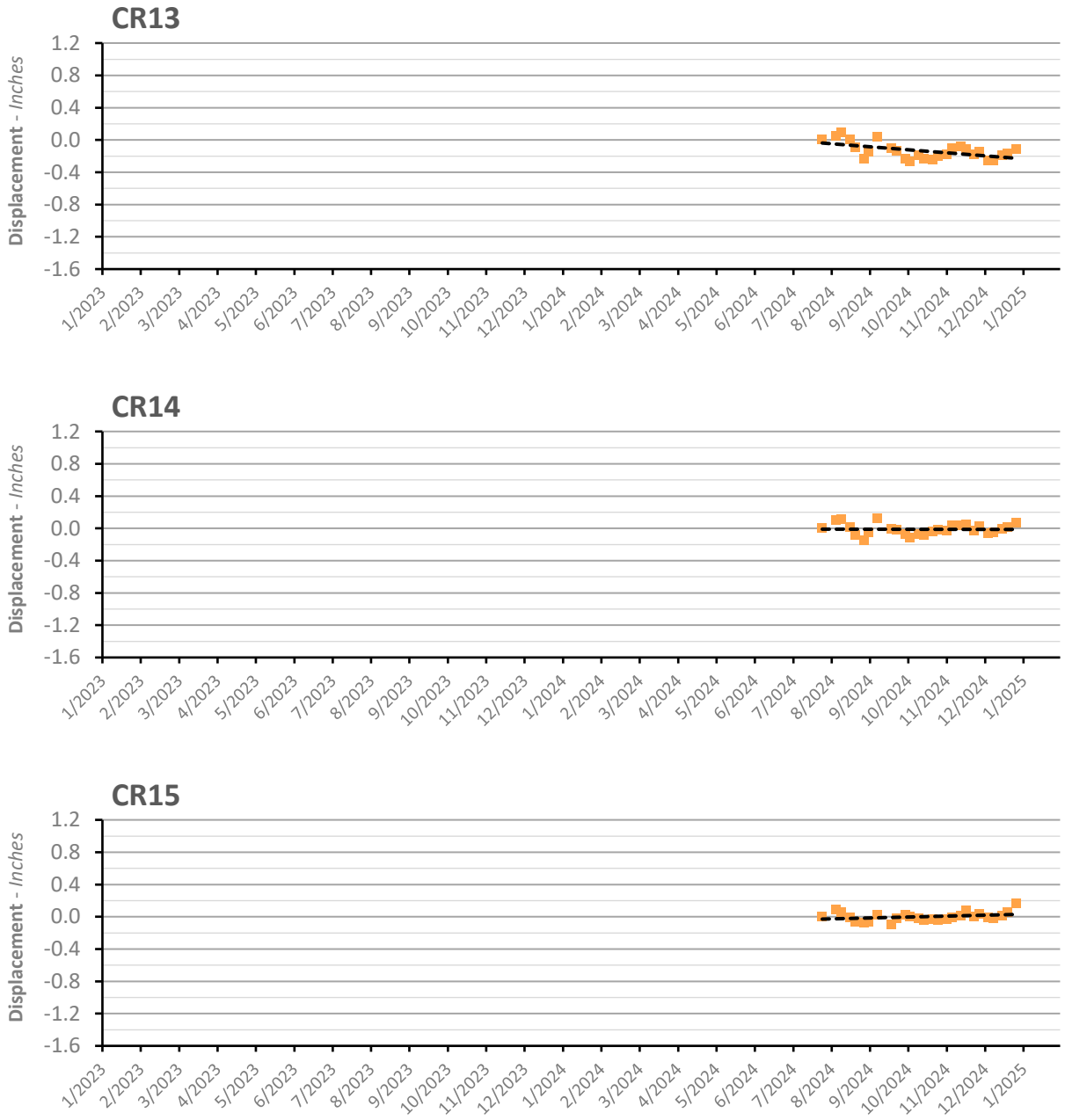

Appendix F – TRE-Altamira InSAR Analysis of Ground Displacement

TRE ALTAMIRA
A CLS Group Company

InSAR Analysis of Ground Displacement at Sulphur Mines, Louisiana

June 2025
Technical Report

Report Specifications

Client:	**Lonquist & Co. LLC**
Attention:	Nathaniel Byars, P.E.
Address:	12912 Hill Country Blvd. Suite F-200, Austin Texas 78738

Reference:	
Title:	InSAR Analysis of Ground Displacement at Sulphur Mines, Louisiana – June 2025
TRE ALTAMIRA Delivery Reference:	JO24-2868-CA
Client Reference (Proposal Reference)	TRE Ref: TREA_LON_2024_207R1

Prepared by:	**TRE ALTAMIRA Inc.**
Address:	#410 - 475 West Georgia Street Vancouver, BC, V6B 4M9, Canada
Author:	Hannah Raffler & Kenny Yue
Verified and Approved by:	Giacomo Falorni
Date:	25 June 2025
Document Number and Version:	1.0

Executive Summary

TRE Altamira Inc. is monitoring ground displacement at the Sulphur Mines Salt Dome in Louisiana, USA, for Lonquist & Co. LLC. The 2024 monitoring employs Interferometric SAR (InSAR) technology, coupled with high-resolution TerraSAR-X (TSX)/PAZ satellite imagery acquired from a descending orbit and low-resolution Sentinel (SNT) from the opposing ascending orbit. A second high-resolution TSX data set, also acquired from an ascending orbit, has also been tasked since early 2023. This new data set will replace the low-resolution ascending SNT for the forward monitoring over the site.

The 2024 monitoring plan provided frequent ground displacement updates aligned with satellite image acquisitions. This included two high-resolution TerraSAR-X/PAZ updates every 11 days (alternating 4 and 7 days) from a descending orbit, lower resolution Sentinel updates every 12 days from an ascending orbit, and 2-D (vertical and E-W) updates also every 12 days. In early 2025, the monitoring plan was adjusted to utilize the new ascending orbit data so that fully high-resolution updates are now delivered every 11 days for the ascending, descending (alternating 4 and 7 days), vertical and E-W data.

In July 2024, 15 Corner Reflectors (CR) were installed on and adjacent to the dome for additional monitoring. Corner Reflectors act as high-quality measurement points at known locations. The CR monitoring plan follows the same frequency as above as it utilizes the same satellite data as the regular InSAR monitoring.

The observations section of the present report focuses on the 2D (vertical and east-west) data over the areas of interest specified by Lonquist, up to the end of 2024.

Key Findings (see Section 4 for additional information):

- Subsidence observed across the entire dome, with an average displacement rate of -1.52 in/yr at AOI 16.
- AOIs 16, 18, and 8 exhibit the highest subsidence rates.
- AOIs 1, 2, 7, and 8 show the most significant lateral eastward displacement rate.
- AOIs 18, 19, and 20 show the most significant lateral westward displacement rate.
- Westward displacement concentrated at AOI 20, with an average displacement rate at -0.69 in/yr.
- Eastward displacement concentrated at AOI 7, reaching an average displacement rate at +0.45 in/yr.

Corner Reflectors:

- Highest subsidence rate observed at CR 12 (AOI 16), reaching -1.4 in/yr.
- Highest eastward displacement rate observed at CR 2 (AOI 1), reaching +0.3 in/yr.

- Highest westward displacement rate observed at CR 13 (AOI 1), reaching -0.5 in/yr.
- The displacement rates observed at the co-located CRs and GNSS stations are comparable

Additional Notes:

TSX/PAZ satellites continue to maintain their image acquisition frequencies (11 days). Monitoring will continue based on these high-resolution image acquisitions. SNT will be used as a back up in case of any issues with the current acquisition plan.

TREA recommends periodically resetting the Sulphur Mines baseline (approximately every 12-24 months) to continuously optimize measurement quality. This interval can be adjusted based on data quality, coverage, and local conditions. The latest baseline reset of the descending TSX/PAZ and new baseline for the ascending TSX was performed in May 2025. The new and re-baselined data forms the basis for the current monitoring campaign.

Table of Contents

Acronyms and Abbreviations

AOI	Area of Interest
ATS	Average Time Series
CR	Corner Reflector
DEM	Digital Elevation Model
DInSAR	Differential Interferometric SAR
DS	Distributed Scatterer(s)
GIS	Geographic Information System
InSAR	Interferometric Synthetic Aperture Radar
LOS	Line of Sight
MP	Measurement Point
NR	Natural Reflector
PS	Permanent Scatterer(s)
SAR	Synthetic Aperture Radar
SNT	Sentinel Satellite
SqueeSAR®	The most recent InSAR algorithm patented by TRE
TS	Time Series
TSX	TerraSAR-X satellite

1. Introduction

TRE Altamira Inc. (TREA) is contracted by Lonquist & Co. LLC (Lonquist) to monitor ground displacement at the Sulphur Mines Salt Dome in Louisiana, USA (Figure 1). This monitoring utilizes Interferometric SAR (InSAR) technology and our proprietary SqueeSAR® algorithm to provide precise measurements of ground movement over the assets and caverns on the salt dome, with the area of interest (AOI) covering 13.70 mi². We process data from both low-resolution Sentinel (SNT) imagery (65 x 16 ft resolution) and high-resolution TerraSAR-X (TSX)/PAZ satellites (3 x 3 ft resolution) for the monitoring and focus on the high-resolution TSX for the analysis.

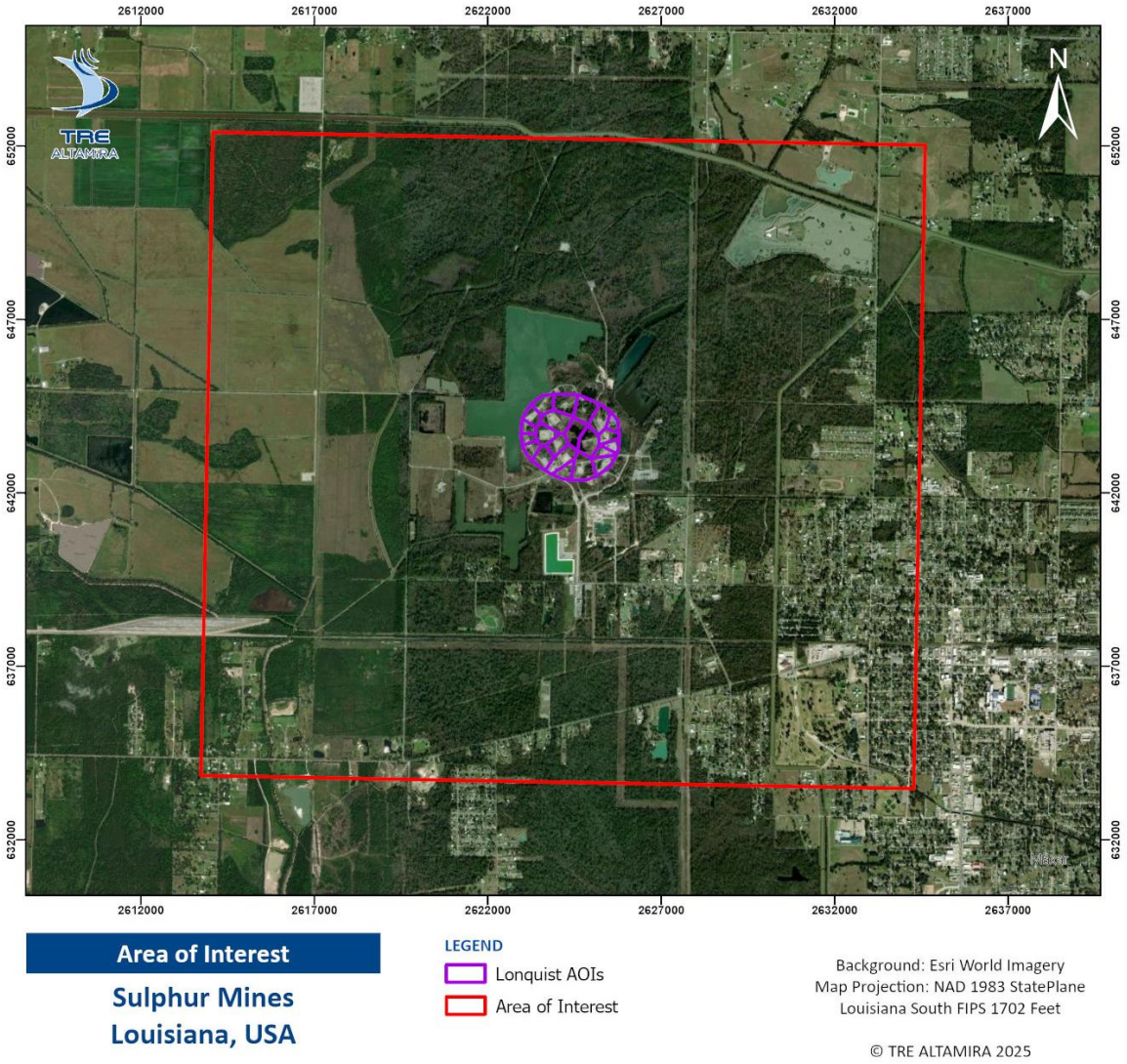

Figure 1. Area of interest (red) and focus areas of interest provided by Lonquist (purple).

The current monitoring plan delivers:

- Descending high-resolution TSX/PAZ updates every 4 and 7 days.
- Ascending high-resolution TSX updates every 11 days.
- 2-D (Vertical and E-W) updates every 11 days.

This Technical Report presents the findings up to the end of 2024 with a special focus on Lonquist's designated areas of interest.

2. Radar Imagery

The present report utilizes radar data acquired from both low- and high-resolution satellites up to the end of 2024:

- Sentinel (SNT): Low-resolution (65 x 16 ft pixel resolution), ascending orbit, with images acquired between October 2016 and December 2024.
- TerraSAR-X (TSX): High-resolution (3 x 3 ft), descending orbit, with images acquired between January 2023 and December 2024 and February 2023 and December 2024 from an ascending orbit.

Key Points:

- Satellite orbits are referred to as ascending or descending according to the direction of travel of the satellite: Ascending orbits move from south to north, imaging to the east. Descending orbits move from north to south, imaging to the west.
- Line of Sight (LOS): The satellite's LOS is angled relative to the vertical direction (see Figure 3). InSAR measurements project the actual displacement onto this LOS, indicated as θ (theta) in Table 2.

This report focuses on the high-resolution TSX/PAZ data collected through the end of 2024 (see Figure 2 and Table 2 for details).

Table 1: Satellite characteristics.

Satellite	Band	Wavelength	Pixel Resolution	Revisit frequency
SNT	C-band	2.32 in	65 x 16 ft	12 days
TSX/PAZ (*Spotlight*)	X-band	1.22 in	3 x 3 ft	11 days

Table 2: Satellite acquisition parameters and image acquisition information.

Satellite	Orbit	LOS Angle (Θ)	# of Images	Date Range
SNT	Ascending	42.45°	216	04 Oct 2016 – 21 Dec 2024
TSX/PAZ	Ascending	44.00°	56	04 Feb 2023 – 28 Dec 2024
	Descending	37.05°	123	24 Jan 2023 – 28 Dec 2024

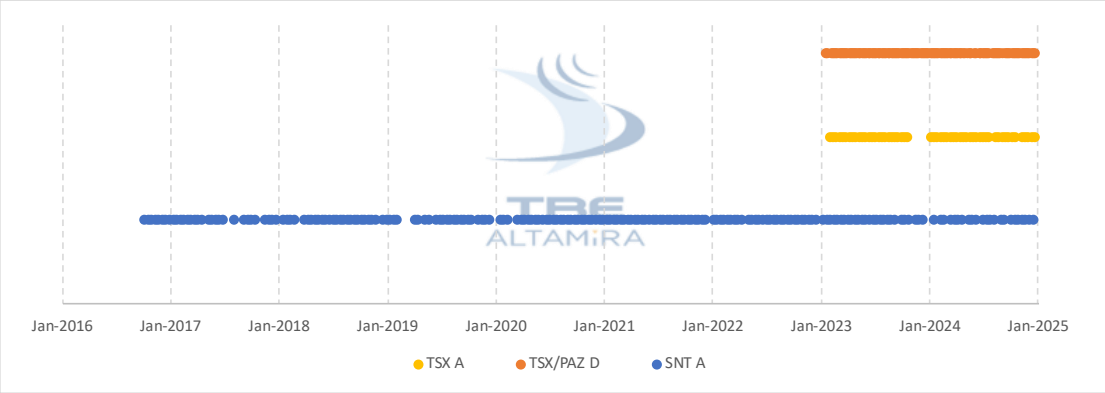

Figure 2: Temporal distribution of the radar images processed over the site.

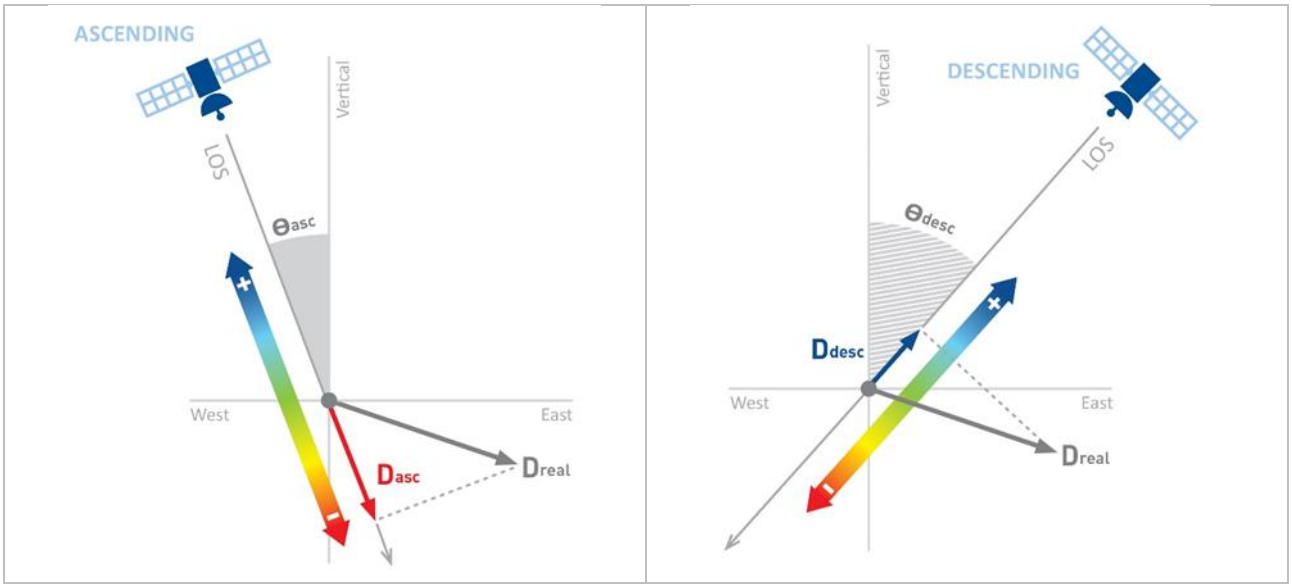

Figure 3: Ascending & Descending InSAR Geometries: InSAR projects real displacement (Dreal) onto the satellite's Line of Sight (LOS). LOS angle and orbit direction impact the measured value. Positive values (green-blue) denote movement towards the satellite, negative values (green-red) indicate movement away.

3. Results

The SqueeSAR® processing of radar imagery provided detailed point clouds of ground displacement measurements for both ascending and descending orbits. Each point cloud contains:

- Individual Measurement Points (MP): Each MP contains:
  - Cumulative Displacement: Total movement relative to the initial reference image.
  - Average Displacement Rate: Average annual movement rate over the analysis period (February 2023 – December 2024 for ascending, January 2023 - December 2024 for descending).
  - Acceleration: Change in displacement rate over the analysis period.
- Line-of-Sight (LOS) readings: Ascending and descending measurements are 1-D, obtained by projecting real displacement onto the satellite's LOS (see Figure 3).
- 2-D Analysis: Spatially overlapping LOS data is combined on a 33 x 33 ft grid to calculate:
  - Vertical Displacement: Up/down movement.
  - East-West Displacement: Horizontal E-W movement.

Additional Details:

This section provides an overview of:

- TSX and SNT LOS and 2-D TSX SqueeSAR results.
- LOS and 2-D TSX Corner Reflector results.

Focus areas of interest: Section 4 offers in-depth observations.

Appendix 1: Lists all deliverables.

Appendix 2: Information on the SqueeSAR® technique.

3.1. Line of Sight (LOS) Results

High-resolution ascending and descending results are shown in Figure 4 and Figure 5, respectively. Lower resolution SNT ascending results are shown in Figure 6. The analysis provides good coverage over most of the dome while, as expected, the density of points is lower over areas with heavy vegetation and water.

In Figure 4, Figure 5 and Figure 6:

- Measurement points are colour-coded according to the annual displacement rate between February 2023 – December 2024 (TSX ascending), January 2023 – December 2024 (TSX/PAZ descending) and October 2016 – December 2024 (SNT ascending).
- Yellow to red indicates movement away from the satellite (negative values), pale to dark blue indicates movement towards the satellite (positive values) (Figure 3).

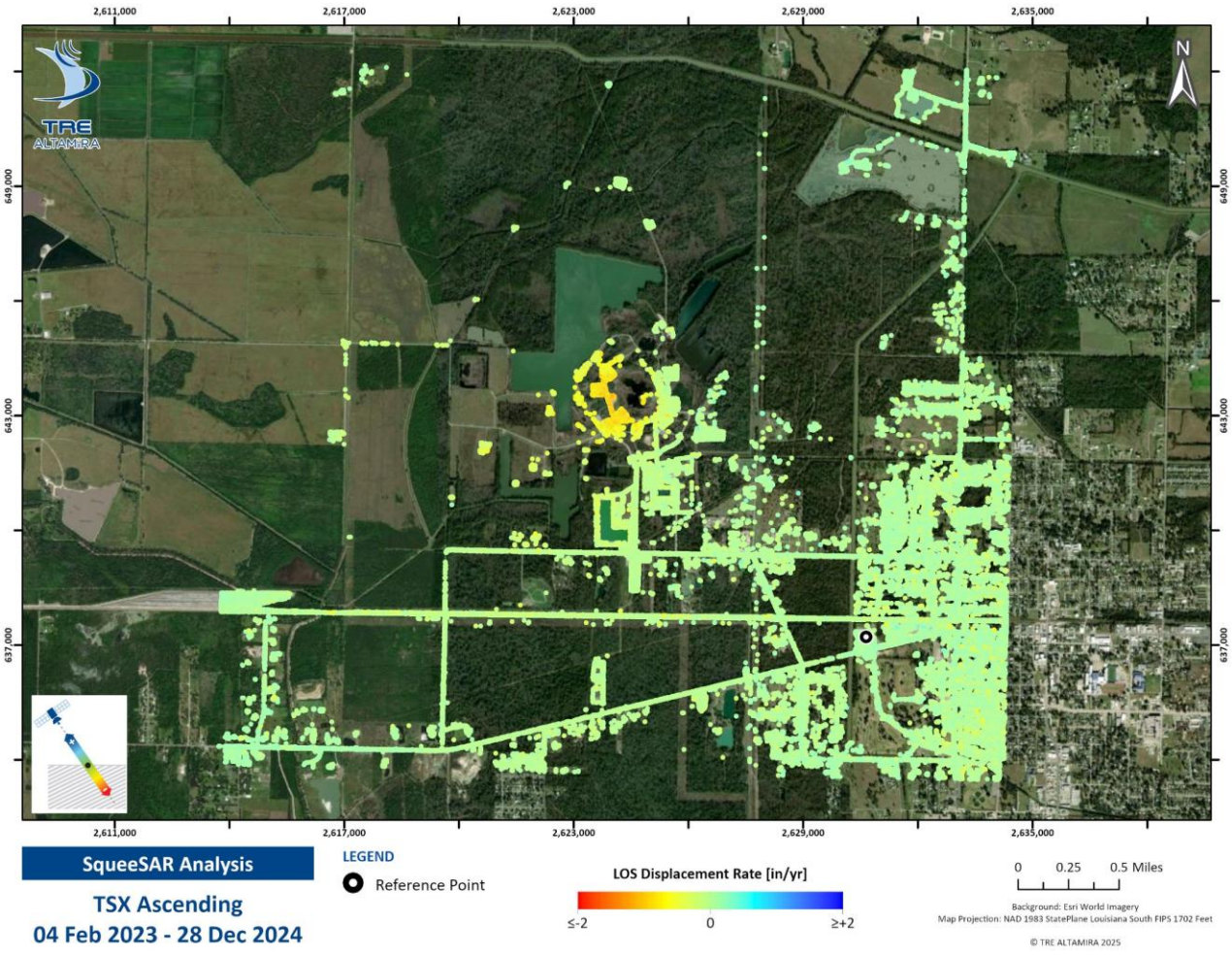

Figure 4. TerraSAR-X ascending LOS SqueeSAR annual displacement rate (February 2023 – December 2024).

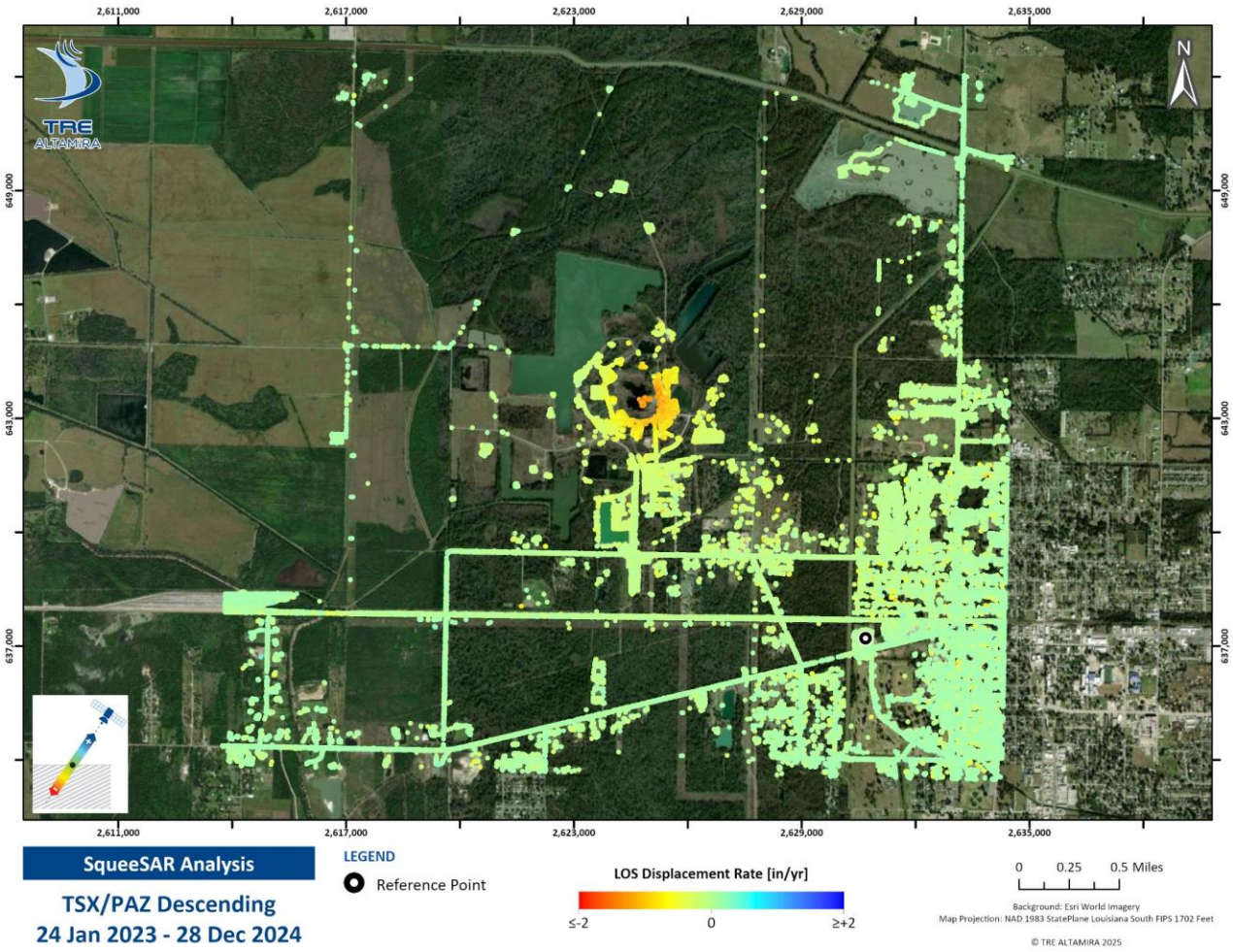

Figure 5. TerraSAR-X descending LOS SqueeSAR annual displacement rate (January 2023 – December 2024).

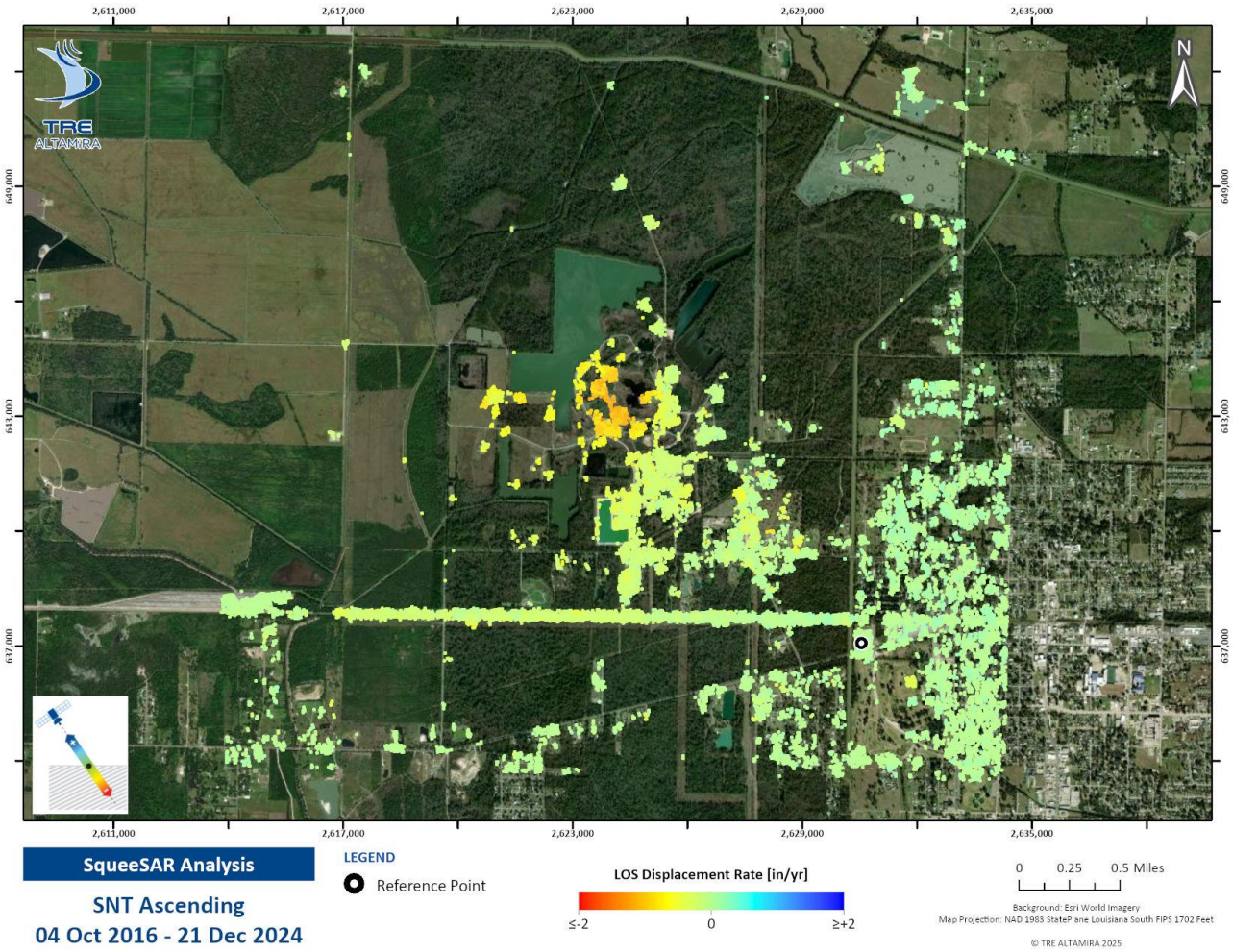

Figure 6: Sentinel ascending LOS SqueeSAR annual displacement rate (October 2016 – December 2024).

SqueeSAR measurements are differential compared to a local reference point (REF), and contain two precision indices:

- Displacement rate standard deviation (V_STDEV): Indication of the error bar associated to the annual rate measurements with respect to the REF.
- Time series error bar (STD_DEF): Indication of the error bar associated to the displacement time series of each measurement point.

A summary of the LOS SqueeSAR results, REF location and precision indices obtained with the analysis are reported in Table 3.

Table 3: Summary of the SqueeSAR analyses characteristics.

Analysis characteristics	LOS Ascending (TSX)	LOS Ascending (SNT)	LOS Descending (TSX/PAZ)
Period covered	04 Feb 2023 – 28 Dec 2024	04 Oct 2016 – 21 Dec 2024	24 Jan 2023 – 28 Dec 2024
N. of images processed	56	216	123
Reference point location (NAD 1983 StatePlane Louisiana South FIPS 1702 (US Feet))	Long = 2,630,644.6596 Lat = 637,213.7457	Long = 2,630,542.0994 Lat = 637,077.2118	Long = 2,630,680.79156 Lat = 637,207.4842
Number of measurement points (PS/DS)	106,384 PS: 105,248 DS: 1,136	25,744 PS: 8,507 DS: 17,237	129,421 PS: 128,319 DS: 1,102
Average Point Density	3,000 pts/mi^2	1,880 pts/mi^2	3,649 pts/mi^2
Average displacement rate standard deviation (V_STDEV)	< ± 0.04 in/yr	< ± 0.04 in/yr	< ± 0.04 in/yr
Average time series error bar (STD_DEF)	± 0.06 in	± 0.20 in	± 0.07 in

3.2. 2-D (Vertical and East-West) Results

High-resolution TSX ascending and descending Line-of-Sight (LOS) results are combined to generate 2-D (vertical and east-west) ground displacement measurements over the shared data period (04 February 2023 – 28 December 2024). The 2-D readings are obtained by means of the following steps:

- A 33 x 33 ft spatial grid is overlaid onto the area of interest. LOS readings from both orbits that fall within a grid cell are averaged.
- 2-D measurements are obtained only where both ascending and descending readings fall within the same grid cell.

In Figure 7 & Figure 8:

- Vertical (Figure 7): Yellow to red indicates subsidence (downward), pale to dark blue indicates uplift (upward).
- East-West (Figure 8): Yellow to red/brown indicates westward motion, pale to dark blue indicates eastward motion.
- Note: with current satellite configurations, InSAR is not able to measure north-south movement.

Data Details:

- Reference Point (REF): 2-D measurements are calculated relative to a reference point.
- Precision: The standard deviation of the displacement rate indicates measurement precision.
- Table 4: Summarizes 2-D results, REF location, and precision indices.

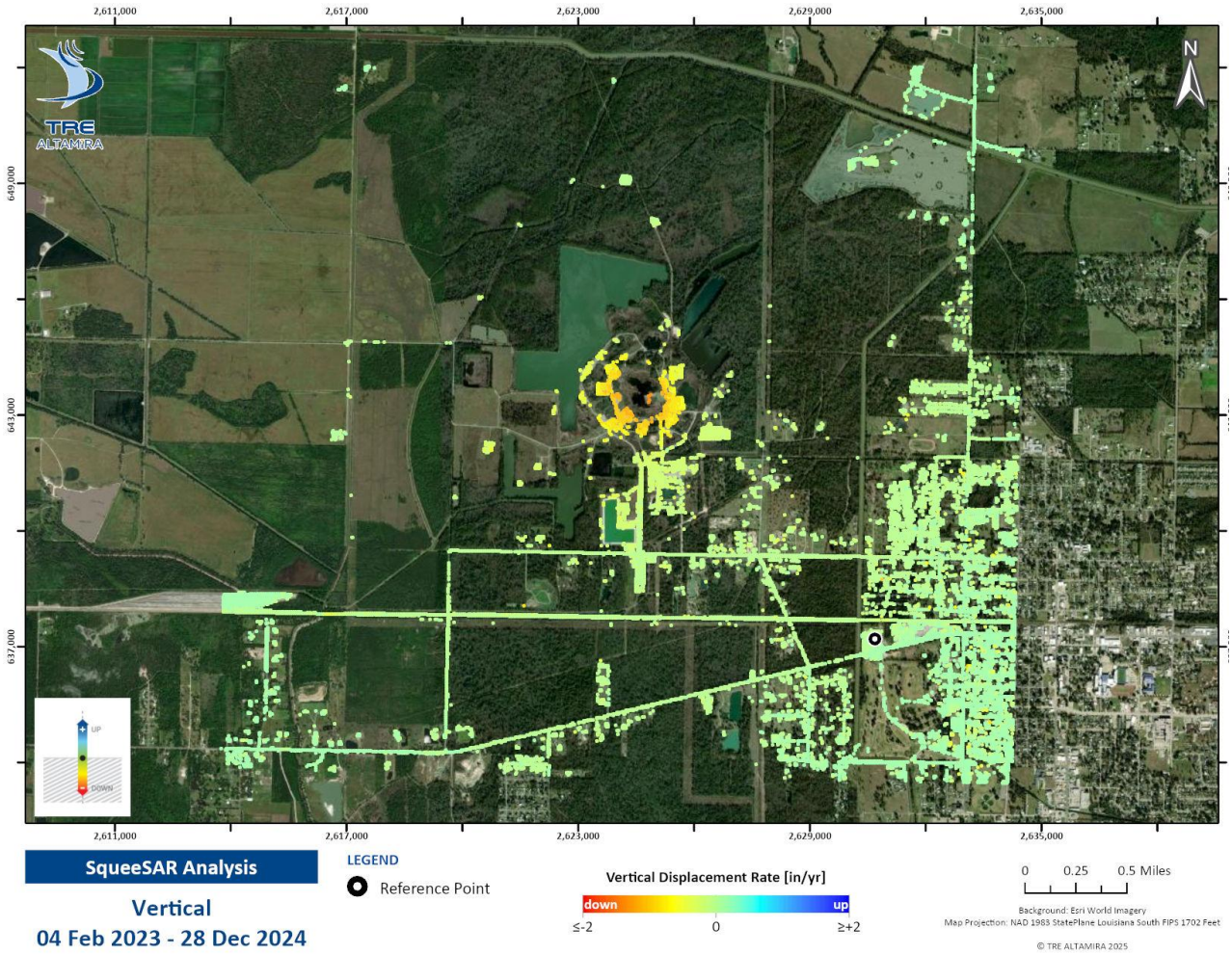

Figure 7: Vertical annual displacement rate (February 2023 – December 2024).

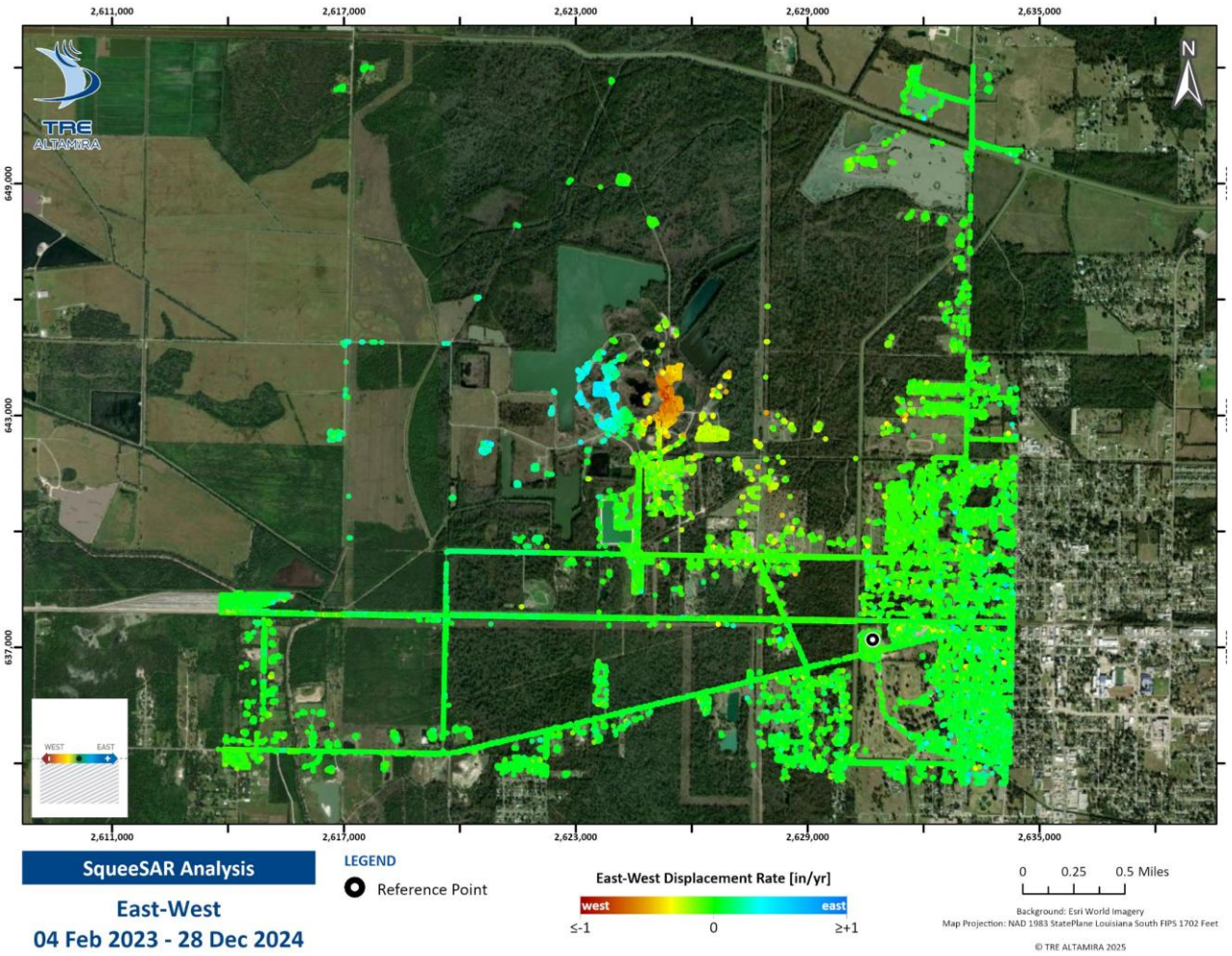

Figure 8: East-West annual displacement rate (February 2023 – December 2024).

Table 4: Summary of the 2-D SqueeSAR analysis.

Analysis characteristics	Vertical	East-West
Period covered	04 February 2023 – 28 December 2024	
N. of images	117	
Reference point location (NAD 1983 StatePlane Louisiana South FIPS 1702 (US Feet))	Long = 2,630,682.1970 Lat = 637,200.5047	
Number of cells	17,187	
Cell size	33 x 33 ft	
Average displacement rate standard deviation (V_STDEV)	±0.02 in/yr	±0.02 in/yr

3.3. Corner Reflector Results

Ascending and descending results of the 15 Corner Reflectors installed over the Sulphur Mine dome are used to provide vertical and E-W movement (Figure 9 and Figure 10). Corner Reflector (CR) measurements are differential compared to the reference CR (CR10). Note that the CR monitoring commences after the installation date of all CRs.

Comparisons of the 2-D SqueeSAR analysis with the CR monitoring should consider that the SqueeSAR 2-D data is derived using a grid (average of LOS measurement within each cell) while 2-D CR measurements are derived directly from each CR. Furthermore, the periods covered by the two analyses are different (Table 5).

Table 5: Comparison of TerraSAR-X satellite characteristics for annual SqueeSAR analysis and monthly CR monitoring over Sulphur Mine.

Satellite	Analysis	Orbit	Date Range
TerraSAR-X	SqueeSAR (NR)	Ascending	04 Feb 2023 – 28 Dec 2024
		Descending	24 Jan 2023 – 28 Dec 2024
	Corner Reflector (CR)	Ascending	27 Jul 2024 – 28 Dec 2024
		Descending	27 Jul 2024 – 28 Dec 2024

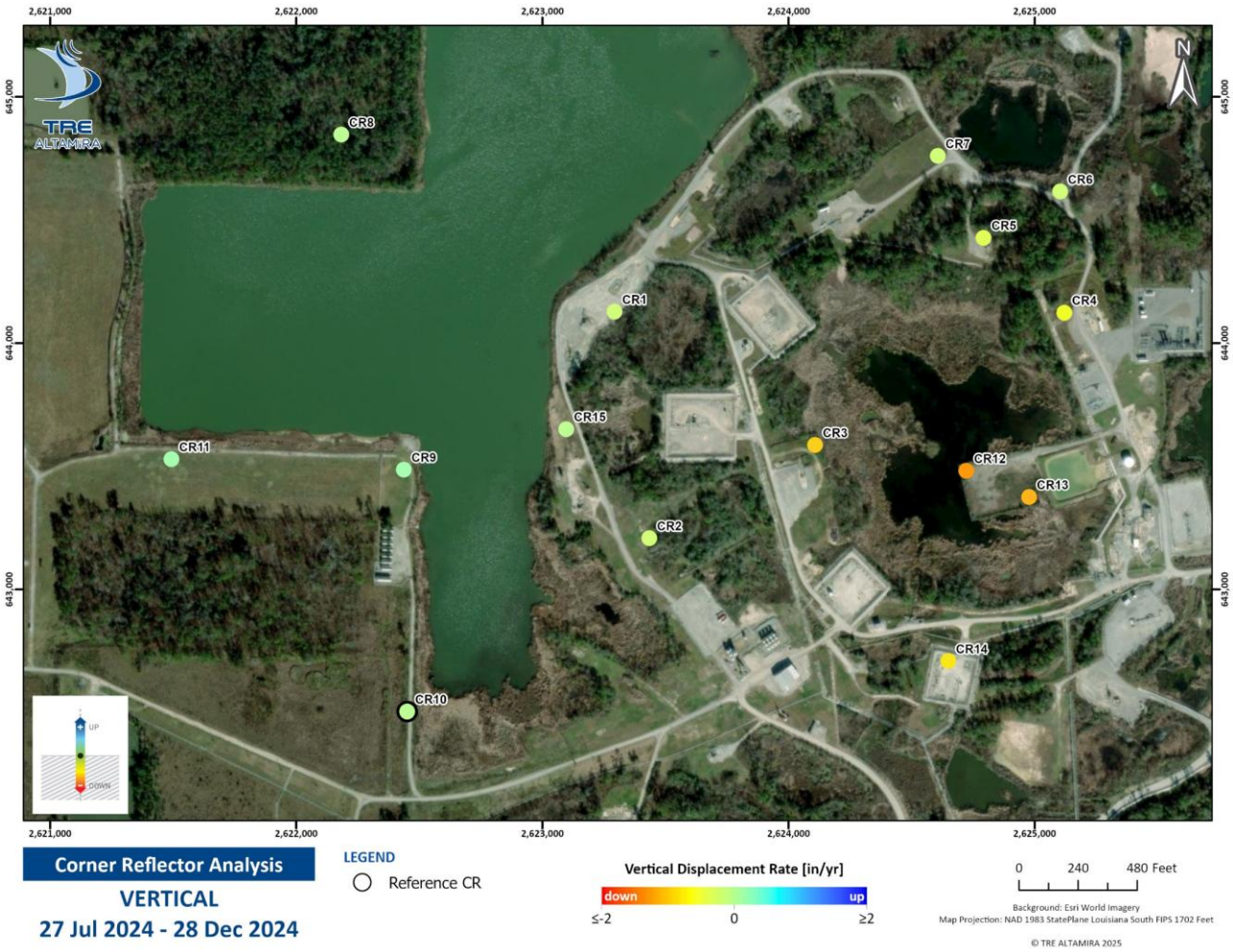

Figure 9: Vertical corner reflector annual displacement rate (July 2024 – December 2024).

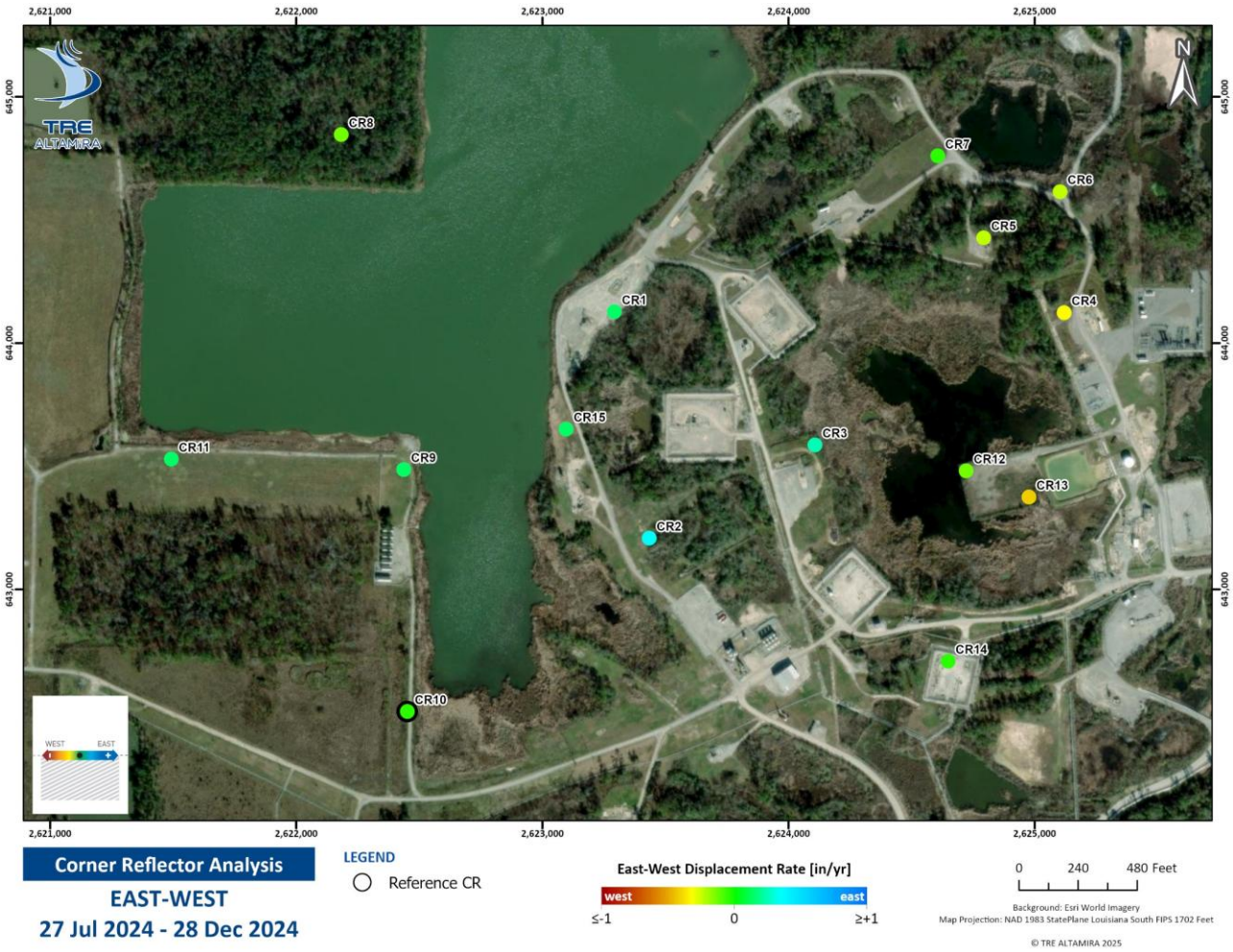

Figure 10: East-West corner reflector annual displacement rate (July 2024 – December 2024).

4. Observations

Ground displacement observations are based on the 2-D results (vertical and east-west) over the areas of interest (Figure 11) provided by Lonquist (InSAR_AOIs_2-12-2024), by means of maps of the displacement rate and average time series (ATS). Subsection 4.2 focuses on the Corner Reflectors installed in July 2024.

- ATS: calculate the average displacement of all measurement points within a polygon/area.
- The displacement rate, cumulative displacement and displacement rate error bar values are displayed in the legend at the top of each figure in imperial units.

In areas where the 2-D results are sparser or do not have good coverage, it is recommended to refer to the LOS results for greater detail.

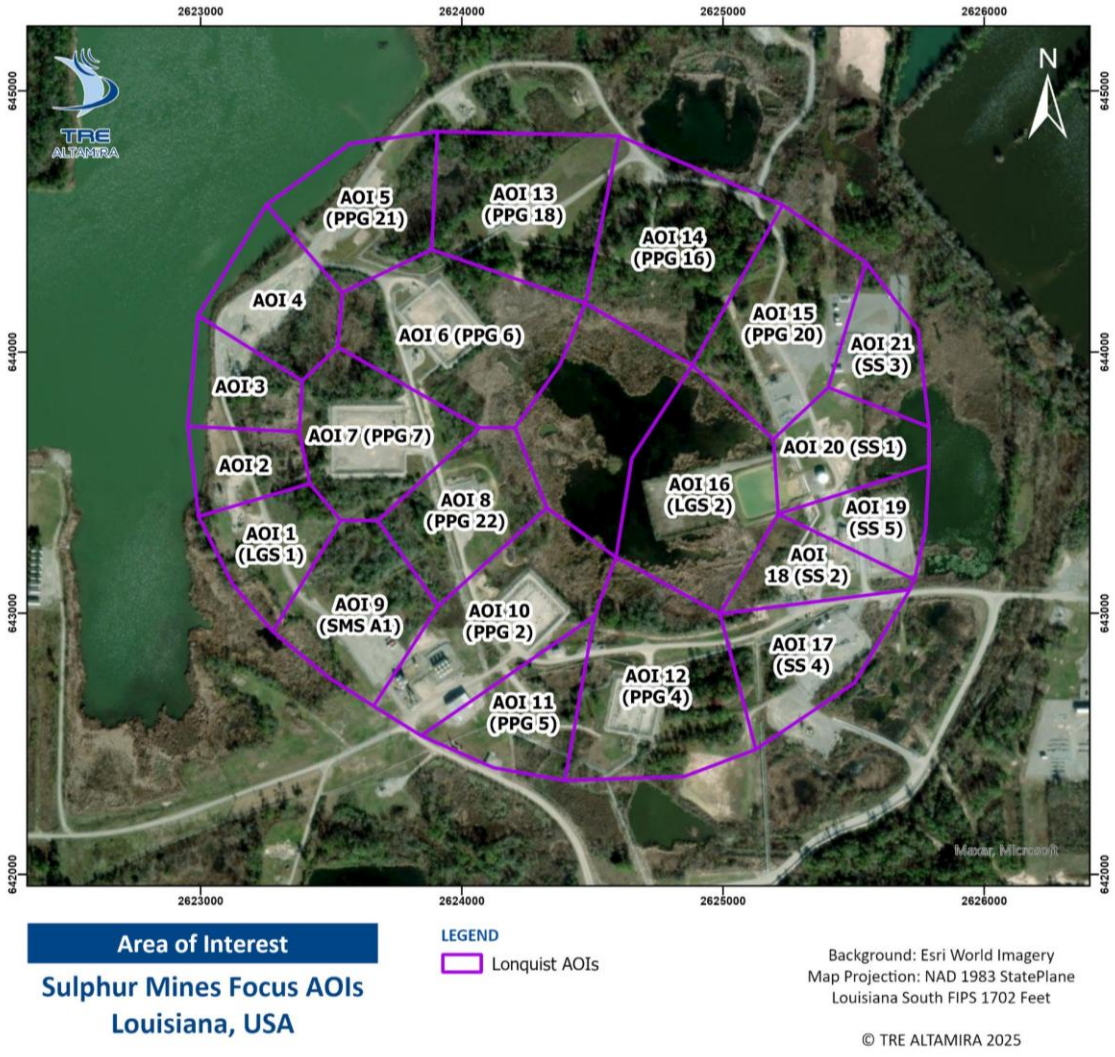

Figure 11: Focus areas of interest provided by Lonquist.

4.1. Average Time Series over Focus Areas of Interest

Average Time Series calculate the average displacement of all measurement points that fall within the polygon (note that the number of points will vary for each polygon). Figure 12 indicates the AOIs used for the ATS, along with the vertical and east-west displacement rates, respectively.

Key Findings:

- The highest average vertical displacement rate was observed at Area 16, reaching -1.52 in/yr of subsidence (Figure 13).
- The highest average E-W horizontal displacement rate was observed at Area 20, reaching -0.69 in/yr westward (Figure 13).

A summary of the displacement rates measured within all ATS polygons is shown in Table 6 and the individual average time series are shown in Appendix 3. Limited 2-D displacement rate information is available for Area 14 as there are too few overlapping LOS points in this polygon – for additional information in this area refer to the LOS data.

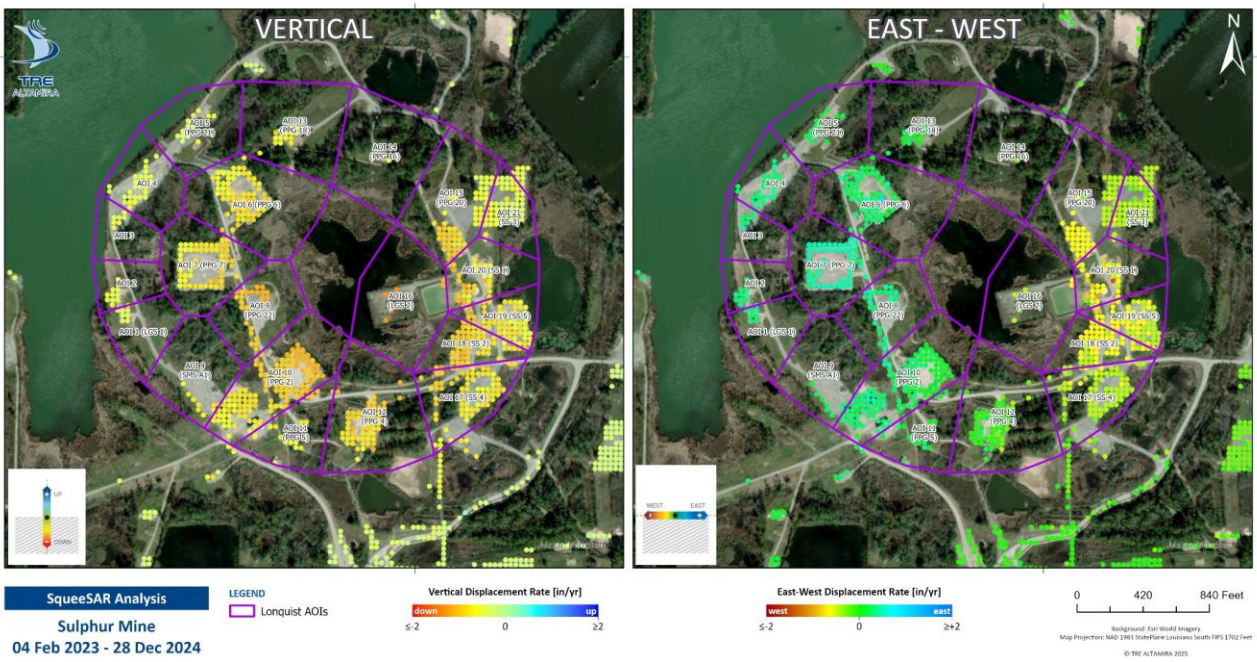

Figure 12: Vertical and East-West displacement rates over the focus AOIs used for ATS polygons.

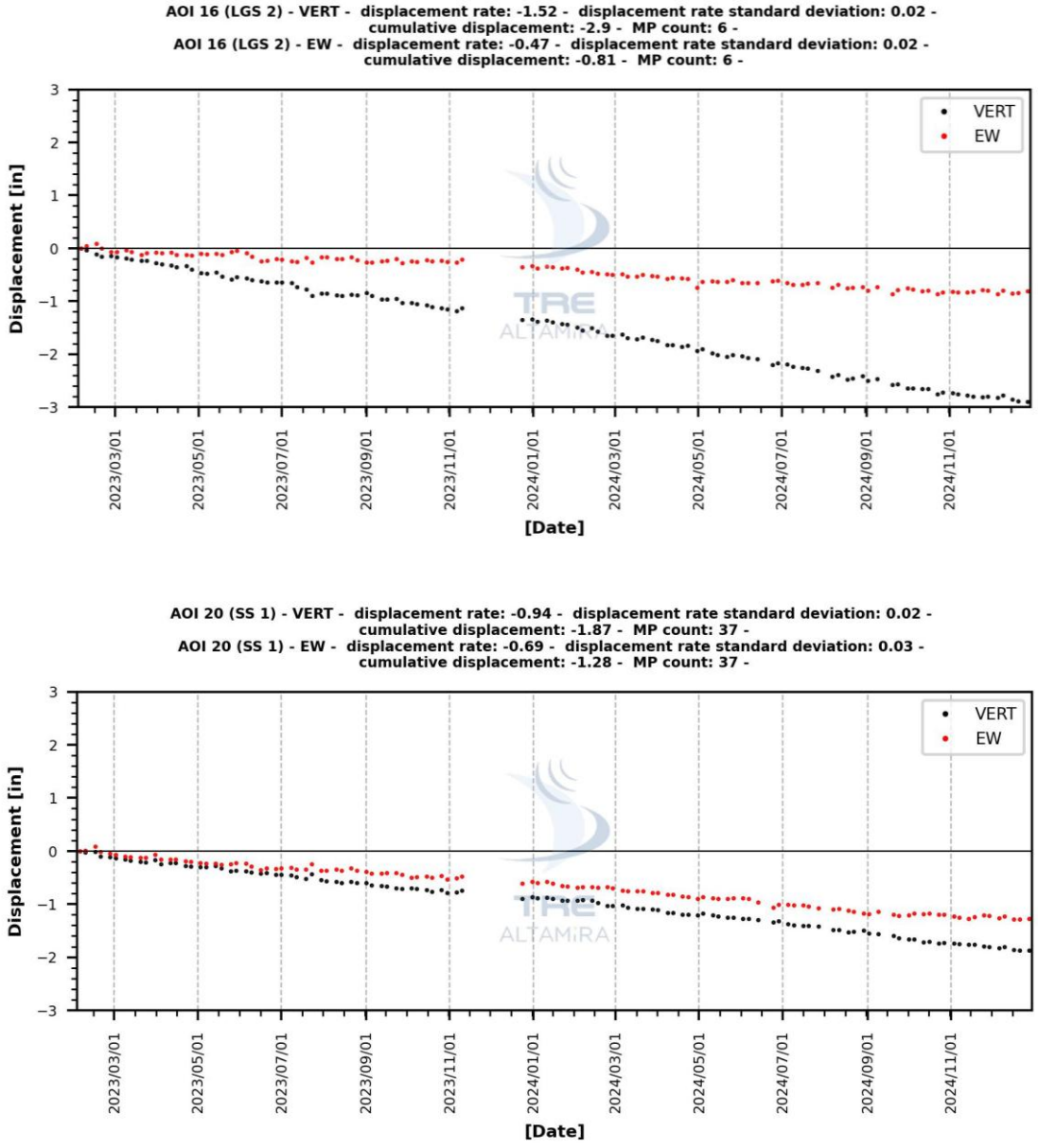

Figure 13: Average time series of Area 16 and Area 20 showing the highest vertical and east-west displacement rates, respectively.

Table 6. Summary of the Vertical and East-West displacement rates and associated standard deviation values observed within each of the focus area ATS polygons.

Monument	VERT Displacement Rate ± Standard Deviation (in/yr)	EW Displacement Rate ± Standard Deviation (in/yr)	Measurement Points count
AOI 1 (LGS 1)	-0.57 ± 0.02	+0.37 ± 0.02	9
AOI 2	-0.61 ± 0.02	+0.38 ± 0.03	10
AOI 3	-0.55 ± 0.02	+0.34 ± 0.03	6
AOI 4	-0.51 ± 0.02	+0.33 ± 0.03	32
AOI 5 (PPG 21)	-0.56 ± 0.02	+0.22 ± 0.03	19
AOI 6 (PPG 6)	-0.87 ± 0.02	+0.27 ± 0.03	66
AOI 7 (PPG 7)	-0.86 ± 0.02	+0.45 ± 0.03	61
AOI 8 (PPG 22)	-1.17 ± 0.02	+0.38 ± 0.03	25
AOI 9 (SMS A1)	-0.74 ± 0.02	+0.33 ± 0.03	15
AOI 10 (PPG 2)	-1.0 ± 0.02	+0.24 ± 0.02	131
AOI 11 (PPG 5)	-0.89 ± 0.02	+0.11 ± 0.03	21
AOI 12 (PPG 4)	-1.02 ± 0.02	-0.16 ± 0.03	60
AOI 13 (PPG 18)	-0.72 ± 0.02	+0.08 ± 0.03	15
AOI 14 (PPG 16)	-0.81 ± 0.02	-0.4 ± 0.03	4
AOI 15 (PPG 20)	-0.83 ± 0.02	-0.6 ± 0.03	59
AOI 16 (LGS 2)	-1.52 ± 0.02	-0.47 ± 0.02	6
AOI 17 (SS 4)	-0.87 ± 0.02	-0.49 ± 0.03	75
AOI 18 (SS 2)	-1.01 ± 0.02	-0.63 ± 0.03	56
AOI 19 (SS 5)	-0.85 ± 0.02	-0.63 ± 0.03	61
AOI 20 (SS 1)	-0.94 ± 0.02	-0.69 ± 0.03	37
AOI 21 (SS 3)	-0.59 ± 0.02	-0.49 ± 0.03	56

4.2. Time Series over Corner Reflectors

There are three GNSS stations (GPS NW, GPS SW, and GPS SE) that are co-located with the corner reflectors - GPS SW is co-located with the CR InSAR reference point. Figure 14 indicates the GNSS stations, along with the InSAR vertical and east-west displacement rates, respectively.

Key Findings:

- The highest vertical displacement rate was observed at CR 12, reaching -1.4 in/yr of subsidence (Figure 15).
- The highest E-W horizontal movement was observed at CR 13, reaching -0.45 in/yr westward (Figure 15).
- Displacement time series are shown for both the GNSS and the CRs for the co-located stations (GPS NW and GPS SE) positioned at CR 8 and CR 14, respectively (Figure 16 and Figure 17)
- The displacement rates observed at the co-located CRs and GNSS stations are comparable.

A summary of displacement rates of each CR is shown in Table 7 and the individual time series are shown in Appendix 4. Displacement for CR10 is set to zero as it is the reference point.

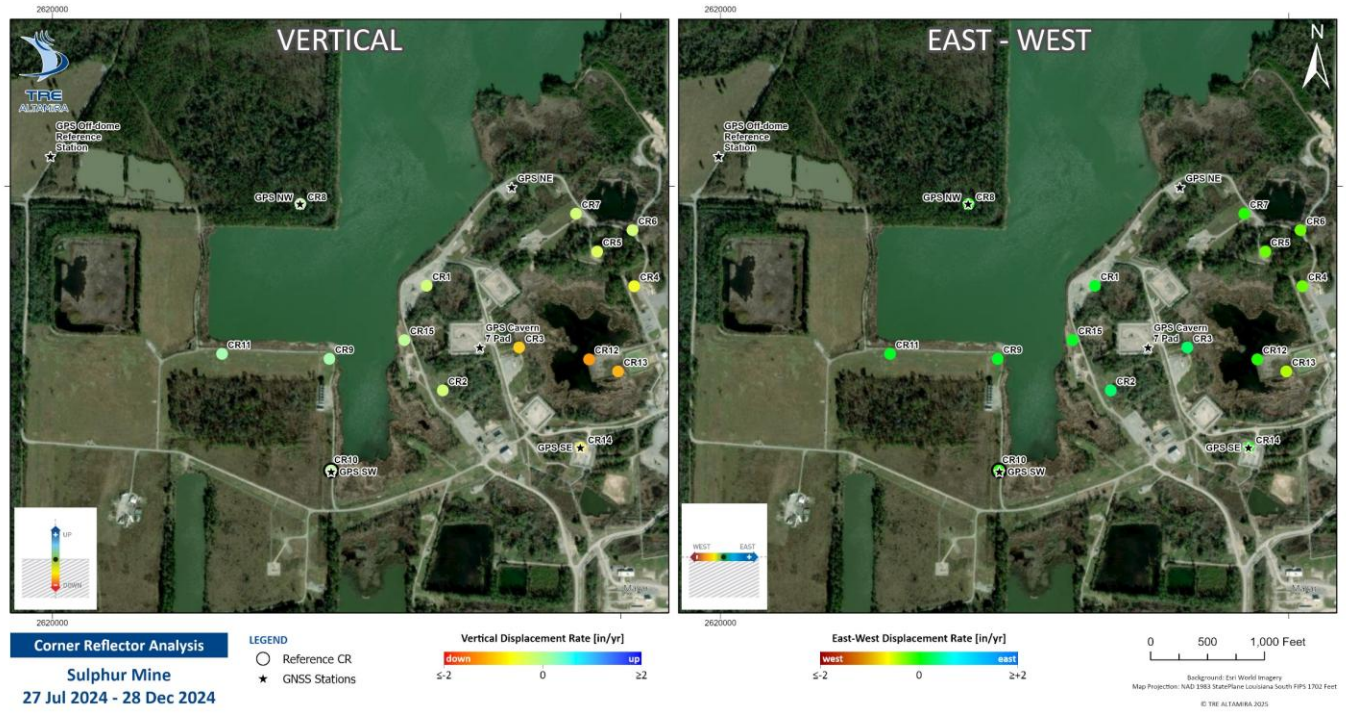

Figure 14: Vertical and East-West displacement rates overlay with GNSS station over the dome.

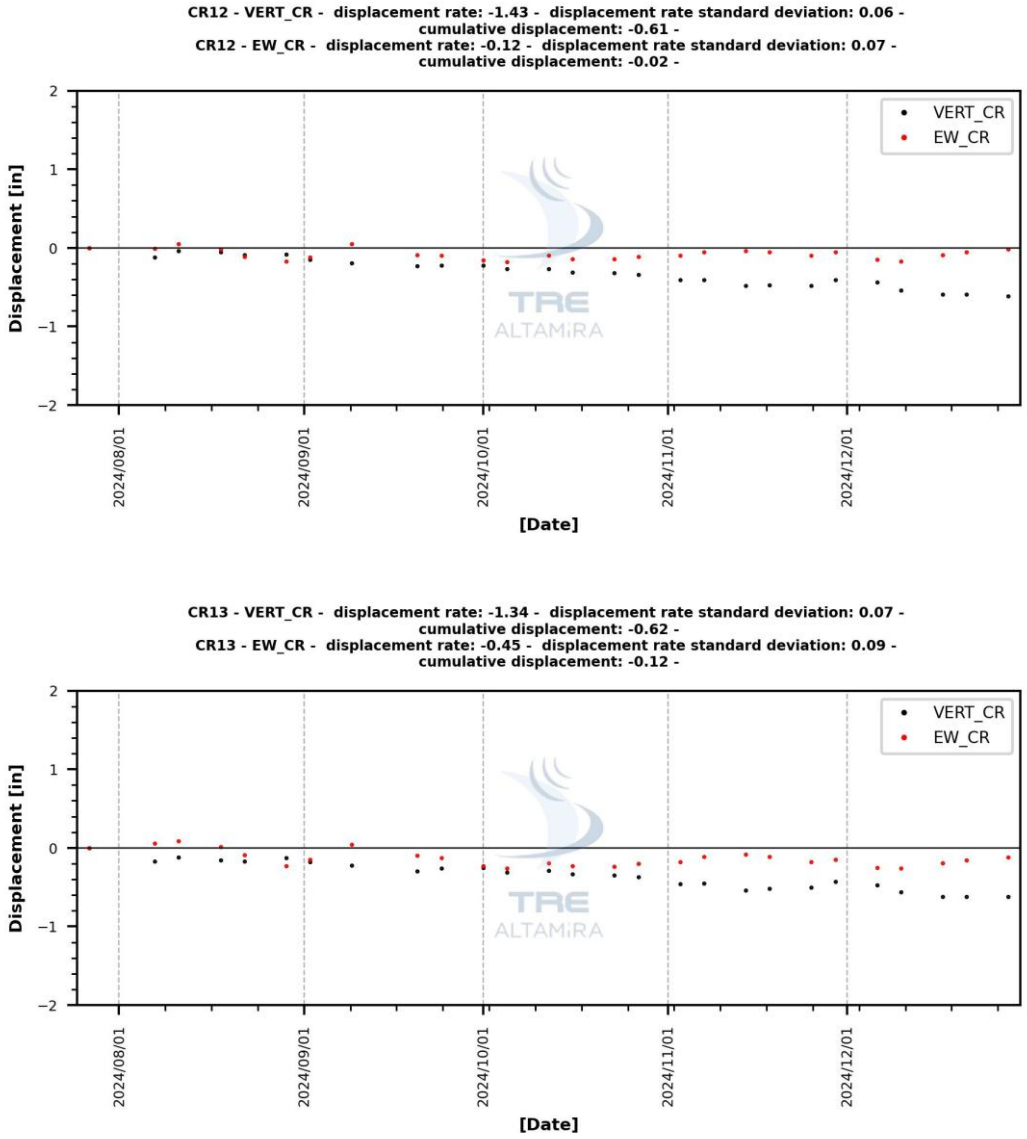

Figure 15: Time Series of CR 12 and CR 13 showing the highest vertical and east-west displacement rates, respectively.

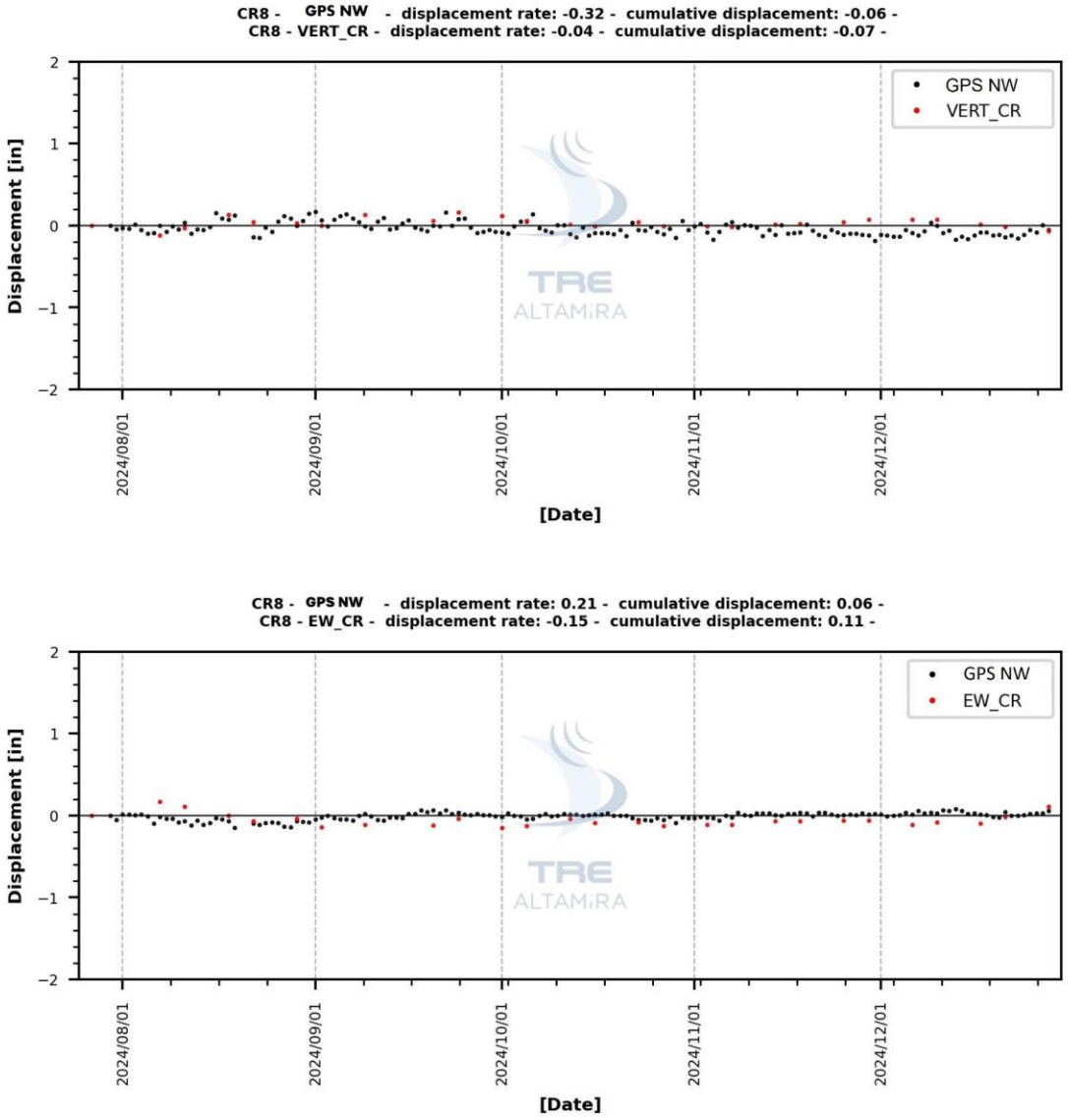

Figure 16: Time Series of CR 8 and GPS NW showing the vertical and east-west displacement rates, respectively.

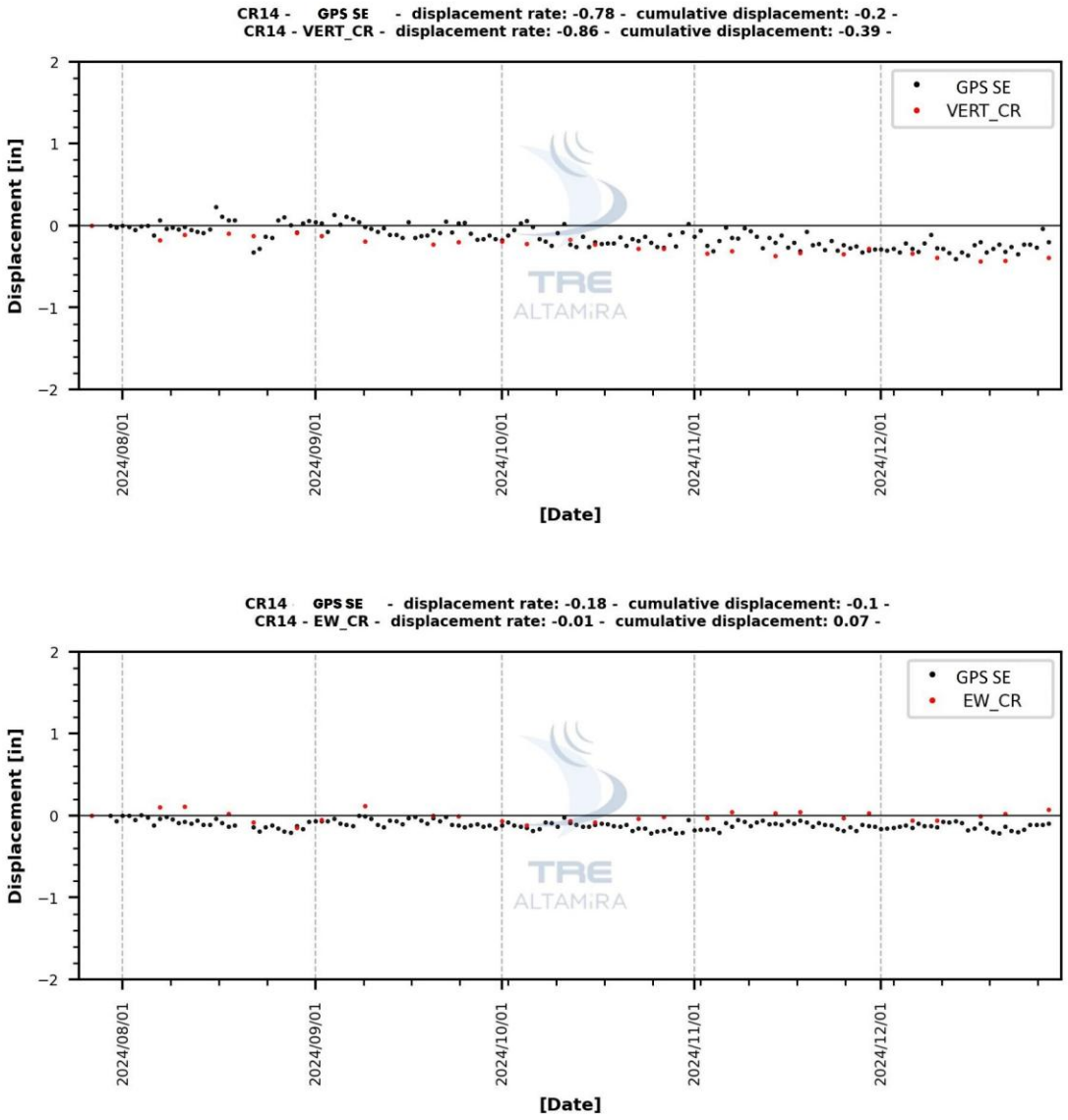

Figure 17: Time Series of CR 14 and GPS SE showing the vertical and east-west displacement rates, respectively.

Table 7. Summary of the Vertical and East-West displacement rates and associated standard deviation values observed at each of Corner Reflector.

CR	VERT Displacement Rate ± Standard Deviation (in/yr)	EW Displacement Rate ± Standard Deviation (in/yr)
CR 1	-0.32 ± 0.04	+0.11± 0.06
CR 2	-0.26 ± 0.06	+0.33 ± 0.07
CR 3	-1.0 ± 0.05	+0.25 ± 0.07
CR 4	-0.68 ± 0.07	-0.36 ± 0.09
CR 5	-0.41 ± 0.06	-0.27 ± 0.08
CR 6	-0.3 ± 0.07	-0.21 ± 0.09
CR 7	-0.28 ± 0.07	-0.04 ± 0.09
CR 8	-0.04 ± 0.06	-0.15 ± 0.08
CR 9	+0.03 ± 0.04	+0.12 ± 0.06
CR 10	-	-
CR 11	+0.06 ± 0.04	+0.15 ± 0.06
CR 12	-1.43 ± 0.06	-0.12 ± 0.07
CR 13	-1.34 ± 0.07	-0.45 ± 0.09
CR 14	-0.86 ± 0.07	-0.01 ± 0.09
CR 15	-0.19 ± 0.05	+0.13 ± 0.06

5. Summary

The InSAR monitoring of the Sulphur Mines Salt Dome has been upgraded over time and now includes high resolution satellite imagery for both the ascending and descending orbits, with high-resolution TSX data now replacing the lower-resolution SNT data, leading to a higher density of measurement points. 15 Corner Reflectors have also been added, with 3 CRs co-located with GNSS stations, to further enhance the monitoring.

This annual technical report (covering 04 February 2023 – 28 December 2024) draws upon the monitoring of the past year to provide observations over the key areas of interest designated by Lonquist.

Key Findings:

SqueeSAR Analysis:

- Subsidence was observed across the entire dome, with an average displacement rate of -1.52 inches/year at AOI 16. Westward displacement was concentrated at AOI 20, reaching an average displacement rate of -0.69 inches/year, while eastward displacement was noted at AOI 6, reaching an average displacement rate of +0.45 inches/year. AOIs 8, 12, 16, and 18 exhibited the highest subsidence rates.
- Eastward displacement was most significant eastward in AOIs 1, 2, 7, and 8.
- Westward displacement was highest in AOIs 18, 19, and 20.

Corner Reflector Data:

- The highest subsidence rate was observed at CR 12 in AOI 16 (-1.43 inches/year).
- The highest eastward displacement was at CR 2 in AOI 1 (0.33 inches/year).
- The highest westward displacement was at CR 13 in AOI 1 (-0.45 inches/year).

Monitoring:

- Ongoing monitoring is continuing with descending images in 4/7-day frequency (TSX/PAZ) and ascending images in 11-day (TSX and 2-D) frequency.

Recommendation:

To maintain optimal data quality, TREA recommends periodically resetting the Sulphur Mines baseline approximately every 12-24 months. This interval depends on data coverage and local conditions.

Appendix 1: Delivered Files

All results are delivered via TREmaps® web platform (https://tremaps.com/) our proprietary online GIS platform to view and interrogate the SqueeSAR data. For login instructions and main functionalities, please use the Help page (https://help.tremaps.com/tremaps/)

Table 8 lists the deliverables including the present report and the InSAR data files, delivered via the TREmaps platform.

The SqueeSAR data is provided in shapefile (.shp) format, imperial units and NAD 1983 State Plane Louisiana South FIPS 1702 ft coordinate system. The shapefile of each elaboration contains details about the measurement points, such as displacement rate, acceleration rate, cumulative displacement, and quality indexes. The information associated within the database files (dbf) are described in Table 9.

Description		File name
SqueeSAR Data	**ASC**	SULPHUR_MINE_SNT_T136_A_20241221_IMP_3452_Xflxkp3v9A007S.shp SULPHUR_MINE_SNT_T136_A_20241221_Xflxkp3v9A3S.shp SULPHUR_MINE_TSX_T52_A_20241228_IMP_3452_DEC2024.shp SULPHUR_MINE_TSX_T52_A_20241228_DEC2024.shp
	DESC	SULPHUR_MINE_TSX_T67_D_20241228_IMP_3452_DEC2024.shp SULPHUR_MINE_TSX_T67_D_20241228_DEC2024.shp
	2-D	SULPHUR_MINE_VERT_20241228_IMP_3452_DEC2024.shp SULPHUR_MINE_VERT_20241228_DEC2024.shp SULPHUR_MINE_EW_20241228_IMP_3452_DEC2024.shp SULPHUR_MINE_EW_20241228_DEC2024.shp
CR Data	**ASC**	SULPHUR_CR_A_3452_IMP_DEC2024.shp SULPHUR_CR_A_DEC2024
	DESC	SULPHUR_CR_D_3452_IMP_DEC2024.shp SULPHUR_CR_D_DEC2024
	2-D	SULPH_CR_VERT_3452_IMP_DEC2024.shp SULPHUR_CR_VERT_DEC2024 SULPHUR_CR_EW_3452_IMP_DEC2024.shp SULPHUR_CR_EW_DEC2024
Technical Report		TREA_Lonquist_SulphurMines_InSAR_Monitoring_Report_Jun2025.pdf

Table 8: List of deliverables.

Field	Description
CODE	Measurement Point (MP) identification code.
HEIGHT	Topographic Elevation referred to input DEM [ft].
H_STDEV	Height standard deviation of the measurement point [ft].
VEL	MP displacement rate [in/yr]. – **LOS:** Positive values correspond to motion toward the satellite; negative values correspond to motion away from the satellite. – **Vertical (VEL_V):** Positive values indicate uplift; negative values indicate downward movement. – **E-W Horizontal (VEL_E):** Positive values indicate eastward movement; negative values westward movement.
V_STDEV	Displacement rate standard deviation [in/yr].
ACC	Acceleration rate [in/yr^2].
A_STDEV*	Standard deviation of the acceleration value [in/yr^2].
COHERENCE*	Quality measure between 0 and 1.
STD_DEF*	Displacement time series error bar [in]
EFF_AREA*	This parameter represents the effective extension of the area [ft^2] covered by Distributed Scatterers (DS). For permanent scatterers (PS), its value is set to 0.
CH_TIME*	Date in which an image has been identified with either a change in amplitude or date of intiial loss of coherence.
Dyyyymmdd	Series of columns that contain the displacement values of successive acquisitions relative to the first acquisition available [in].

Table 9: Description of the fields contained in the LOS and 2-D database. *Field is only present in LOS data sets.

Appendix 2: Technique Description

6. SqueeSAR®

SqueeSAR® is the advanced multi-image InSAR algorithm patented by TREA that provides high precision measurements of ground displacement in the form of a point cloud. By analyzing a stack of SAR images acquired over a site, the SqueeSAR algorithm identifies and measures the movement of radar reflectors on the ground surface that remain visible and coherent throughout the period of the analysis.

Radar reflectors belong to two different families (Figure 18):

- Permanent Scatterers (PS): point-wise radar targets characterized by highly stable radar signal returns (e.g. buildings, rocky outcrops, infrastructures, etc.)
- Distributed Scatterers (DS): patches of ground exhibiting a lower but homogenous radar signal return (e.g. rangeland, debris fields, arid areas, etc.). DS are represented as individual points, but the information does not refer to a single target, but rather to the patch of ground associated with each DS (the size [km2] but not the exact shape of the patch is provided).

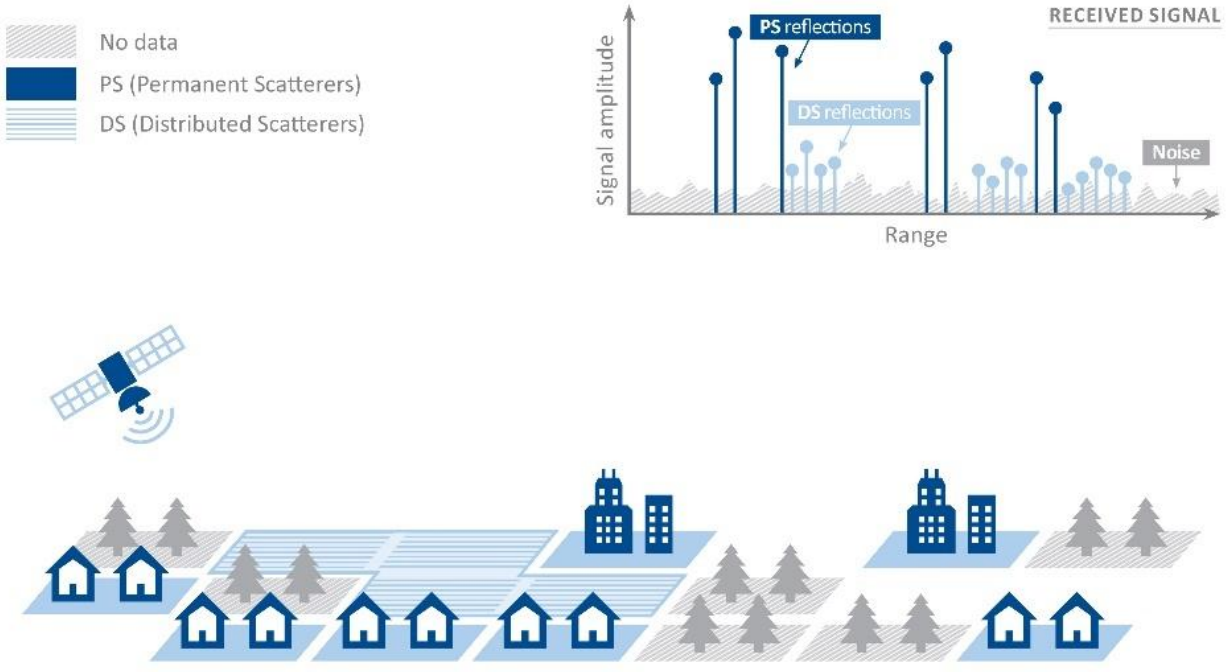

Figure 18: Schematic of PS and DS radar targets.

6.1. 1-D (LOS) Measurements

SAR satellites image the ground from ascending and descending orbits, according to the flight direction, from south to north (imaging to the east) and from north to south (imaging to the west) respectively (Figure 19). InSAR measures the projection of the real vector of displacement onto the satellite line-of-sight (LOS) and provides 1-D measurements along the LOS, which is inclined with respect to the vertical and north-south direction (θ and δ angle, respectively).

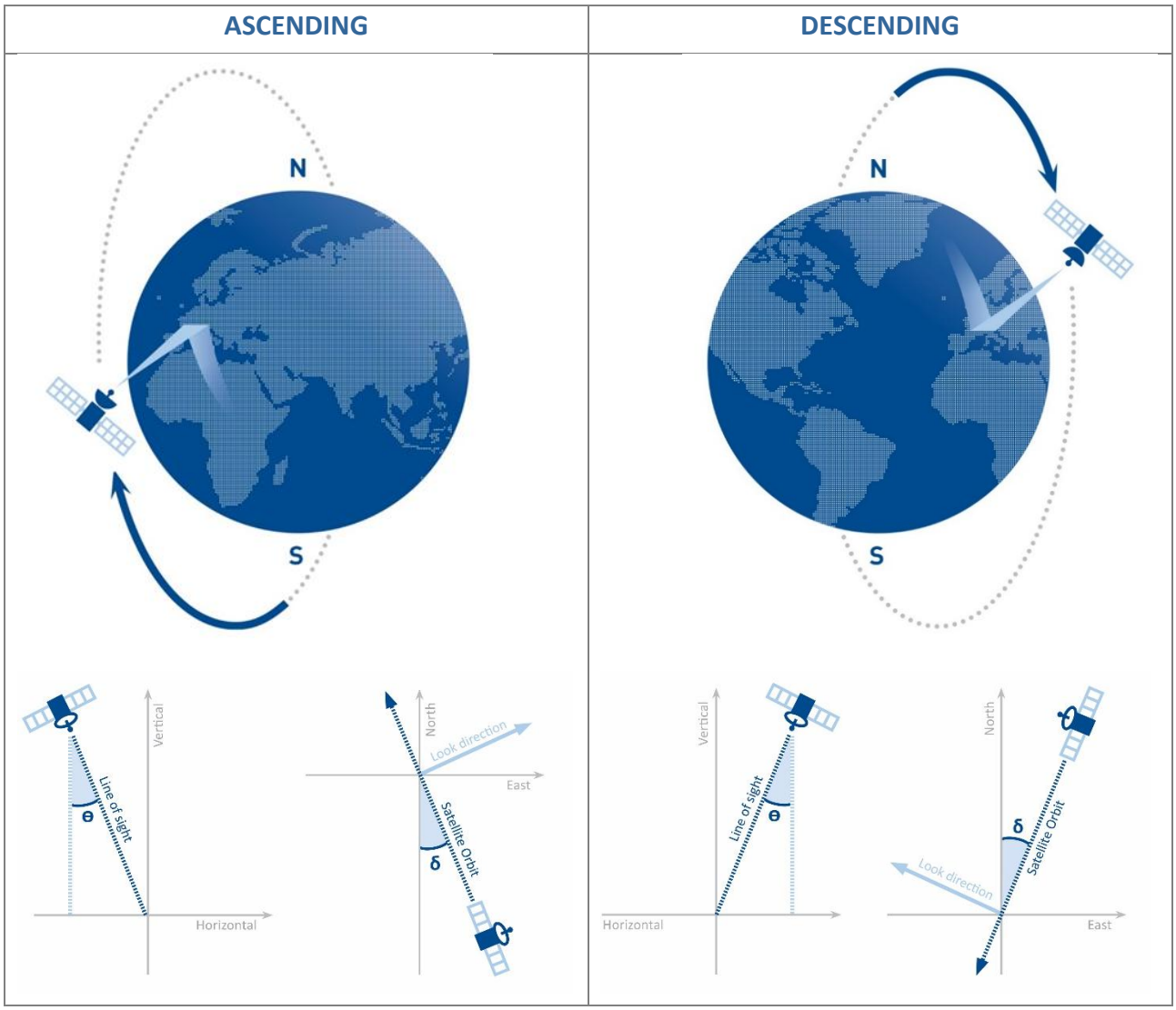

Figure 19: SAR satellites image the ground from ascending and descending orbits, according to the flight direction, from south to north (imaging to the east) and from north to south (imaging to the west), respectively. The satellite Line Of Sight (LOS) is inclined with respect to the vertical and north-south direction (θ and δ angle, respectively).

As SqueeSAR measurements are 1-D (i.e. away or toward the satellite), the sign and value of the displacement depends on the orientation of the real displacement with respect to the LOS (Figure 20). Negative values (from green to red) indicate movement away from the satellite, while positive values (from green to blue) indicate movement towards the satellite. A same displacement produces different readings when viewed from different LOS angles (Figure 20).

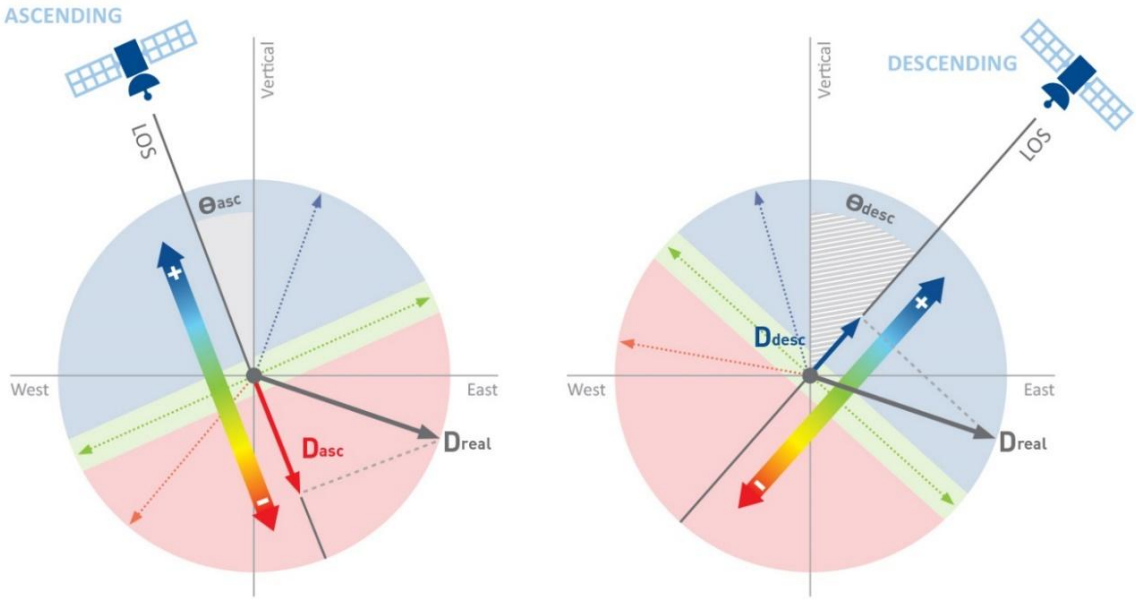

Figure 20: SqueeSAR measures the projection of real movement (Dreal) onto the LOS. The same real movement (Dreal) produces a different value from a different LOS (different inclination or different orbits). Real displacement vectors (Dreal) within the blue areas will produce positive LOS measurements while those within the red areas will produce negative LOS values. Real displacement vectors within the green band (i.e. perpendicular to the satellite LOS) will produce small (i.e. close to zero) LOS measurements.

SqueeSAR measurements are differential in space and time: spatially they are related to a local reference point (REF) and temporally to the date of the first available satellite image. The REF is assumed to be motionless and selected for its radar properties to optimize the quality of the measurements. It corresponds to a radar target with a high coherence signal in all the images of the archive and that is not affected by displacement rate variations (non-linear movement or cyclical deformations) in the analysis period. The selection of the REF is imagery dependent. If the imagery changes (number of images and/or time span), the MP selected as the REF can change. The absolute movement of the REF point can be defined only with calibration to a GNSS network.

For each measurement point (MP), SqueeSAR provides the following main information:

- Position and elevation estimated with respect to the input DEM [ft].
- Displacement time series (TS) representing the evolution of the displacement for each acquisition date [mm or in] and measured along the LOS direction.
- Annual average displacement rate [in/yr], calculated from a linear regression of the displacement time series over the analysis period and referred to the REF.

SqueeSAR is best suited for displacement rates < 3.3ft /yr.

6.1.1. Measurement Point Density and Coverage

The density and distribution of MPs identified by the analysis depends on the resolution of the imagery, the surface characteristics, changes over time and topography of the area. In detail, MP density and coverage increases with satellite resolution and decreases over (Figure 21):

- Vegetated and low reflectivity areas (i.e., areas where the signal backscattered to the satellite is low).
- Areas affected by temporal decorrelation (i.e. radar signal is not coherent over time), which is generally associated with rapid surface changes (such as active operations areas), seasonal surface changes (such as floods or snow-coverage) or fast movement (displacement rate >3.3ft/yr)
- Areas where the satellite has visibility limitations, because of the Line of Sight (LOS) orientation with respect to the local topography.

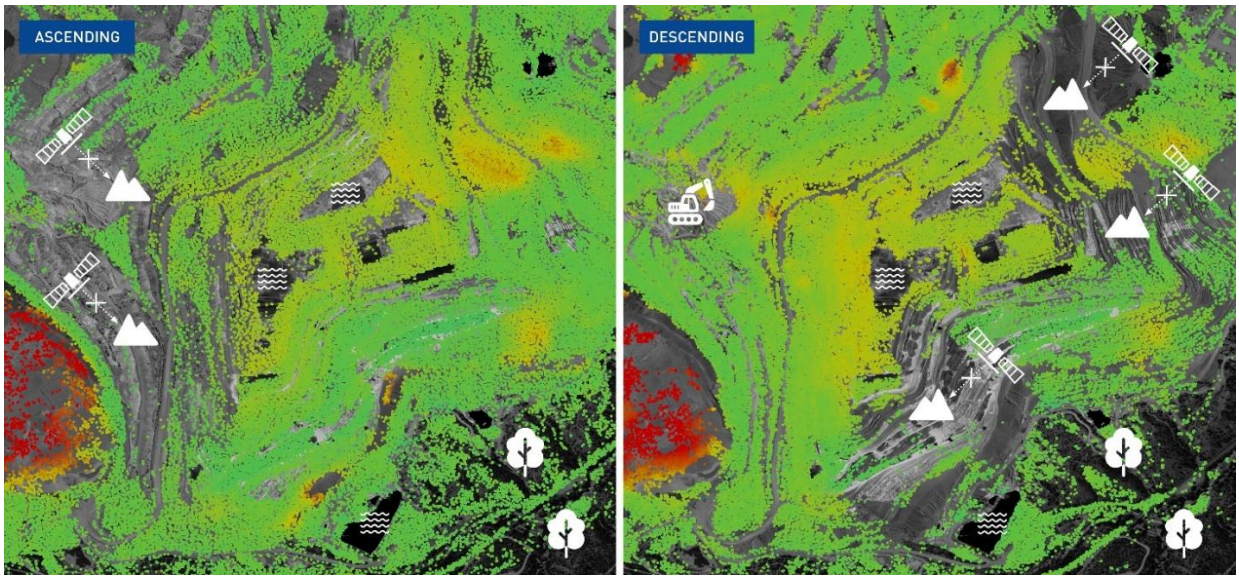

Figure 21: Example of point coverage over a mine site. The MPs coverage is low over areas with vegetation, areas of surface operations or where the visibility is limited due to the orientation of the slope with respect to the satellite line of sight. Generally, west-facing slopes have a better coverage in ascending orbit while east-facing slopes has a better visibility on descending orbit.

6.1.2. Measurement Precision

SqueeSAR can measure displacement with precision up to one-hundredth of an inch. The precision depends on a correct phase unwrapping and atmospheric contribution estimation and increases with the quality of the imagery and the coherence of the signal. In particular, the precision:

- Increases with the number of processed images, the length of the period of the analysis, the frequency of acquisitions, the coherence of the signal (i.e. the absence of vegetation or surface disturbances) and the density of points.
- Decreases with the presence of gaps in the acquisitions, strong atmospheric disturbances, and surface variations in the period of the analysis (e.g. snow, floods, changes to the ground surface).

Typical displacement precision values obtained with a dataset of at least 30 images are reported in Table 10. SqueeSAR LOS measurements are provided with two displacement precision indices:

- The displacement rate standard deviation (V_STDEV), which provides an indication of the precision of the annual deformation rate with respect to the REF. Given the standard deviation (σ), and assuming that the errors are normally distributed (Gaussian), 95% of the rate values tend to be included in a ±2σ range. The displacement rate standard deviation increases with the distance of the point from the REF.
- The time series error bar (STD_DEF), which provide an indication of the precision of single displacement measurements. It depends on the coherence of the phase signal over time: the higher the coherence, the higher the precision of the measurements. This parameter is calculated as standard deviation of the residuals with respect to an analytic model (i.e. how well the model fits the displacement time series). The model is selected individually for each MP with an advanced Model Order Selection technique that take into consideration the quality of the imagery (number of images, time span and possible gaps in the acquisitions).

LOS measurements	Displacement rate standard deviation	Error bar of single measurement
Precision	±0.04 in/yr	±0.20 in

Table 10: Typical precision values for a MP less than 0.62 mi from the REF and a data set of at least 30 SAR scenes.

While the precision of the displacement measurements is within the order of one-hundredth of an inch, the location of individual measurement points is known with metric accuracy and depends on the satellite system being used (Table 11) As for the measurement precision, the location accuracy increases with the quality of the imagery, the coherence of the signal and the density of points.

Satellite	Band	Wavelength [in]	Resolution RGxAZ [ftxft]	North-South [ft]	East-West [ft]	Elevation [ft]
ERS - ENVI	C-band	2.20	65x16	± 6	± 23	± 5
RSAT (*Standard Beam*)	C-band	2.20	65x16	± 6	± 23	± 5
SNT	**C-band**	**2.32**	**16x65**	**± 26**	**± 39**	**±26**
CSK	X-band	1.23	10x10	± 3	± 3	±1.6
TSX (*Stripmap*)	X-band	1.22	10x10	± 3	± 10	± 5
TSX (*Spotlight*)	**X-band**	**1.22**	**3x3**	**± 1.6**	**± 10**	**± 5**
ALOS-1 (*Fine Beam*)	L-band	9.29	54x54	± 5	± 10	± 3
ALOS-2 (*Fine SM3 Beam*)	L-band	9.37	32x32	± 5	± 10	± 3

Table 11: Typical precision values (1 sigma) associated to the UTM coordinates of a MP at mid-latitudes. Values are referred to a MP less than 0.62 mi from the REF and a dataset of at least 30 SAR scenes. Satellites used in this analysis are in bold.

6.1.3. Fast Movements and Phase Unwrapping

SqueeSAR is best suited to measure displacement rates below 3.3 ft/yr. In a case of rapid deformation, the measurements can be affected by phase unwrapping inaccuracies.

Figure 22 represents a schematic of a radar target affected by a phase unwrapping error. The target is represented at an initial distance R_0 (in blue), while in red there are three possible cases that are shifted by different amounts. Without prior information, the radar system is not able to estimate the correct number of wavelengths ($n\lambda$), therefore, all three cases will produce equivalent ΔRs.

In theory, on a single isolated radar target, only displacement that is below half a wavelength can be correctly detected. A greater displacement may be underestimated. In extreme cases, if the target moved exactly half a wavelength between two acquisitions the target would still be observed as perfectly stable.

These theoretical limits refer to movements affecting single isolated radar targets. The limits increase significantly in cases where the movement is spatially correlated, and the MP density is adequate. Figure 23 shows a schematic of spatially correlated subsidence. When the radar target density is adequate, the phase can be correctly unwrapped and displacement exceeding the $\lambda/2$ limit can be measured. In cases where the radar target distribution is not adequate, incorrect phase unwrapping can occur and will usually cause displacement to be underestimated.

The temporal distribution of the acquisitions also impacts the phase unwrapping procedure: a higher acquisition frequency means a higher sampling frequency and thus the ability measure more rapid movement.

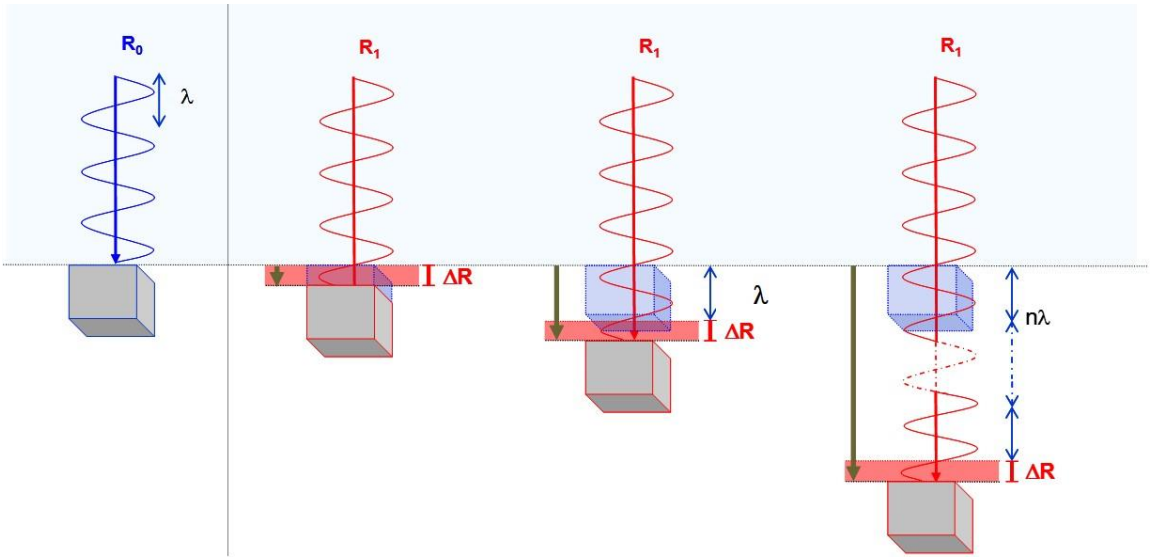

Figure 22: Schematic of a sinusoidal phase of the electromagnetic wave incident on a moving target (grey solid). Without prior information, it is not possible to estimate the correct number of wavelengths (nλ) which occur and in all three cases an equivalent ΔR shift is measured.

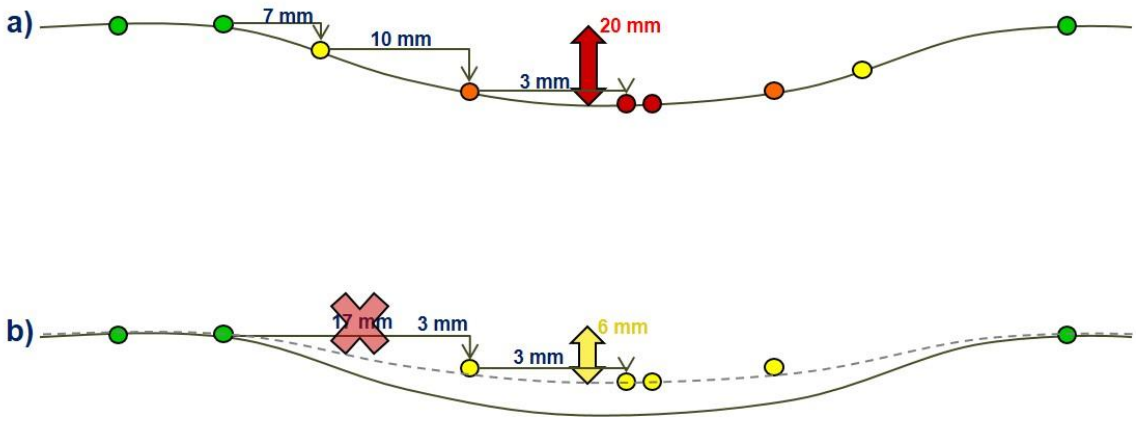

Figure 23: Schematic of spatially correlated subsidence. The MPs are colour-coded according to the displacement measured. Considering a X-band satellite (λ=1.22), a total displacement of 0.79 in (higher than the λ/2 limit of 0.61 in) can be measured when the MP are well distributed along the subsiding profile (a). When the MP distribution is not adequate, an underestimation of the real displacement occurs (b).

6.2. 2-D (Vertical and East-West) Measurements

The combination of 1-D (LOS) SqueeSAR results obtained from ascending and descending orbits over the same area and overlapping period, produces 2-D (vertical and east-west) measurements.

The estimation of the 2-D measurements requires the following steps and assumptions:

- Satellites travelling in ascending and descending orbits identify different radar targets on the ground, entailing that the 2-D procedure requires a spatial grid to capture MPs from both orbits within each cell. It is assumed that MPs that fall within the same cell are affected by the same motion. All MPs within a same cell are then averaged. This entails that the 2-D cells do not represent radar targets on the ground, but rather synthetic points located at the centre of the cells (Figure 24).
- A 2-D time series is calculated by combining all ascending and descending time series using trigonometry. Only cells that contain points from both input LOS data sets will produce a 2-D time series. This entails that the spatial coverage of the 2-D information is thus generally lower than that of the individual LOS data sets (Figure 24).
- Since the images are acquired on different dates from each orbit, the LOS displacement time series must be re-sampled in time. The final output includes all ascending and descending acquisition dates and covers the overlapping period in common for the two data sets.
- North-south movement cannot be measured with InSAR as SAR satellites are not sensitive to movement parallel to their travel direction.

As in LOS analyses, average annual displacement rates in a 2-D analysis are calculated from a linear regression of the displacement measured over the entire period of the study and all measurements are relative to a reference point that is assumed to be stable.

The convention for displacement sign and point colour is the following (Figure 25):

- In a vertical data set, negative values (from yellow to red) indicate downward displacement (subsidence), while positive values (from pale to dark blue) indicate upward displacement (uplift or heave).
- In an east-west data set, negative values (from yellow to red) indicate westward motion, while positive values (from pale to dark blue) indicate eastward motion.

Although 2-D measurements are generally easier to interpret than LOS data, but they have a lower spatial resolution, which means that in detailed analysis of localized features it may be beneficial to use the full resolution LOS results.

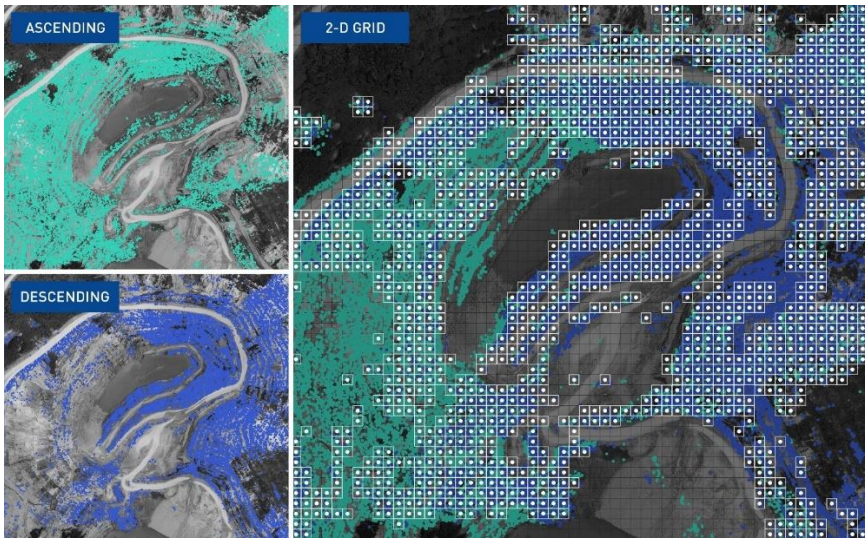

Figure 24: 2-D measurements are estimated by subsampling ascending and descending data on a common spatial grid. The measurements of all MPs contained within the same cell are averaged to produce 2-D measurement points located at the centre of the cell. The 2-D procedure only produces readings for cells containing MP from both orbits (white cells).

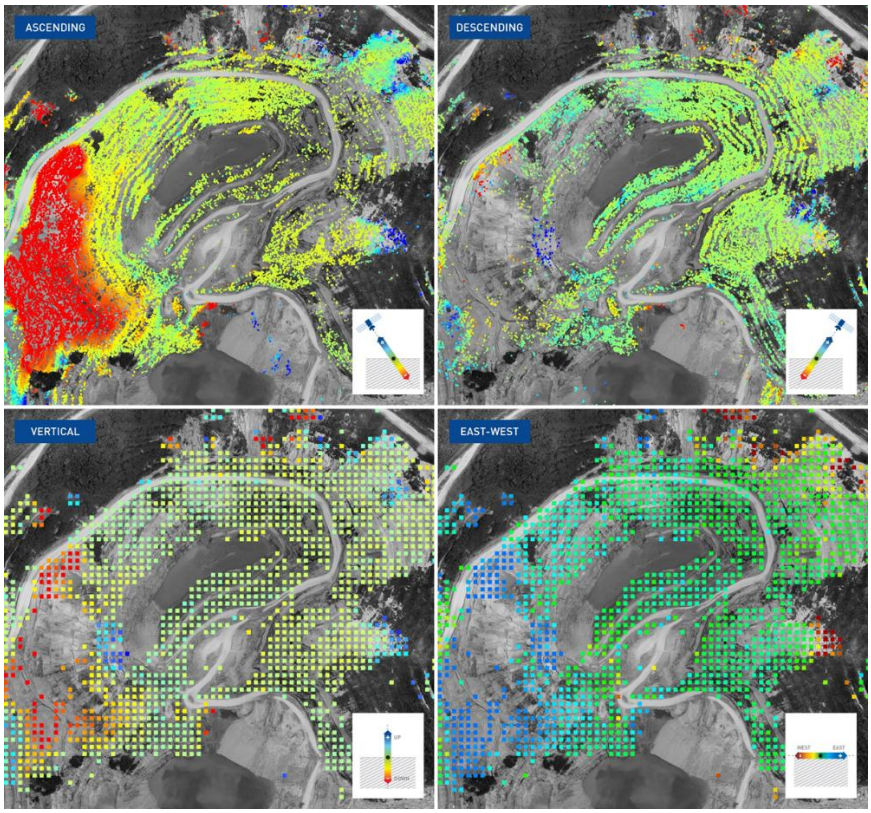

Figure 25: Ascending and descending LOS measurements correspond to the full resolution network of natural reflectors identified on the ground and provide the projection of the real movement to the specific LOS The combination of ascending and descending data produces a regular grid of vertical and east-west measurements.

6.3. SqueeSAR vs Other Surface Monitoring Techniques

When comparing SqueeSAR data with other measurements, the main characteristics to take into consideration are the following:

- SqueeSAR measurements are referred to a local REF. The REF is selected for its radar properties to optimize the quality of the measurements and corresponds to a radar target with high coherence signal and not affected by displacement rate variations in the period of the analysis. The “absolute” stability of the REF point can be verified with a GNSS network.
- SqueeSAR provides displacement measurements with precision in the order of one-hundredth of an inch but point location accuracy is in the order of feet.
- SqueeSAR provides a dense network of measurement points (from 259 to over 25,900 MP/mi^2, depending on the satellite resolution and the land cover) that is not achievable with other in-situ monitoring techniques. This dense network of natural benchmarks allows InSAR to provide very accurate relative movement (estimation of how a point is moving with respect to another point) but less accurate absolute measurements because all the measurements are referred to a local reference point.
- InSAR does not measure the full displacement vector but its projection onto the satellite line of sight. SqueeSAR measurements are 1-D (LOS) and an accurate estimation of the vertical motion component is only possible by combining LOS measurements obtained from ascending and descending orbits over the same area and overlapping period.
- InSAR is not sensitive to movement along the orbit direction (Azimuth), which is approximately north-south (i.e. SqueeSAR do not provide north-south measurements).

Table 12 reports a comparison between the main characteristics of InSAR measurements with respect to other conventional surface monitoring techniques.

Main Characteristics	SqueeSAR	Manual GNSS	Permanent GNSS	Levelling
Spatial density of points	259 - >125,900 points/mi^2	few points/mi^2	few points/mi^2	few points/mi^2
Measurement precision* [1σ]	± 0.20 in (LOS and vert)	± 0.40 in (horizontal) ± 0.80 in (vertical)	± 0.40 in (horizontal) ± 0.40 in (vertical)	±0.04-0.08 in **
Measurement accuracy	High relative accuracy but low absolute accuracy	High absolute accuracy	High absolute accuracy	High absolute accuracy
Location accuracy**	feet	inches	inches	inches
Components	1-D (LOS) and 2-D	3-D	3-D	1-D (vert)
Acquisition frequency	Weekly to monthly	Quarterly to yearly	Hourly to daily	Quarterly to yearly

Table 12: Main characteristics of InSAR and other conventional monitoring techniques. *Precision refers to the error bar of a single measurement (i.e. the consistency of repeated measurements). **Accuracy refers to how close a measurement is to the absolute value. GNSS precision values refer to a 1-hour static session.

In general, to perform a comparison of InSAR data with other measurements it is necessary:

1. To compare the measurements along a same direction.

- As InSAR provides 1-D (LOS) measurements, it is more rigorous to project 3-D measurements to the LOS direction. The projection of the LOS measurements to the vertical direction can be performed only under the assumption of negligible horizontal motion components. Alternatively, the use of SqueeSAR measurements obtained from ascending and descending orbits over the same area and overlapping period allows an accurate estimation of the vertical motion component.

2. Define a co-location rule between the InSAR measurement points and other stations/benchmarks.

- In general, it is unusual for SqueeSAR measurement points to fall exactly at benchmark locations. It is therefore recommended to perform the comparison using all of the most coherent (highest

quality) points located within a certain radius from the benchmark, rather than just an individual SqueeSAR point.

3. Use the same reference point or verify the absolute stability of the local InSAR reference point (REF).
4. Use the same reference period and consider the accuracy and frequency of the measurement techniques being compared.

6.3.1. Integration and Calibration of InSAR Data with a GNSS Network – Best Practices

InSAR and GNSS (Global Navigation Satellite System) are complementary techniques for monitoring surface movements and are generally integrated to take advantage of the strengths of both technologies, in terms of spatial density, precision and accuracy (Table 12). The integration of InSAR and GNSS measurements provides a high spatial density of information with optimal precision and accuracy of the measurements when a common reference system is used.

To achieve this, the SqueeSAR data is generally calibrated to an absolute GNSS network based on the following steps:

1) Projection of the GNSS measurements to the satellite LOS. The GNSS 3-D measurements are projected to the satellite 1-D LOS to create a GNSS LOS time series. This step allows a direct comparison of the two independent measurements (InSAR and GPS). The projection of the 3-D GNSS measurements onto the LOS direction can be calculated as follows:

$$D_{LOS} = D_{VERT}*V_{LOS} + D_{EW}*E_{LOS} + D_{NS}*N_{LOS}$$

with V_{LOS}, E_{LOS} e N_{LOS} are the LOS versors along the 3 directions and D_{VERT}, D_{EW} e D_{NS} are the 3 components of the GNSS measurements. The LOS versors are provided in the metadata associated to the SqueeSAR data (Figure 26) and represent the cosines of the angles between the LOS and the 3 coordinate axes.

2) Co-localization of the measurement points. Generally, GNSS benchmarks and InSAR points are not exactly co-located. Additionally, the accuracy of the InSAR point location is known to within a few metres (Table 11). The location of a GNSS benchmark is known with cm precision. For these reasons, InSAR measurement points (MP) within a certain radius of each GNSS are generally selected and used to calculate an average time series (ATS) for the overlapping period with the GNSS time series (one InSAR ATS for each GNSS). This step allows the comparison of data collected at a same location over a corresponding period.
3) Refence point stability check. GNSS measurements are absolute as they are connected to a global network, while InSAR data are referred to a local reference point (REF). GNSS measurements can be

used to verify the "absolute" stability of the REF. If there is no GNSS station close to the REF, it is suggested to just verify the stability of the InSAR points in an area around a stable GPS station.

4) Absolute calibration. If the REF check highlights discrepancies between InSAR and GNSS measurements, the InSAR measurements are calibrated to the absolute GNSS network as follows:

- Plane removal (when only a linear regional trend is present): a difference in average velocity is calculated for each ATS and corresponding GNSS. The average velocity differences calculated for each ATS and GNSS pair is then used to estimate and remove a first order surface (plane) from all InSAR measurement points. The plane is statistically estimated at regional scale by minimizing the residuals of the differences between the ATS and corresponding GNSS.
- Time series calibration (when a not-linear regional trend is present): evaluation of an average time series of residuals by comparing the ATS to the corresponding GNSS time series at each location. All the time series of residuals obtained are then averaged to define a unique common time series of residuals (cRTS) at regional scale. This cRTS represents the movement of the local InSAR reference points with respect to the absolute GNSS reference frame. The cRTS is then removed from every InSAR MP time series.

$$D_{LOS} = D_{VERT} * V_{LOS} + D_{EW} * E_{LOS} + D_{NS} * N_{LOS}$$

Satellite info

Satellite	Wavelength	Satellite geometry	Sensor mode	Satellite track
SNT	5.55 cm	ASCENDING	IW	111

Acquisition geometry

Line of sight angle	ɵ:	35.75°	δ:	15.47°		
Line of sight versors	V:	0.812	N:	-0.156	E:	-0.563

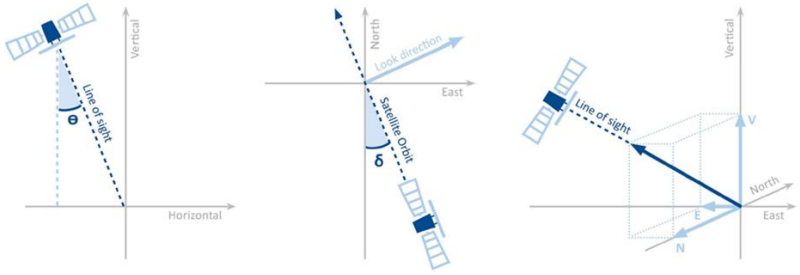

Figure 26: Example of metadata associated to the SqueeSAR measurements. LOS angles and versos can be used to transform a 3-D measurement (D_{VERT}, D_{EW} and D_{NS}) onto a LOS measurement (D_{LO}).

Appendix 3: Average Time Series over Lonquist Areas of Interest

ATS (vertical and east-west) plots for the Lonquist areas of interest (Figure 27).

- Vertical (black): Negative displacement rates indicate subsidence and positive displacement rates indicate uplift.
- East-West (red): Negative displacement rates indicate westward movement and positive displacement rate indicate eastward movement.

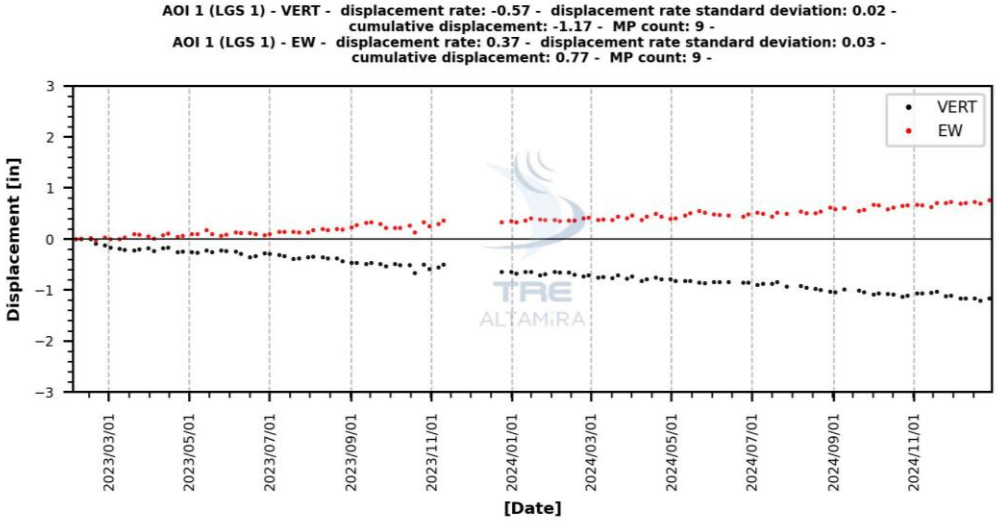

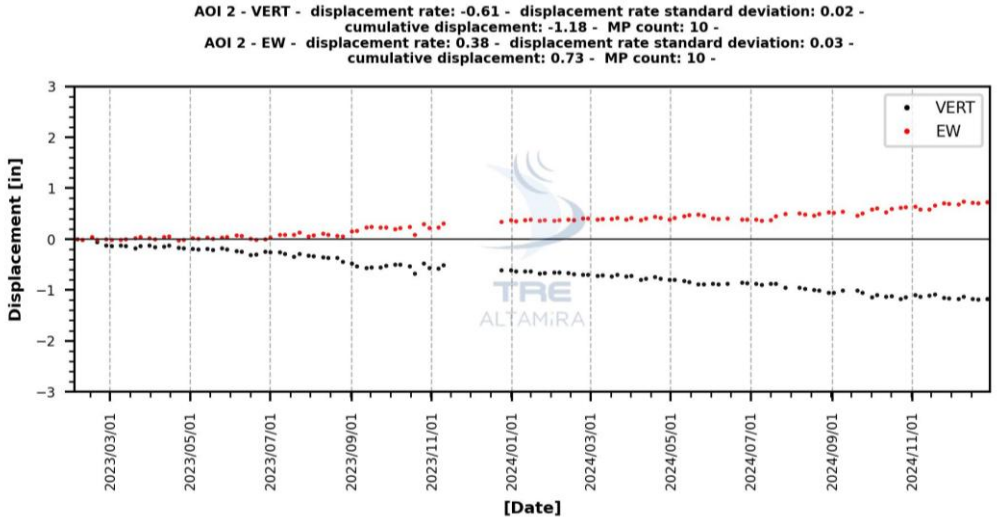

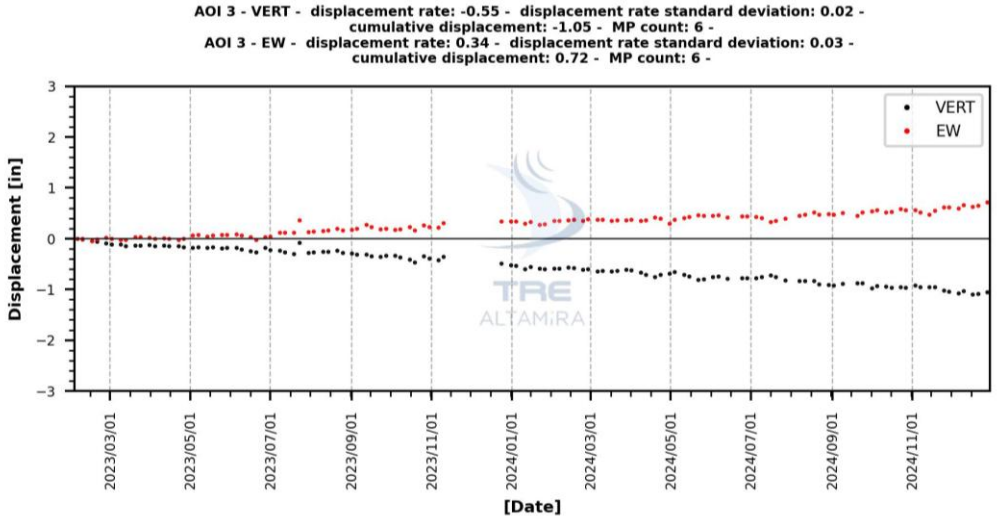
AOI 3 - VERT - displacement rate: -0.55 - displacement rate standard deviation: 0.02 - cumulative displacement: -1.05 - MP count: 6 -
AOI 3 - EW - displacement rate: 0.34 - displacement rate standard deviation: 0.03 - cumulative displacement: 0.72 - MP count: 6 -
VERT
EW
Displacement [in]
[Date]

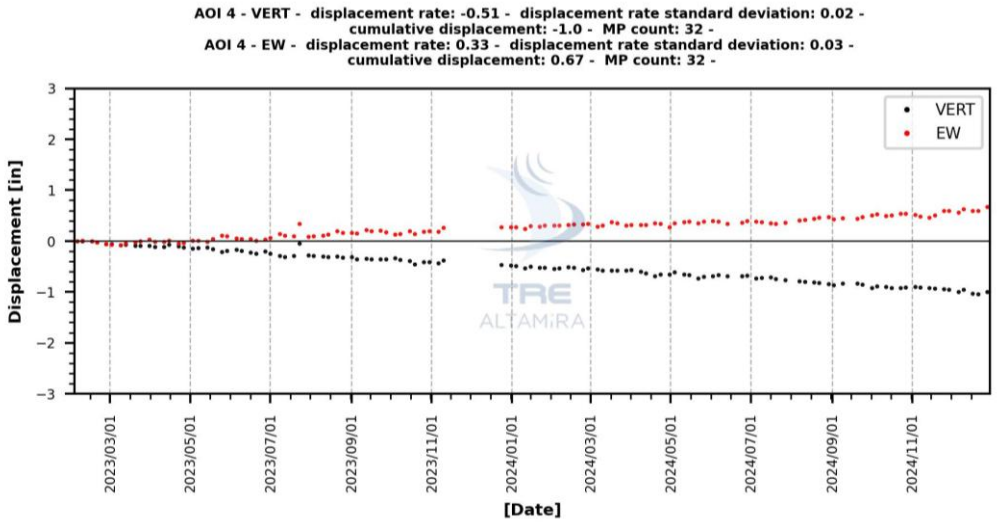
AOI 4 - VERT - displacement rate: -0.51 - displacement rate standard deviation: 0.02 - cumulative displacement: -1.0 - MP count: 32 -
AOI 4 - EW - displacement rate: 0.33 - displacement rate standard deviation: 0.03 - cumulative displacement: 0.67 - MP count: 32 -
VERT
EW
Displacement [in]
[Date]

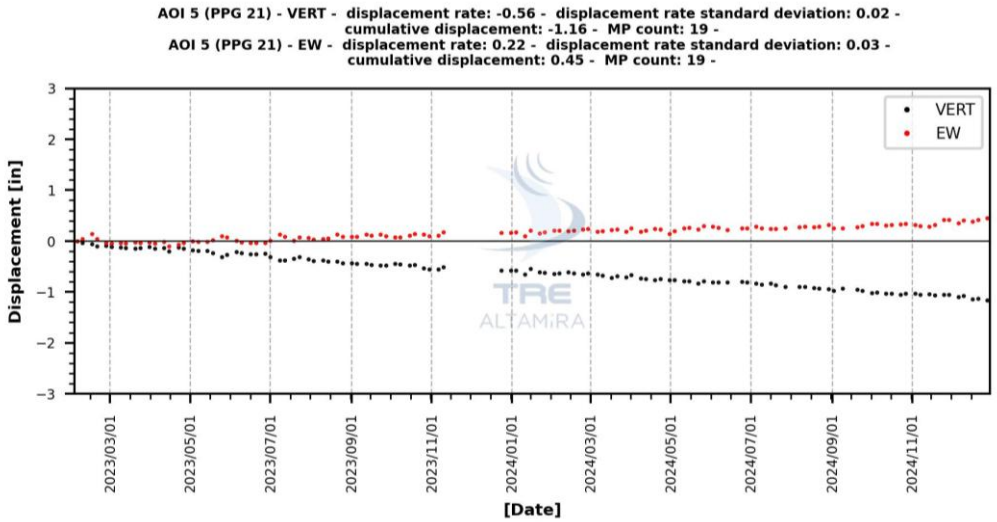
AOI 5 (PPG 21) - VERT - displacement rate: -0.56 - displacement rate standard deviation: 0.02 - cumulative displacement: -1.16 - MP count: 19 -
AOI 5 (PPG 21) - EW - displacement rate: 0.22 - displacement rate standard deviation: 0.03 - cumulative displacement: 0.45 - MP count: 19 -
VERT
EW
Displacement [in]
[Date]

AOI 6 (PPG 6) - VERT - displacement rate: -0.87 - displacement rate standard deviation: 0.02 - cumulative displacement: -1.72 - MP count: 66 -
AOI 6 (PPG 6) - EW - displacement rate: 0.27 - displacement rate standard deviation: 0.03 - cumulative displacement: 0.56 - MP count: 66 -

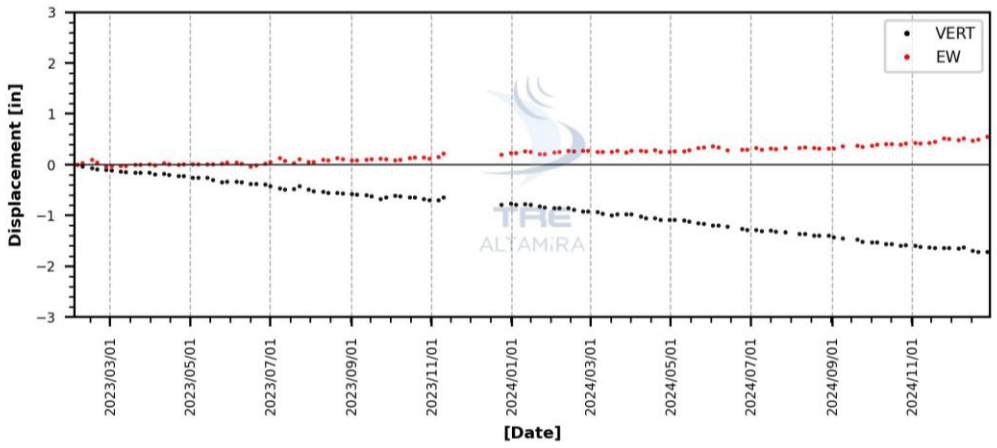

AOI 7 (PPG 7) - VERT - displacement rate: -0.86 - displacement rate standard deviation: 0.02 - cumulative displacement: -1.68 - MP count: 61 -
AOI 7 (PPG 7) - EW - displacement rate: 0.45 - displacement rate standard deviation: 0.03 - cumulative displacement: 0.88 - MP count: 61 -

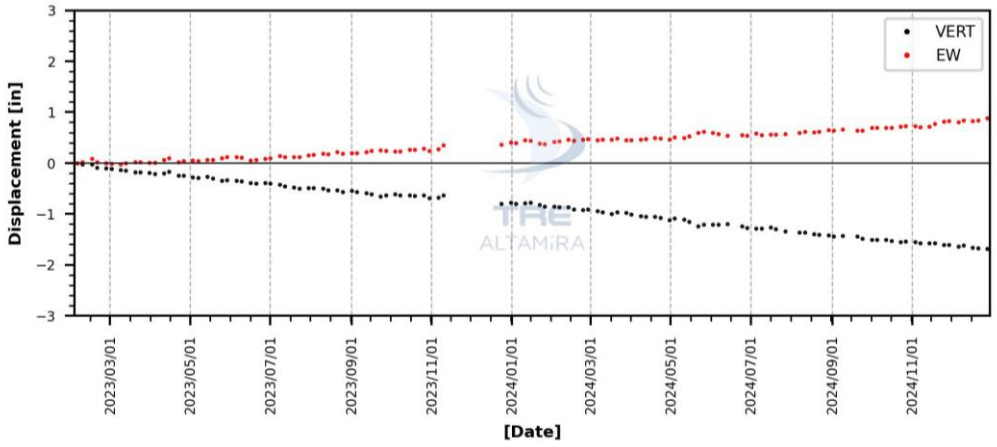

AOI 8 (PPG 22) - VERT - displacement rate: -1.17 - displacement rate standard deviation: 0.02 - cumulative displacement: -2.28 - MP count: 25 -
AOI 8 (PPG 22) - EW - displacement rate: 0.38 - displacement rate standard deviation: 0.03 - cumulative displacement: 0.75 - MP count: 25 -

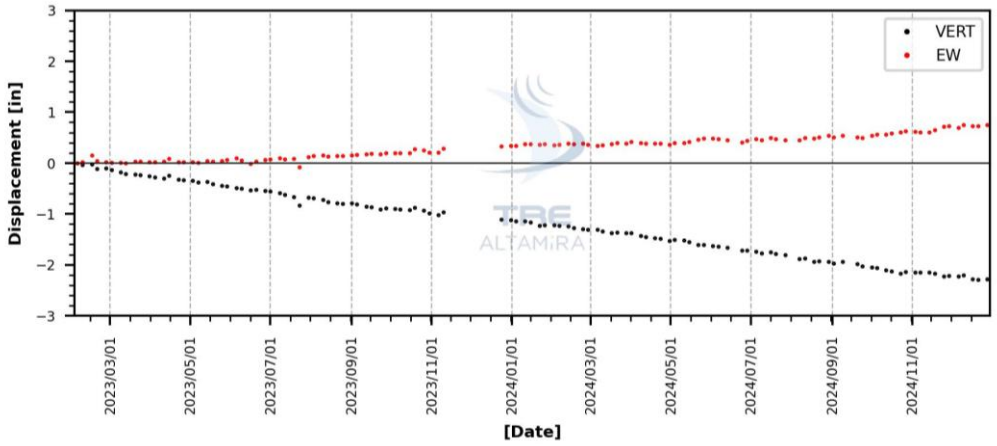

AOI 9 (SMS A1) - VERT - displacement rate: -0.74 - displacement rate standard deviation: 0.02 - cumulative displacement: -1.47 - MP count: 15 -
AOI 9 (SMS A1) - EW - displacement rate: 0.33 - displacement rate standard deviation: 0.03 - cumulative displacement: 0.61 - MP count: 15 -

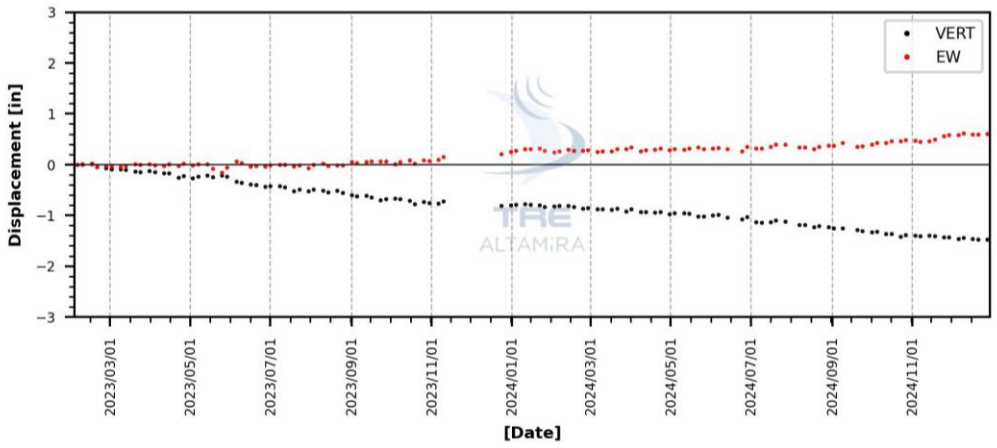

AOI 10 (PPG 2) - VERT - displacement rate: -1.0 - displacement rate standard deviation: 0.02 - cumulative displacement: -1.94 - MP count: 131 -
AOI 10 (PPG 2) - EW - displacement rate: 0.24 - displacement rate standard deviation: 0.03 - cumulative displacement: 0.5 - MP count: 131 -

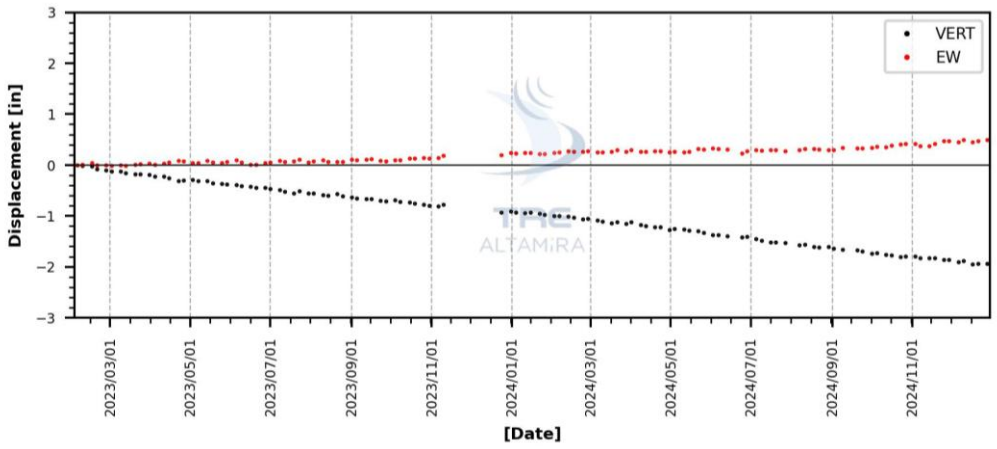

AOI 11 (PPG 5) - VERT - displacement rate: -0.89 - displacement rate standard deviation: 0.02 - cumulative displacement: -1.75 - MP count: 21 -
AOI 11 (PPG 5) - EW - displacement rate: 0.11 - displacement rate standard deviation: 0.03 - cumulative displacement: 0.29 - MP count: 21 -

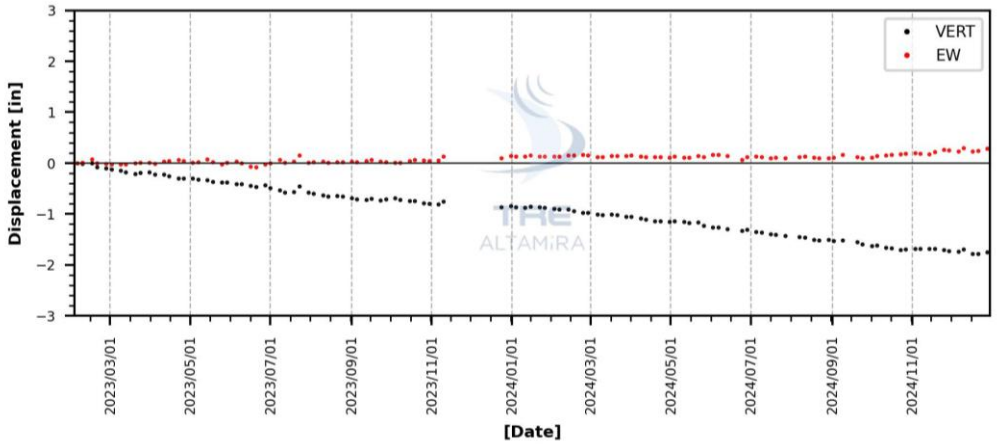

AOI 12 (PPG 4) - VERT - displacement rate: -1.02 - displacement rate standard deviation: 0.02 - cumulative displacement: -2.0 - MP count: 60 -
AOI 12 (PPG 4) - EW - displacement rate: -0.16 - displacement rate standard deviation: 0.03 - cumulative displacement: -0.25 - MP count: 60 -

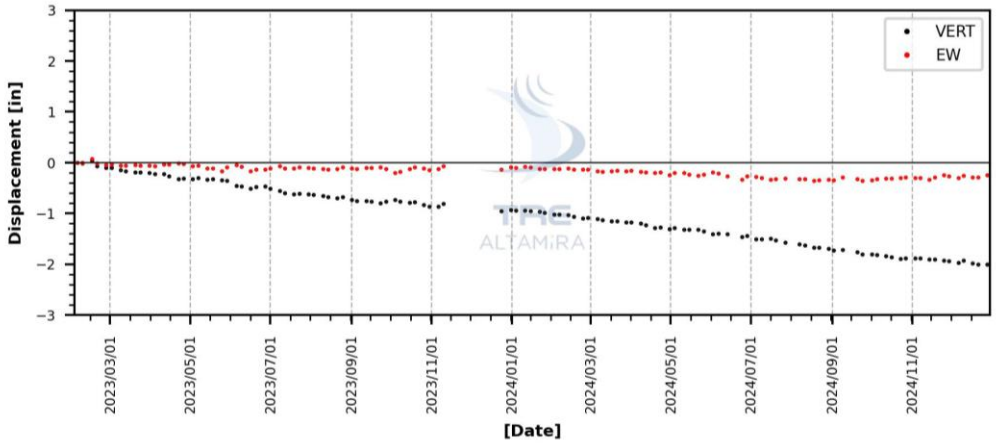

AOI 13 (PPG 18) - VERT - displacement rate: -0.72 - displacement rate standard deviation: 0.02 - cumulative displacement: -1.46 - MP count: 15 -
AOI 13 (PPG 18) - EW - displacement rate: 0.08 - displacement rate standard deviation: 0.03 - cumulative displacement: 0.22 - MP count: 15 -

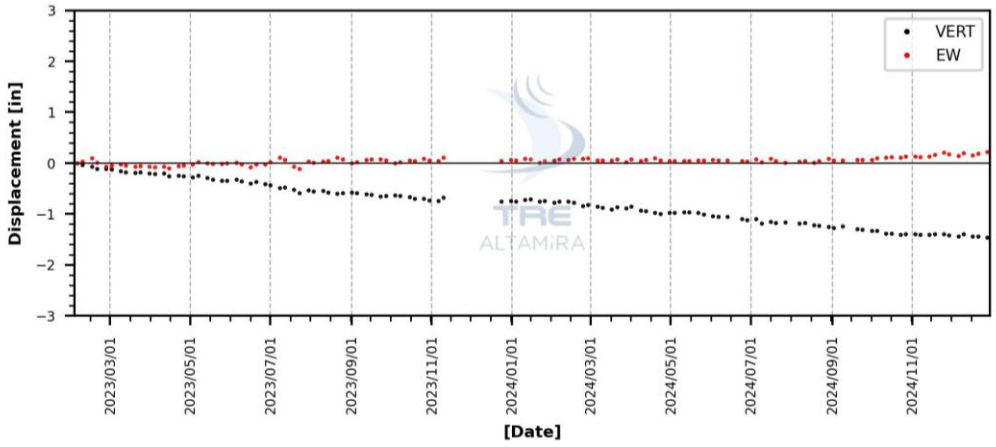

AOI 14 (PPG 16) - VERT - displacement rate: -0.81 - displacement rate standard deviation: 0.02 - cumulative displacement: -1.63 - MP count: 4 -
AOI 14 (PPG 16) - EW - displacement rate: -0.4 - displacement rate standard deviation: 0.03 - cumulative displacement: -0.75 - MP count: 4 -

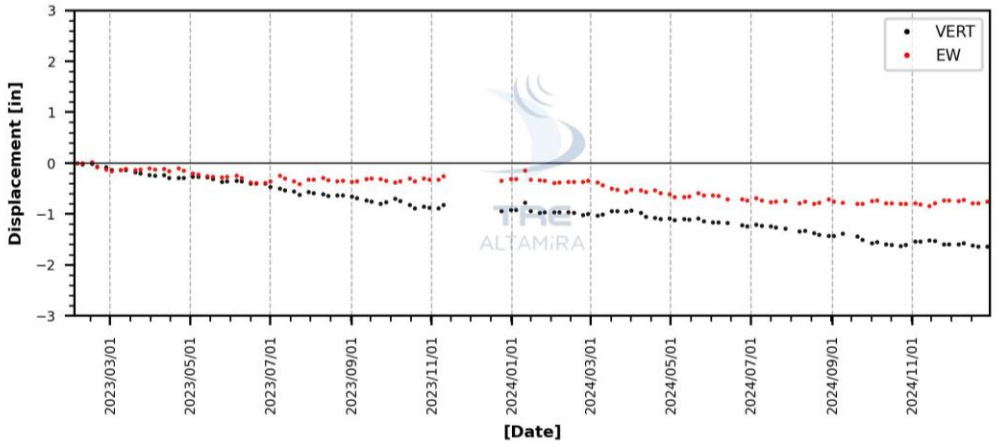

AOI 15 (PPG 20) - VERT - displacement rate: -0.83 - displacement rate standard deviation: 0.02 - cumulative displacement: -1.65 - MP count: 59 -
AOI 15 (PPG 20) - EW - displacement rate: -0.6 - displacement rate standard deviation: 0.03 - cumulative displacement: -1.09 - MP count: 59 -

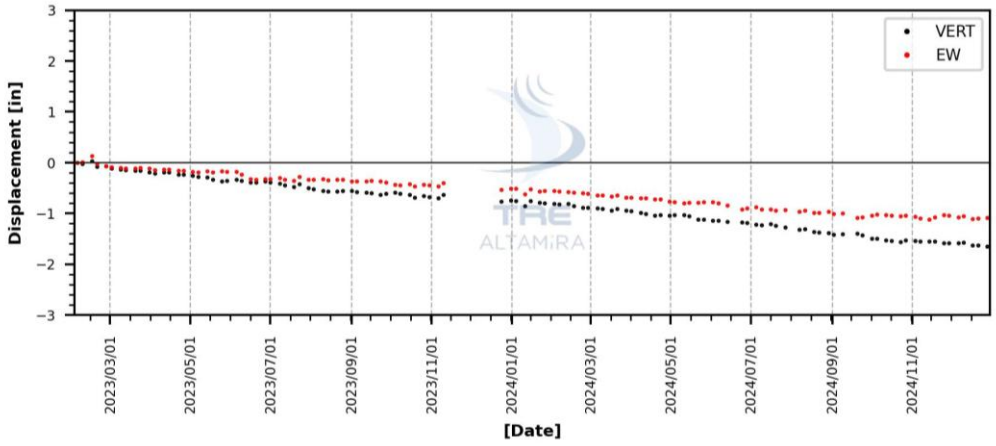

AOI 16 (LGS 2) - VERT - displacement rate: -1.52 - displacement rate standard deviation: 0.02 - cumulative displacement: -2.9 - MP count: 6 -
AOI 16 (LGS 2) - EW - displacement rate: -0.47 - displacement rate standard deviation: 0.02 - cumulative displacement: -0.81 - MP count: 6 -

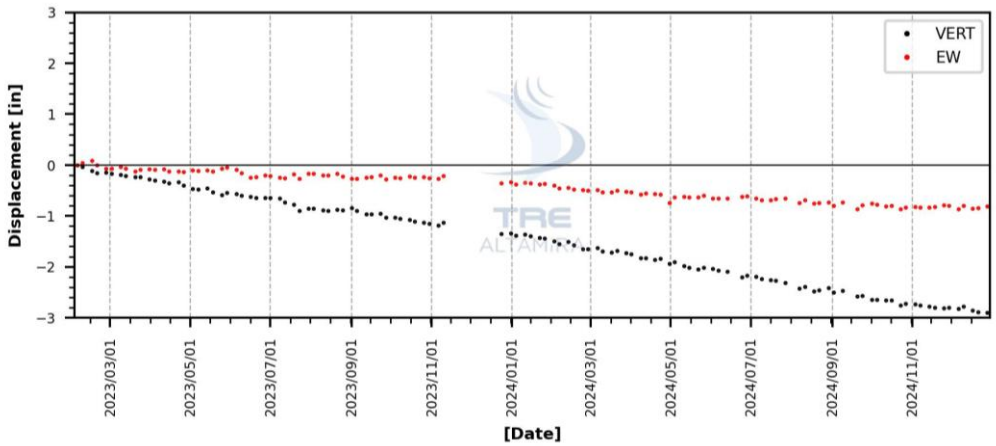

AOI 17 (SS 4) - VERT - displacement rate: -0.87 - displacement rate standard deviation: 0.02 - cumulative displacement: -1.68 - MP count: 75 -
AOI 17 (SS 4) - EW - displacement rate: -0.49 - displacement rate standard deviation: 0.03 - cumulative displacement: -0.85 - MP count: 75 -

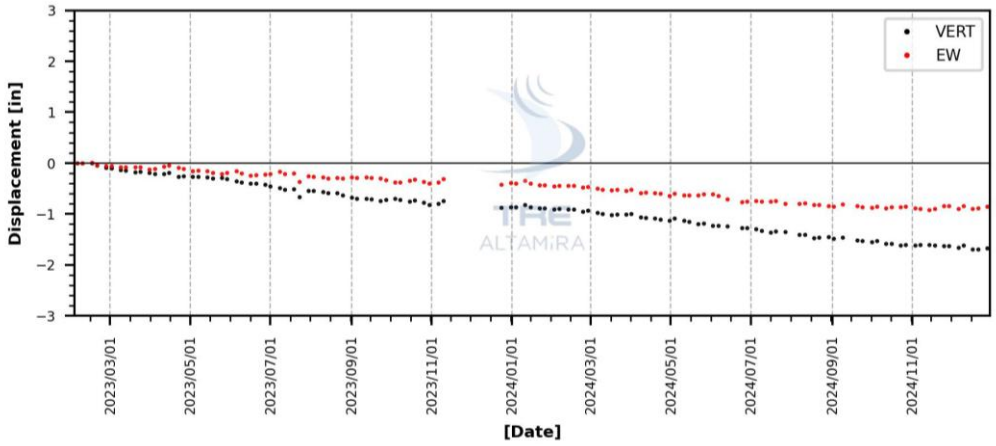

AOI 18 (SS 2) - VERT - displacement rate: -1.01 - displacement rate standard deviation: 0.02 - cumulative displacement: -1.94 - MP count: 56 -
AOI 18 (SS 2) - EW - displacement rate: -0.63 - displacement rate standard deviation: 0.03 - cumulative displacement: -1.15 - MP count: 56 -

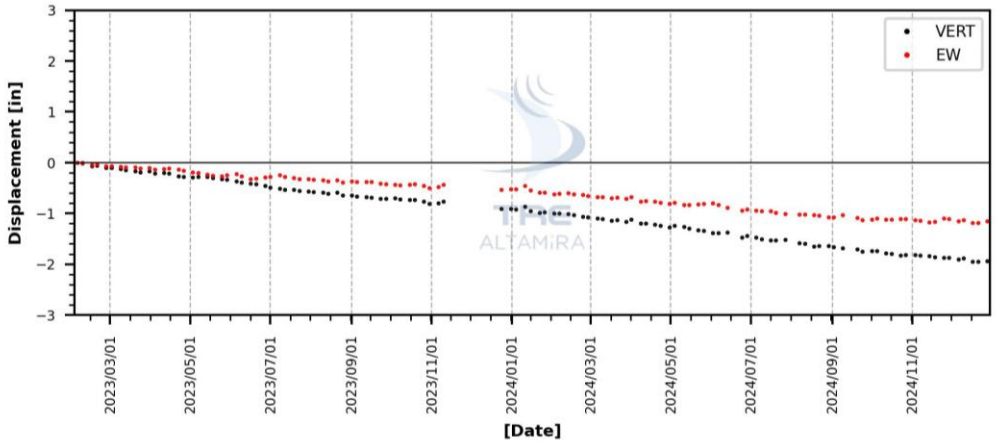

AOI 19 (SS 5) - VERT - displacement rate: -0.85 - displacement rate standard deviation: 0.02 - cumulative displacement: -1.63 - MP count: 61 -
AOI 19 (SS 5) - EW - displacement rate: -0.63 - displacement rate standard deviation: 0.03 - cumulative displacement: -1.17 - MP count: 61 -

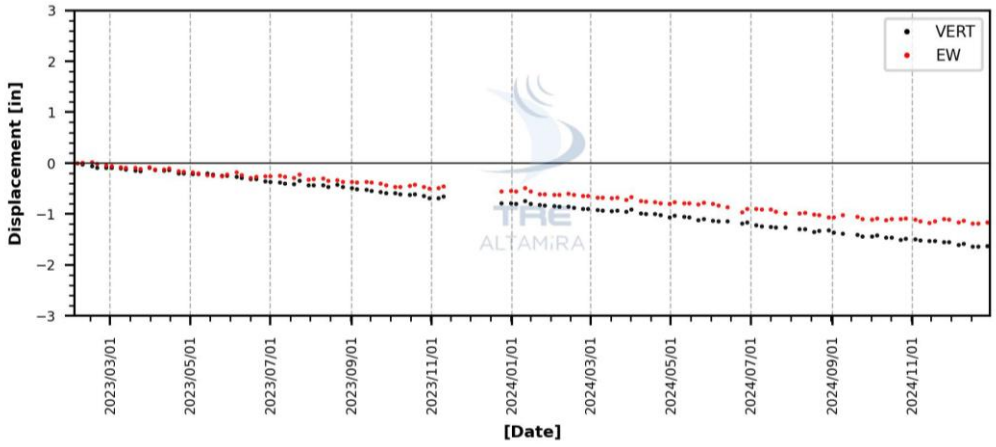

AOI 20 (SS 1) - VERT - displacement rate: -0.94 - displacement rate standard deviation: 0.02 - cumulative displacement: -1.87 - MP count: 37 -
AOI 20 (SS 1) - EW - displacement rate: -0.69 - displacement rate standard deviation: 0.03 - cumulative displacement: -1.28 - MP count: 37 -

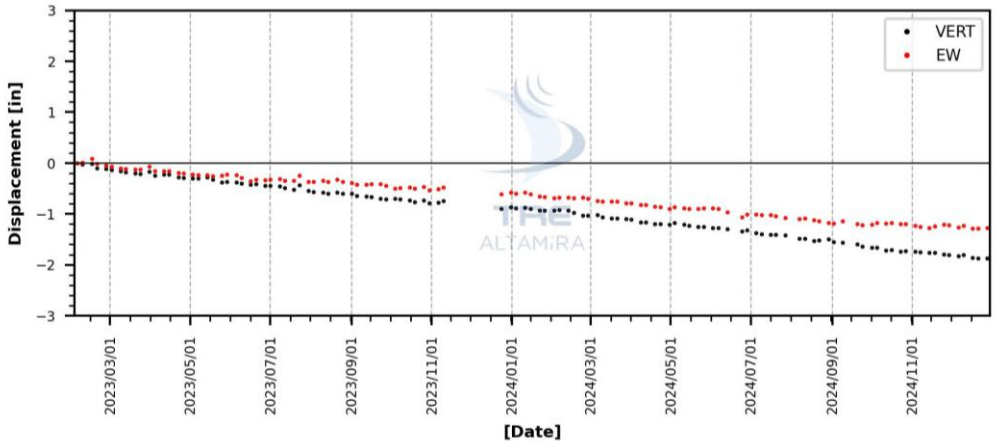

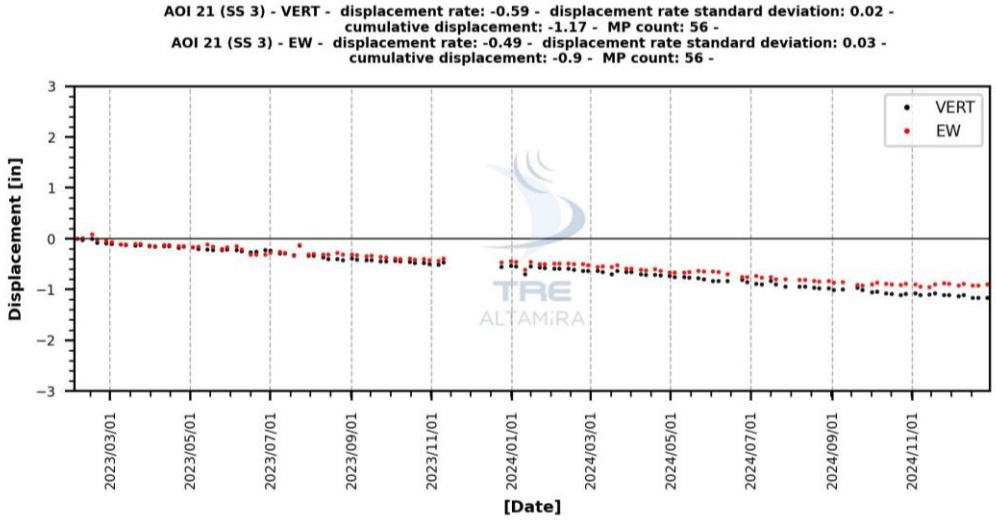

Figure 27: Average time series of the vertical and east-west displacement rates of all measurement points within Lonquist areas of interest.

Appendix 4: Time Series over Corner Reflectors

Vertical and East-West time series plots over Corner Reflectors within the area of interest (Figure 28).

- Vertical (black): Negative displacement rates indicate subsidence and positive displacement rates indicate uplift.
- East-West (red): Negative displacement rates indicate westward movement and positive displacement rate indicate eastward movement.

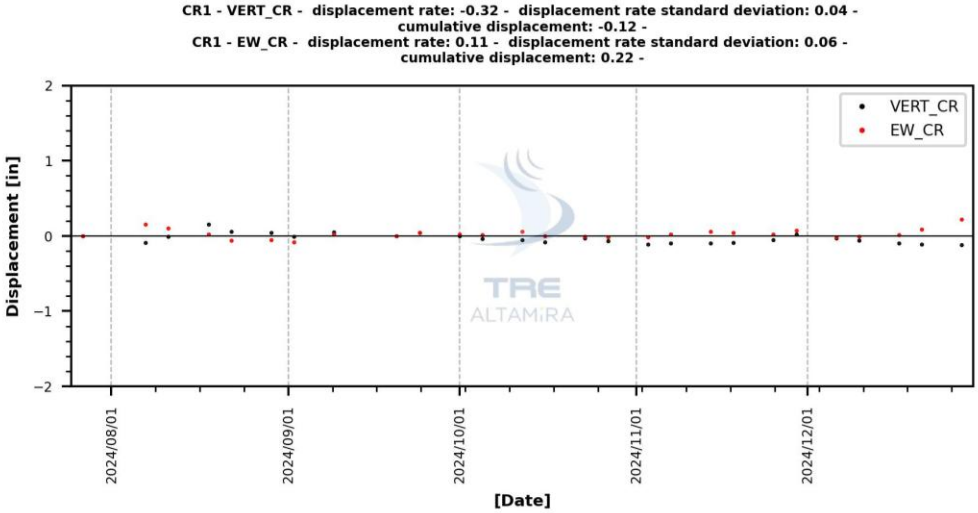

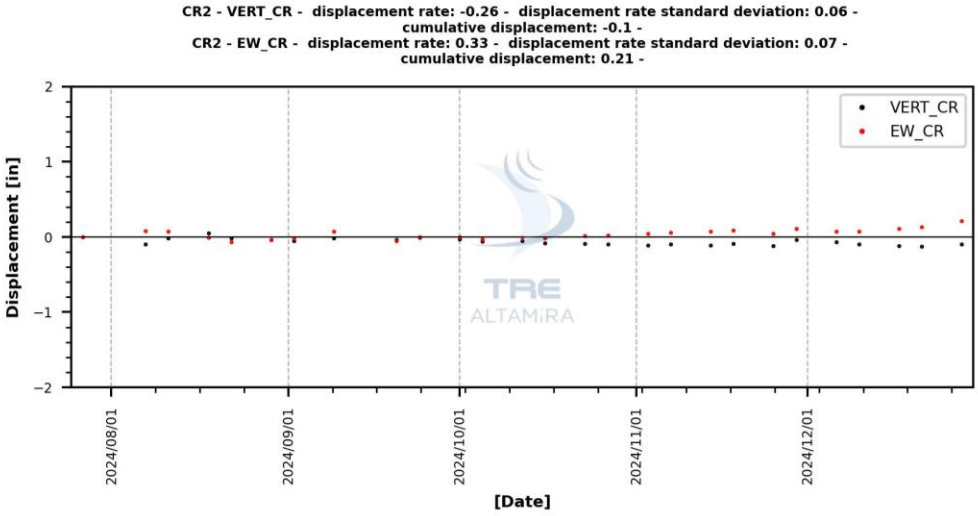

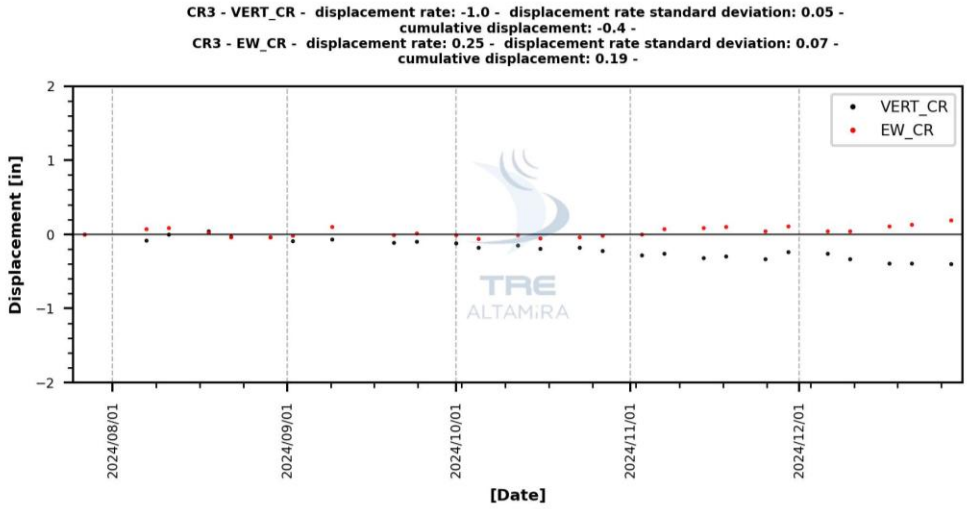
CR3 - VERT_CR - displacement rate: -1.0 - displacement rate standard deviation: 0.05 - cumulative displacement: -0.4 -
CR3 - EW_CR - displacement rate: 0.25 - displacement rate standard deviation: 0.07 - cumulative displacement: 0.19 -
VERT_CR
EW_CR
Displacement [in]
2
1
0
−1
−2
2024/08/01
2024/09/01
2024/10/01
2024/11/01
2024/12/01
[Date]

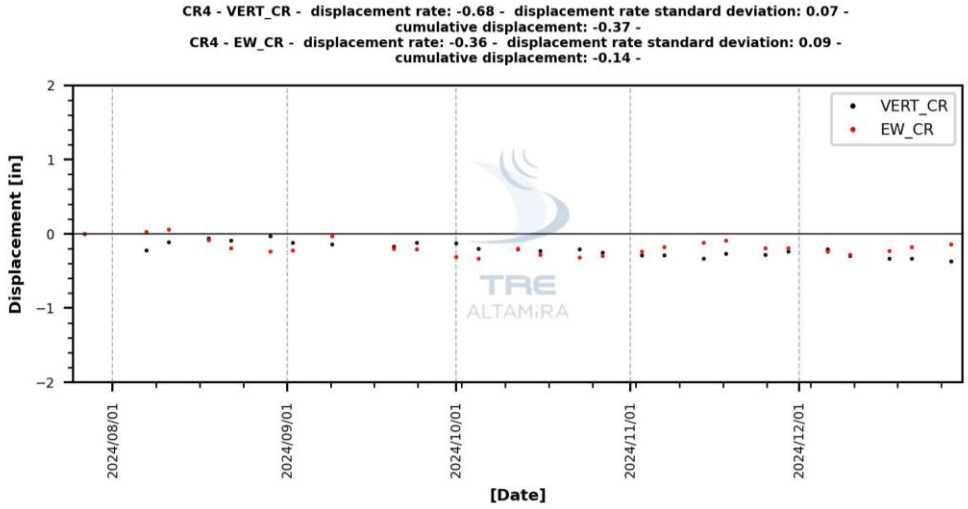
CR4 - VERT_CR - displacement rate: -0.68 - displacement rate standard deviation: 0.07 - cumulative displacement: -0.37 -
CR4 - EW_CR - displacement rate: -0.36 - displacement rate standard deviation: 0.09 - cumulative displacement: -0.14 -
VERT_CR
EW_CR
Displacement [in]
2
1
0
−1
−2
2024/08/01
2024/09/01
2024/10/01
2024/11/01
2024/12/01
[Date]

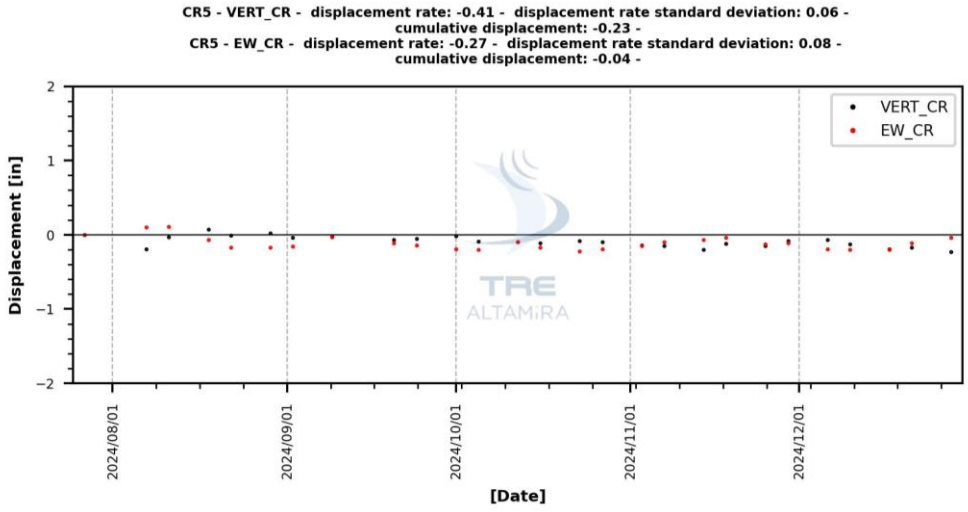
CR5 - VERT_CR - displacement rate: -0.41 - displacement rate standard deviation: 0.06 - cumulative displacement: -0.23 -
CR5 - EW_CR - displacement rate: -0.27 - displacement rate standard deviation: 0.08 - cumulative displacement: -0.04 -
VERT_CR
EW_CR
Displacement [in]
2
1
0
−1
−2
2024/08/01
2024/09/01
2024/10/01
2024/11/01
2024/12/01
[Date]

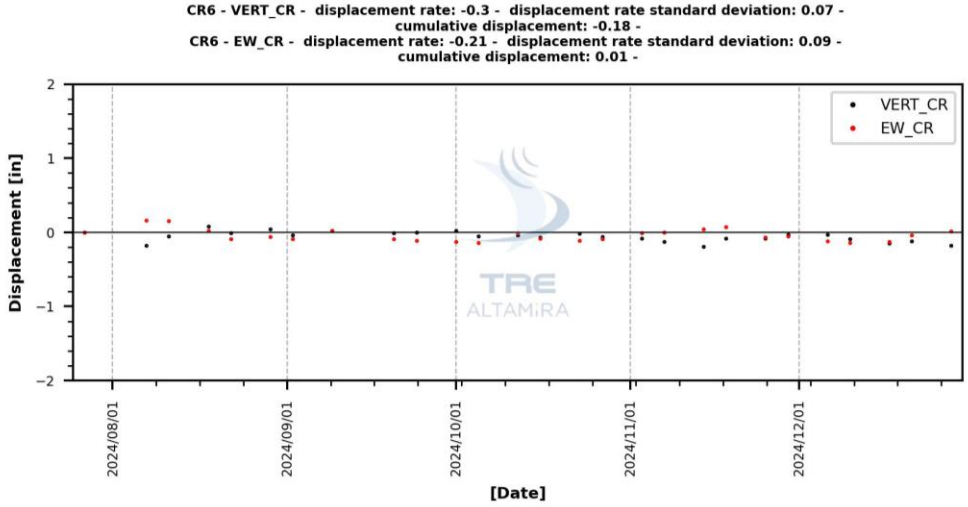
CR6 - VERT_CR - displacement rate: -0.3 - displacement rate standard deviation: 0.07 - cumulative displacement: -0.18 -
CR6 - EW_CR - displacement rate: -0.21 - displacement rate standard deviation: 0.09 - cumulative displacement: 0.01 -
VERT_CR
EW_CR
Displacement [in]
2
1
0
−1
−2
2024/08/01
2024/09/01
2024/10/01
2024/11/01
2024/12/01
[Date]

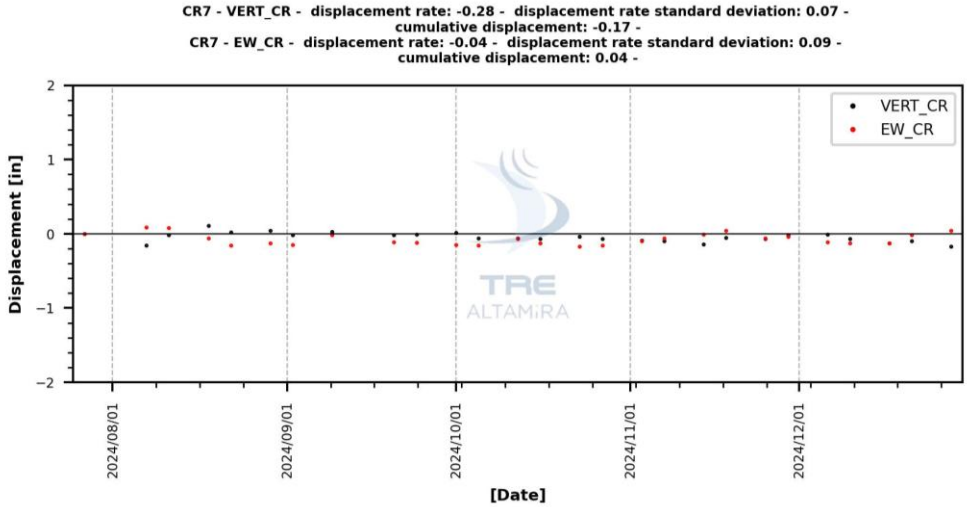
CR7 - VERT_CR - displacement rate: -0.28 - displacement rate standard deviation: 0.07 - cumulative displacement: -0.17 -
CR7 - EW_CR - displacement rate: -0.04 - displacement rate standard deviation: 0.09 - cumulative displacement: 0.04 -
VERT_CR
EW_CR
Displacement [in]
2
1
0
−1
−2
2024/08/01
2024/09/01
2024/10/01
2024/11/01
2024/12/01
[Date]

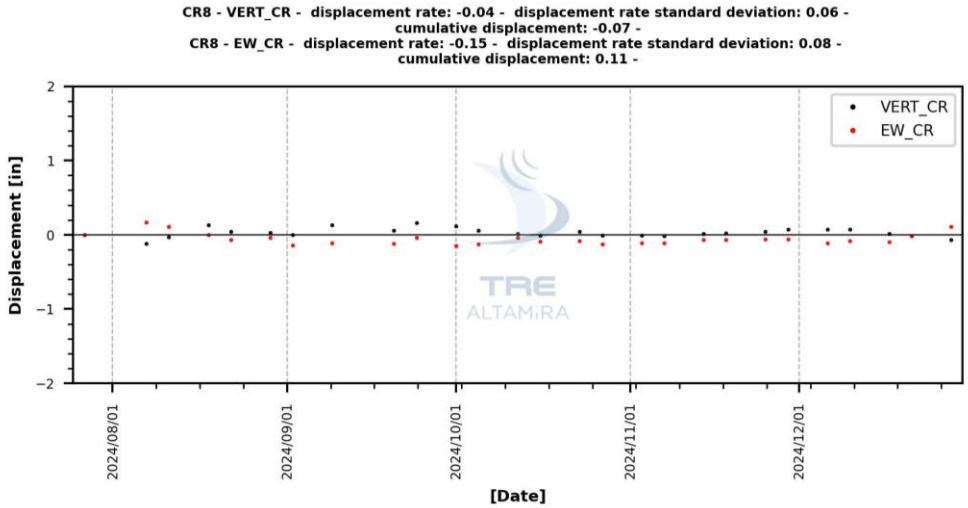
CR8 - VERT_CR - displacement rate: -0.04 - displacement rate standard deviation: 0.06 - cumulative displacement: -0.07 -
CR8 - EW_CR - displacement rate: -0.15 - displacement rate standard deviation: 0.08 - cumulative displacement: 0.11 -
VERT_CR
EW_CR
Displacement [in]
2
1
0
−1
−2
2024/08/01
2024/09/01
2024/10/01
2024/11/01
2024/12/01
[Date]

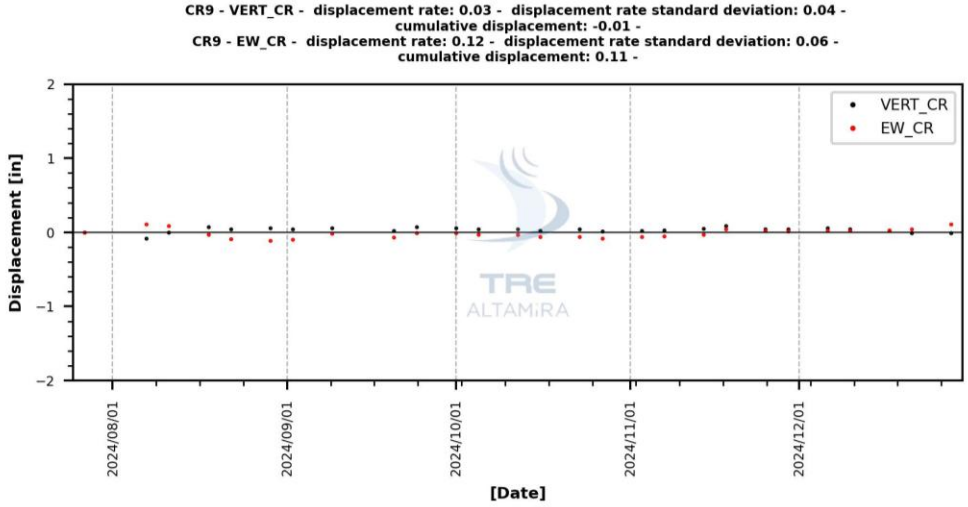
CR9 - VERT_CR - displacement rate: 0.03 - displacement rate standard deviation: 0.04 - cumulative displacement: -0.01 -
CR9 - EW_CR - displacement rate: 0.12 - displacement rate standard deviation: 0.06 - cumulative displacement: 0.11 -
VERT_CR
EW_CR
Displacement [in]
2
1
0
−1
−2
2024/08/01
2024/09/01
2024/10/01
2024/11/01
2024/12/01
[Date]

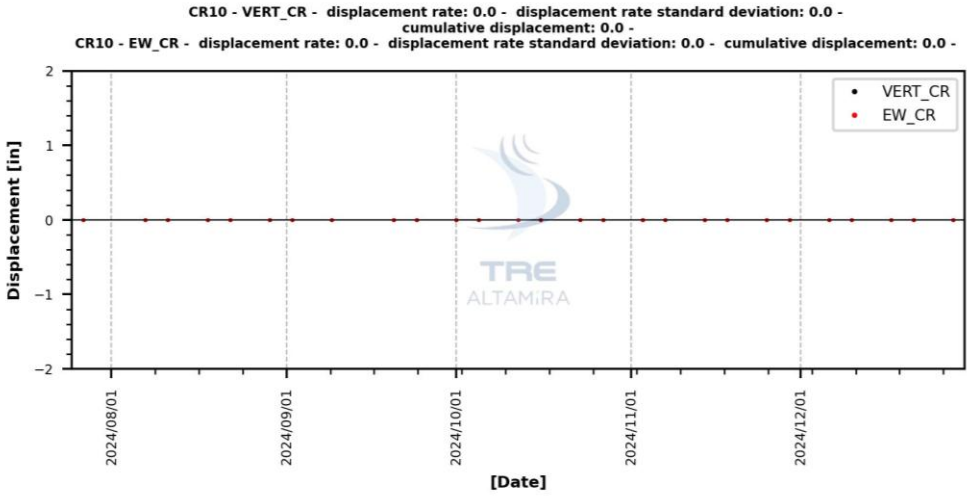
CR10 - VERT_CR - displacement rate: 0.0 - displacement rate standard deviation: 0.0 - cumulative displacement: 0.0 -
CR10 - EW_CR - displacement rate: 0.0 - displacement rate standard deviation: 0.0 - cumulative displacement: 0.0 -
VERT_CR
EW_CR
Displacement [in]
2
1
0
−1
−2
2024/08/01
2024/09/01
2024/10/01
2024/11/01
2024/12/01
[Date]

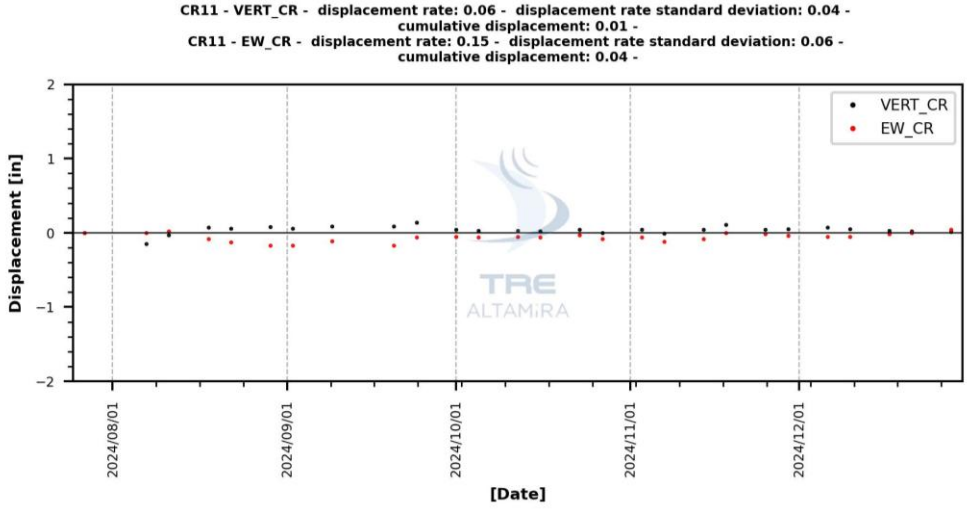
CR11 - VERT_CR - displacement rate: 0.06 - displacement rate standard deviation: 0.04 - cumulative displacement: 0.01 -
CR11 - EW_CR - displacement rate: 0.15 - displacement rate standard deviation: 0.06 - cumulative displacement: 0.04 -
VERT_CR
EW_CR
Displacement [in]
2
1
0
−1
−2
2024/08/01
2024/09/01
2024/10/01
2024/11/01
2024/12/01
[Date]

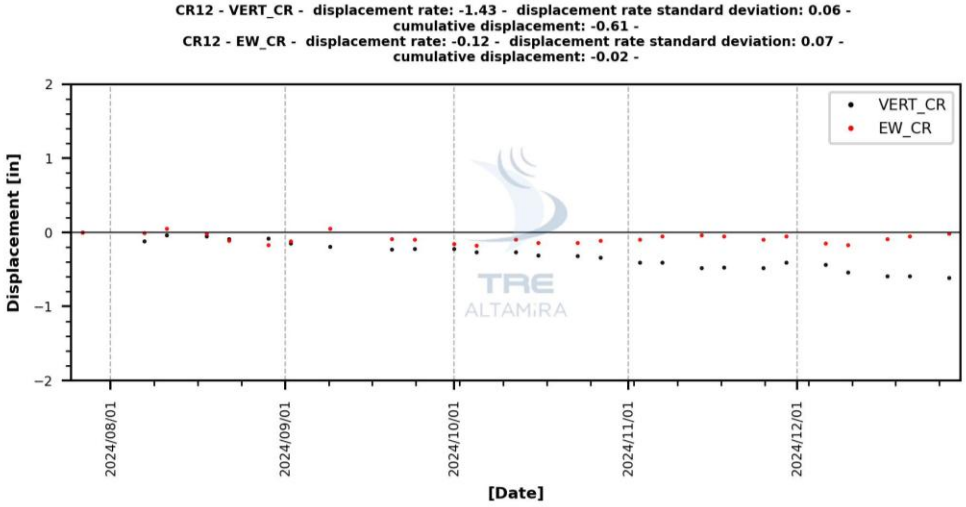
CR12 - VERT_CR - displacement rate: -1.43 - displacement rate standard deviation: 0.06 - cumulative displacement: -0.61 -
CR12 - EW_CR - displacement rate: -0.12 - displacement rate standard deviation: 0.07 - cumulative displacement: -0.02 -
VERT_CR
EW_CR
Displacement [in]
2
1
0
−1
−2
2024/08/01
2024/09/01
2024/10/01
2024/11/01
2024/12/01
[Date]

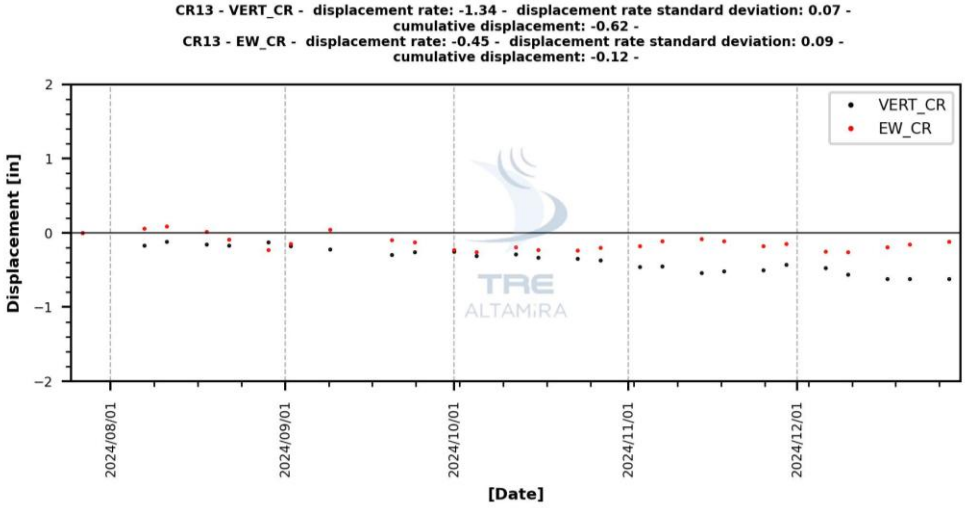
CR13 - VERT_CR - displacement rate: -1.34 - displacement rate standard deviation: 0.07 - cumulative displacement: -0.62 -
CR13 - EW_CR - displacement rate: -0.45 - displacement rate standard deviation: 0.09 - cumulative displacement: -0.12 -
VERT_CR
EW_CR
Displacement [in]
2
1
0
−1
−2
2024/08/01
2024/09/01
2024/10/01
2024/11/01
2024/12/01
[Date]

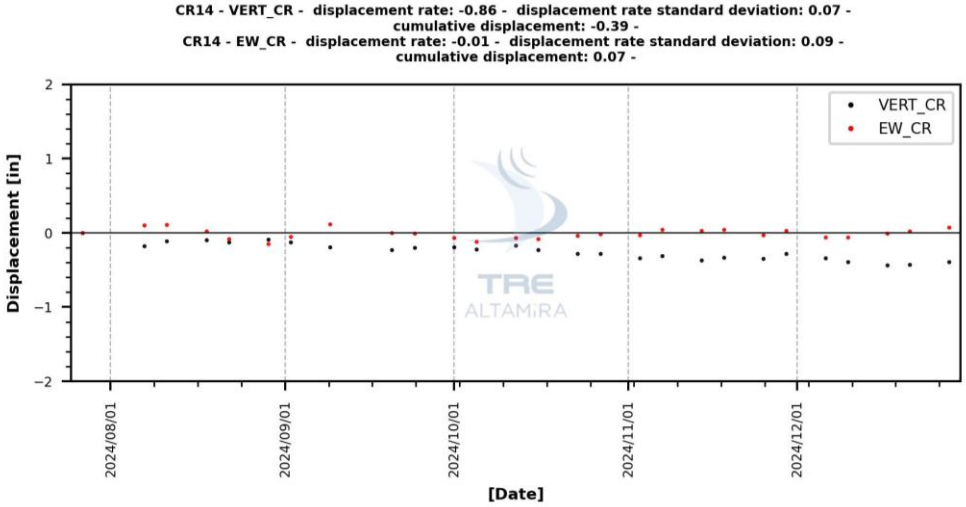
CR14 - VERT_CR - displacement rate: -0.86 - displacement rate standard deviation: 0.07 - cumulative displacement: -0.39 -
CR14 - EW_CR - displacement rate: -0.01 - displacement rate standard deviation: 0.09 - cumulative displacement: 0.07 -
VERT_CR
EW_CR
Displacement [in]
2
1
0
−1
−2
2024/08/01
2024/09/01
2024/10/01
2024/11/01
2024/12/01
[Date]

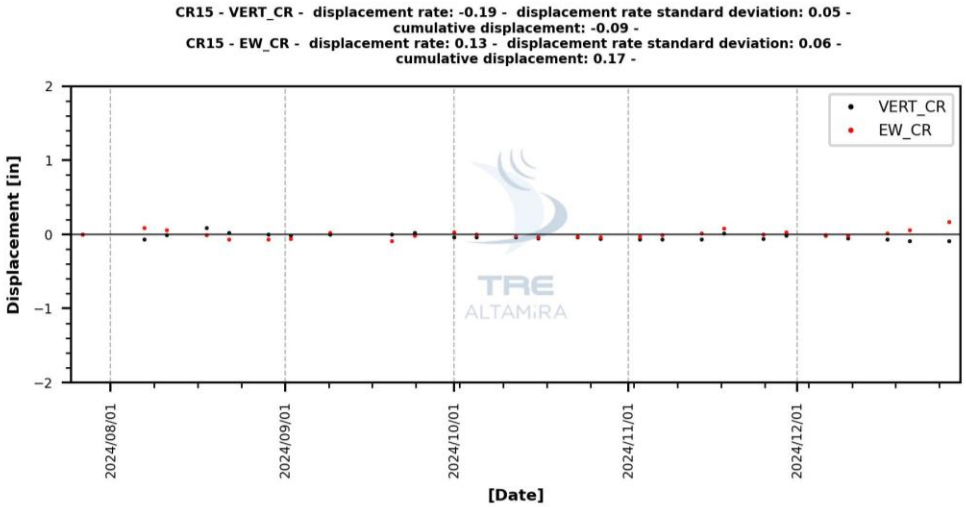

Figure 28: Time series of the vertical and east-west displacement of each CR within Lonquist areas of interest.

TRE ALTAMIRA
A CLS Group Company

TRE ALTAMIRA s.r.l.
Ripa di Porta Ticinese, 79
20143 Milan Italy
Tel: +39 02 4343 121

TRE ALTAMIRA S.L.U.
Carrer de Còrsega, 381-387
08037 Barcelona Spain
Tel.: +34 93 183 57 50

TRE ALTAMIRA Inc.
Suite 410, 475 West Georgia Street
Vancouver, BC V6B 4M9 Canada
Tel: +1 604 331 2512

tre-altamira.com